MIP Plasma Decapsulation of Copper-wired Semiconductor Devices for Failure Analysis

MIP Plasma Decapsulation of Copper-wired Semiconductor Devices for Failure Analysis

PROEFSCHRIFT

ter verkrijging van de graad van doctor
aan de Technische Universiteit Delft,
op gezag van de Rector Magnificus Prof. ir. K. C. A. M. Luyben,
voorzitter van het College voor Promoties,
in het openbaar te verdedigen

op woensdag 15 januari 2014 om 10.30 uur

door

Jiaqi TANG

Master of Science in Materials Science
University of Pennsylvania, Philadelphia, USA
geboren te Beijing, China

Dit proefschrift is goedgekeurd door de promotor:

Prof. dr. C. I. M. Beenakker

Samenstelling promotiecommissie:

Rector Magnificus, voorzitter

Prof. dr. C. I. M. Beenakker, Technische Universiteit Delft (promotor)

Prof. dr. G. Q. Zhang, Technische Universiteit Delft

Prof. dr. P. J. French, Technische Universiteit Delft

Prof. dr. C. J. Bailey, University of Greenwich, UK

Prof. dr. R. A. M. Wolters, Universiteit Twente

Prof. dr. D. C. Schram, Technische Universiteit Eindhoven

Dr. J. H. Gulpen, NXP Semiconductors, Nijmegen

Jiaqi Tang, Ph.D. thesis Delft University of Technology with summary in Dutch.

The work described in this thesis was carried out under project number M21.9.SE2Ab in the framework of the Research Program of the Materials innovation institute M2i and co-funded by ENIAC Joint Undertaking.

Key words: Microwave induced plasma, MIP, afterglow plasma etching, decapsulation, plastic IC package, copper wire bond, failure analysis, resonant cavity, microwave power coupling, etching recipe, etching selectivity, preservation of IC functionality, business development

ISBN: 978-94-91909-05-4

Copyright 2014 by Jiaqi Tang

All rights reserved.

No part of this publication may be reproduced, stored in a retrieval system, or transmitted in any form or by any means without the prior written permission of the copyright owner.

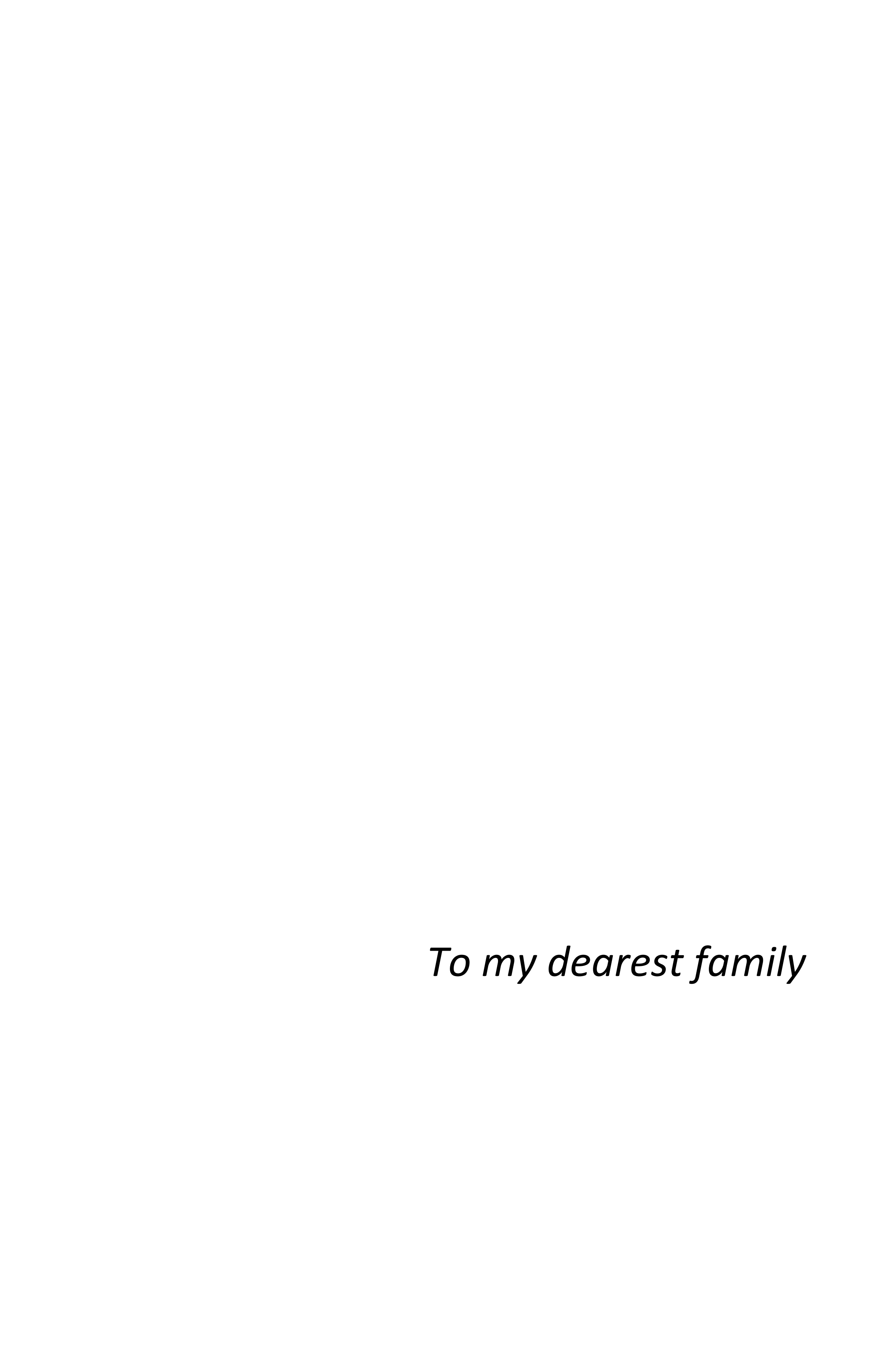

To my dearest family

Contents

1. Introduction

1.1 Integrated Circuit Packaging 1

1.2 Copper Wire Bonding 3

1.3 IC Package Level Quality Control and Failure Analysis 5

1.4 Currently Adopted Decapsulation Techniques and Their Limitations on Copper Wire Packages 7

1.4.1 Acid Decapsulation 7

1.4.2 Conventional Plasma Decapsulation 8

1.4.3 Laser-ablation 9

1.4.4 The Urgent Need for a New Decapsulation Technology 9

1.5 Outline of the Thesis 10

2. Microwave Induced Plasma Decapsulation System

2.1 System Setup 11

2.2 Conclusions 14

3. Microwave Cavity and Atmospheric Pressure Plasma Generation

3.1 Introduction 15

3.2 Beenakker Cavity Modification Design 16

3.2.1 Microwave Properties of the Beenakker Cavity 16

3.2.2 Impedance Mismatch When Sustaining Argon Plasma 19

3.2.3 Solutions to Impedance Mismatch and Literature Study 26

3.2.4 Modifications to Solve Impedance Mismatch 27

3.2.5 Influence of Etchant Gas Addition 32

3.2.6 Modifications to Broaden the Stable Plasma Operation Range 35

3.3 Frequency Tuning 39

3.4 Filamentation of Plasma 40

3.5 Power Efficiency of the MIP System 42
3.6 Conclusions 48
4. Microwave Induced Plasma Afterglow Etching
4.1 Introduction 49
4.2 MIP Afterglow Etching Temperature 50
4.2.1 Numerical Thermal Model 51
4.2.2 Temperature Measurement 52
4.2.3 In-situ Temperature Monitoring 54
4.3 Species and Their Lifetimes in the Plasma Afterglow 56
4.4 MIP Afterglow Etching of Epoxy Molding Compound 58
4.4.1 Ar/O_2 Plasma Etching 58
4.4.2 Ar/CF_4 Plasma Etching 59
4.4.3 $Ar/O_2/CF_4$ Plasma Etching 59
4.4.4 Influence of the Epoxy Molding Compound Composition 60
4.5 MIP Afterglow Etching of Si and SiO_2 63
4.6 MIP Afterglow Etching of Si_3N_4 67
4.7 MIP Afterglow Etching of Silicone 70
4.8 MIP Afterglow Etching of Metals 72
4.8.1 Plasma Etching of Copper 72
4.8.2 Plasma Etching of Aluminum 75
4.8.3 Plasma Etching of Palladium 78
4.8.4 Plasma Etching of Gold 79
4.9 Conclusions 80
5. Microwave Induced Plasma Decapsulation of IC Packages
5.1 Introduction 83
5.2 $Ar/O_2/CF_4$ Plasma Decapsulation 85
5.2.1 The Scan Etching Process 85
5.2.2 The Decapsulation Results 89

5.3 $Ar/O_2/CF_4$ Plasma + Ar/O_2 Plasma Decapsulation 90
5.3.1 $Ar/O_2/CF_4$ Plasma Decapsulation and Over-etch Damage 91
5.3.2 $Ar/O_2/CF_4$ + Ar/O_2 Plasma Decapsulation, No Damage to Si_3N_4 and Si 92
5.3.3 Critical Thickness to Prevent Over-etch Damage to Si_3N_4 and Si 94
5.4 Laser-ablation + Ar/O_2 Plasma Decapsulation 95
5.4.1 Step 1: Laser-ablation 95
5.4.2 Step 2: Ar/O_2 Plasma Etching 96
5.4.3 Comparison with Cold Acid Decapsulation 97
5.5 Laser-ablation + Low Power $Ar/O_2/CF_4$ Plasma Decapsulation 99
5.5.1 The Wire-masking Effect 99
5.5.2 Solution to Wire-masking Effect 102
5.6 Case Study 1: Thermally Stressed IC Packages 103
5.6.1 Bare Copper Wire Bonded Package After HAST 104
5.6.2 Palladium-coated Copper Wire Bonded Package After HTS 105
5.7 Case Study 2: IC Packages with Delamination Defects 106
5.7.1 Plasma Decapsulation Results 107
5.7.2 Comparison with Cold Acid Decapsulation 108
5.8 Case Study 3: Solving Failure Analysis Dilemma by MIP Decapsulation 110
5.9 Conclusions 111
6. Microwave Induced Plasma Decapsulation of LED Packages
6.1 Introduction 113
6.2 Flip-chipped Sapphire Substrate GaN-based High-power LED 114
6.3 Wire-bonded GaN-based High-power LED 117
6.4 Conclusions 118
7. Business Development
8. Conclusions and Recommendations

8.1 Conclusions 125
8.2 Future work 127
List of abbreviations 129
About the Author 131
List of Publications 133
Summary 135
Samenvatting 139
Acknowledgments 143
Bibliography 147

Chapter 1

Introduction

1.1 Integrated Circuit Packaging

Integrated Circuit (IC) devices are normally packaged in little black boxes to protect the chip from the environment and to provide a standard outline for Printed Circuit Board (PCB) design and automatic pick and place (see Fig.1-1). Chip, supporting leadframe and interconnection components are encapsulated inside the IC package. Epoxy molding compound is the most widely used material for IC encapsulation due to the low cost and good performance. Thin metal wires are commonly used to connect the bond pads on the chip to the leadframe that sticks outside the package, thus connecting the micron or submicron dimensions on the chip to the PCB outside world (see Fig.1-2).

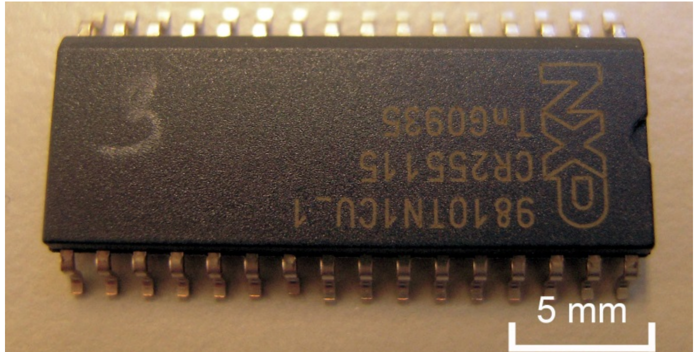

Fig.1-1 Plastic IC package encapsulated in epoxy molding compound.

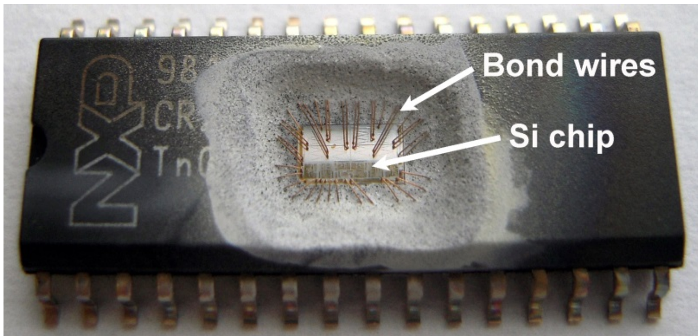

Fig.1-2 Inside an IC package. Once the epoxy molding compound encapsulation material is removed, the chip and bond wires inside the IC package can be seen.

There are many types of IC packages with different package structures (see Fig.1-3). The trends in IC packaging are smaller footprint, lower cost, higher performance, and multi-functionality. Smaller footprint means the size of the IC package is becoming smaller and comparable to the footprint of the semiconductor chip that is inside. Lower cost is made possible by introducing new materials, for example copper wire bonding. Higher performance and multi-functionality can be achieved by adopting new packaging structures that allow integration of multiple chips in one package through heterogeneous integration, for example stacked die package and System in Package (SiP) [1, 2].

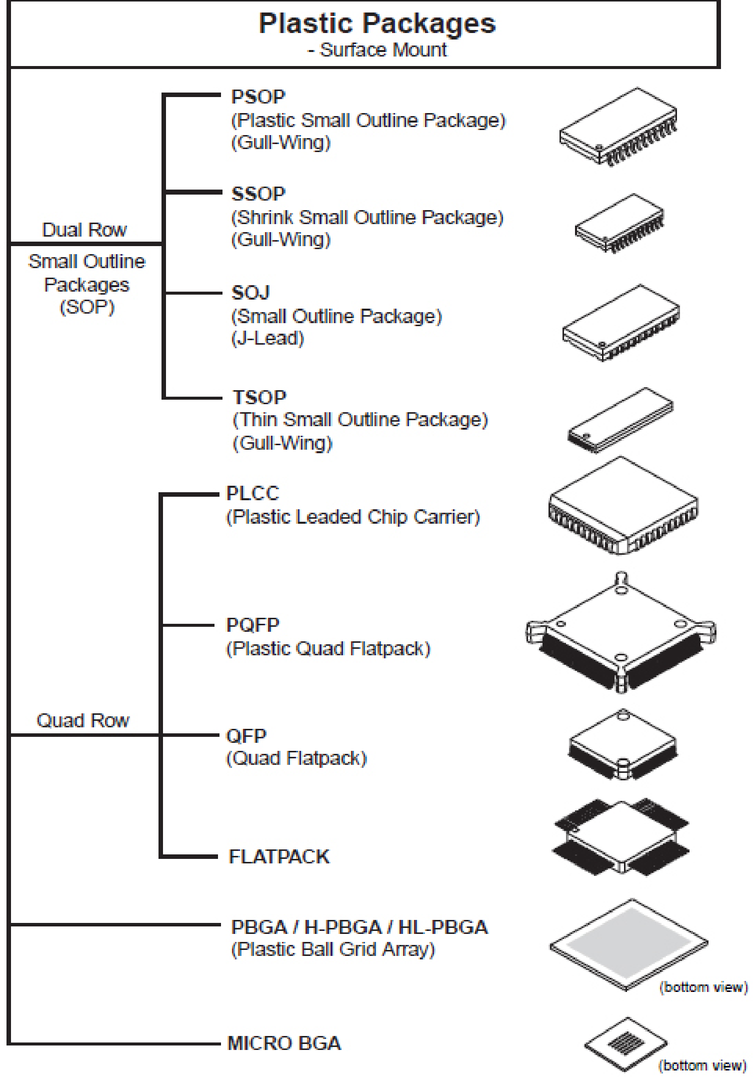

Fig.1-3 Different kinds of surface mount type plastic IC packages [3]. (Source: Intel)

1.2 Copper Wire Bonding

For single chip packages in volume production, the mostly used packaging technologies are wire bonding and flip-chip. In the year 1999, wire bonding accounts for well over 90% of all the chip-to-package interconnections due to technology maturity, cost, and application diversity reasons [1].

For decades, gold has been mostly used as the bonding wire material in fine pitch IC packaging due to its good electrical conductivity, mechanical properties, and excellent chemical resistance. However, the increase of gold material price from 400 USD/ounce in the year 2005 to 1400 USD/ounce in the year 2013 (see Fig.1-4) results in a major portion of the packaging cost to be the cost of the gold wire. The cost issues prompt industry to search for alternative bond wire materials.

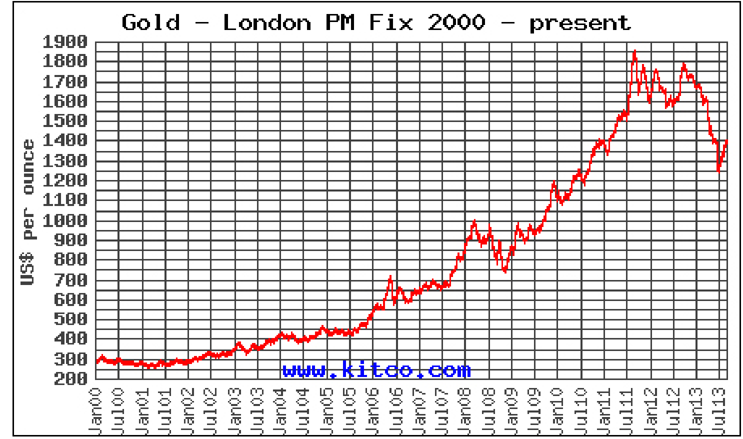

Fig.1-4 Gold price USD/ounce from 2000 to 2013. 1 ounce=0.0625lb (Source: kitco.com)

Copper has excellent electrical, mechanical, and Cu/Al bonding intermetallic properties, thus it has gained much attention in IC packaging industry as the alternative wire bonding material to replace gold. More importantly the material cost of copper is much lower than gold (see Fig.1-5) such that the major cost of thin copper wire bonding does not come from the material itself, but from processing steps. With gold price over 1000 USD/ounce, there is significant motivation to move to copper wire [4]. Cost savings of at least 10% for the overall assembly process is expected when using copper wire bonding [5].

Thick copper wire (>50 micron diameter) bonding has been used for over 20 years in power electronic components [6]. However, fine pitch thin copper wire (about 25 micron or less in diameter) bonding was not implemented in IC packaging until recent years.

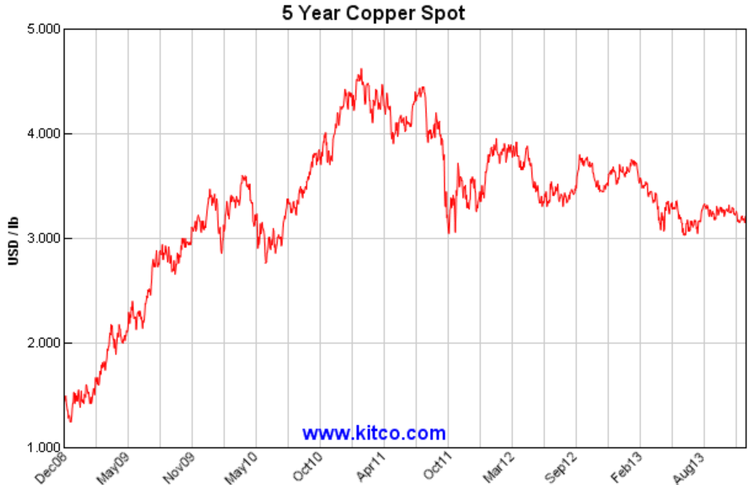

Fig.1-5 Copper price USD/lb from 2008 to 2013. (Source: kitco.com)

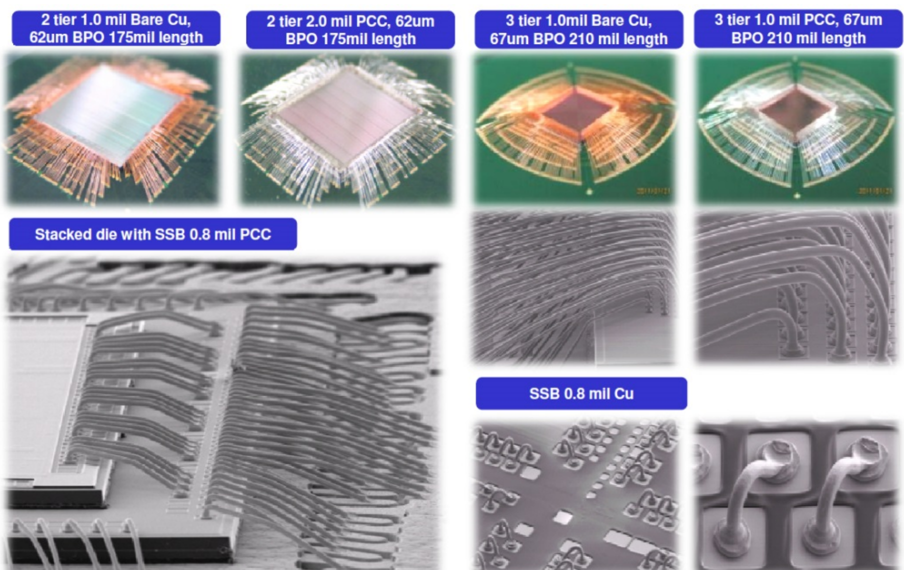

Fig.1-6 Copper and Palladium-coated copper wire bonded IC packages before encapsulation, PCC stands for Palladium-Coated Copper, BPO stands for Bond Pad Opening, SSB stands for Stand-off-Stitch Bond [4]. (Source: Amkor)

The main problem with fine pitch copper wire bonding is that copper oxidizes easily in normal air environment, thus posing difficulty in the ball bonding process and the long term bonding reliability [7]. Ball formation is required to allow for the use of fully automatic wire-bonding machines with speeds of about 10 wires per second. Special fine pitch copper wire bonding machines were designed with forming gas during the free air ball formation process to prevent oxidization. To reduce oxidization on bare copper wire and enhancing long-term reliability, palladium-coated copper wires [8-10] were also introduced and both types of copper wires are now used in IC packaging industry. With continuous efforts on understanding the thermosonic copper wire ball bonding process [9, 11-14], Cu/Al intermetallic compound formation [15, 16], and long-term package reliability [16, 17], copper wire bonding has become a mature process and is now in mass production [4, 6] (see Fig.1-6).

Copper wire bonding is now steadily replacing traditional gold wire bonding in IC packaging. According to International Technology Roadmap for Semiconductors (ITRS) assembly and packaging report in 2011, the share of copper has increased from 1% in 2007 to 10% in 2010 [18] and is expected to increase further.

1.3 IC Package Level Quality Control and Failure Analysis

When a new type of IC component is manufactured, quality tests on samples has to be performed before shipping the product into market. During quality tests, IC packages are exposed to stressing conditions like High Temperature Storage (HTS), Temperature Cycling (TC), and Highly Accelerated Stress Test (HAST) [14-17, 19, 20]. These accelerated tests simulate and predict the behavior of the IC component in real use conditions.

Failure in the IC component may occur after, during, or even before quality tests. When failure happens, the IC component has to go through failure analysis steps to investigate the root cause of failure. Successfully locating the failure site in an early stage during product development is crucial to detect potential defects and prevent disasters like massive malfunction of the IC components after they are on market.

Even if the batch of IC components pass quality test, some still fail during its lifetime. In such cases, the failed component is returned to a lab and failure analysis is performed to find the root cause. The analysis on field-return components should answer whether the failure is due to inappropriate usage or reliability issues, and more importantly, suggest improvement measurements to prevent such component failure from happening again.

Failure analysis on IC components normally follows a general procedure:

1. X-ray of the IC component, sometimes Scanning Acoustic Microscopy (SAM) is also performed to detect delamination in the IC package.
2. Open the IC package, also called decapsulation. The encapsulation material on the IC package is removed, exposing the bond wires and die inside the package without process-induced damage.
3. Optical microscopy or Scanning Electron Microscopy (SEM). Detailed surface microscopy is performed to locate the possible failure sites on the bond wire, bond pad, or die.
4. Focused Ion Beam (FIB) milling, Transmission Electron Microscopy (TEM), Energy-Dispersive X-ray spectroscopy (EDX), etc. Material or structure analysis is made depending on the type of failure and the specific analysis task.

Step #2, IC package decapsulation (see Fig.1-7), is the focus of this thesis. Careful package decapsulation is a crucial step in failure analysis because this step should only remove the molding compound material, while not damage the bond wires and die inside the package. Otherwise, if a failure site is discovered in further analysis one cannot tell whether the failure is due to decapsulation or whether it is an original defect before decapsulation. Also, if the decapsulation process induces unwanted damage the original failure sites may be removed after the package is decapsulated, which also makes further root cause analysis impossible.

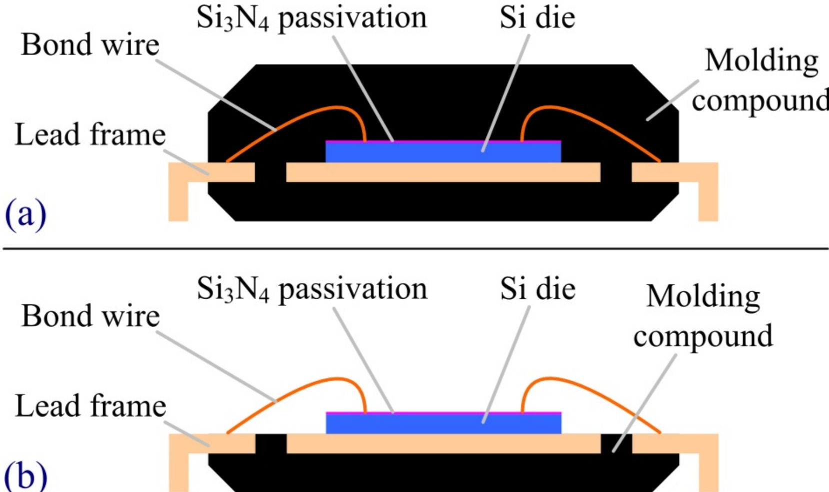

Fig.1-7 Schematic representation of an IC package structure, cross-sectional view (a) Before decapsulation; (b) After decapsulation

1.4 Currently Adopted Decapsulation Techniques and Their Limitations on Copper Wire Packages

In plastic IC packages, epoxy molding compound is used as the encapsulating material. The compositions of the molding compound is a mixture of epoxy (10-30 %Wt), silica fillers (70-90 %Wt), and small amounts of coupling agents, hardener, releasing agents, flame retardants, etc. [21]. Decapsulation is the process to selectively remove this epoxy molding compound layer. A good decapsulation process is important not only for failure analysis but also in packaging process development.

There are two major requirements for a decapsulation technique. One is selectivity, which determines the potential of unwanted damage to bond wires and silicon die. The other one is etching rate, which determines how fast the IC package can be fully decapsulated. It is hard to meet both of the above requirements simultaneously because they are often found contradictory in practice.

The most widely used plastic IC package decapsulation technique is etching by nitric and sulfuric mixture acid. However, the switching from gold to copper wire bonding causes acid decapsulation not suitable any more. Conventional plasma decapsulation and laser-ablation also have inherent disadvantages. These techniques are summarized below.

1.4.1 Acid Decapsulation

The mostly used conventional decapsulation technique is to use hot nitric or nitric and sulfuric mixture acid to etch away the molding compound [21, 22], such process has been routinely used for gold wire bonded plastic IC package decapsulation. The advantage of acid decapsulation is its speed, it often takes only several minutes to decapsulate one package and the process works fine with gold wire bonded packages as gold does not react with the acid.

However, the switch to copper wire bonding in industry has raised a problem for acid decapsulation, because copper wires are more susceptible to be corroded and damaged by the acid (see Fig.1-8) [5, 23-25]. Efforts have been made to reduce corrosion on copper bond wires and aluminum bond pads by reducing the etching temperature [23, 25, 26]. Cold acid etching increases etching selectivity of molding compound to copper bond wires by sacrificing the etching rate. With well-engineered acid etching recipes, decapsulation of copper wire bonded package can be achieved. However, corrosion on the copper wire is often found inevitable and the surface features on the copper wire bonds are always lost.

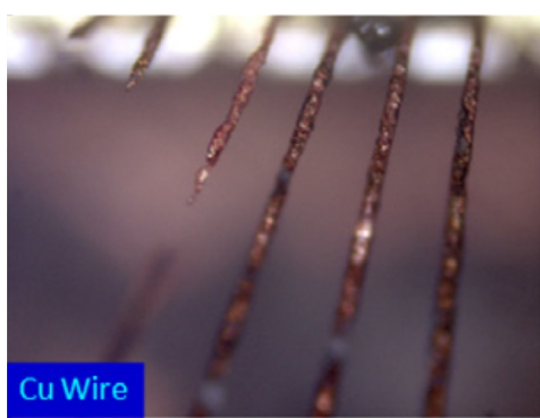

Fig.1-8 Copper bond wires severely corroded after acid decapsulation [25]

Stressed or failed IC components are of the most interest in analysis as they often demonstrate the weak points in design or potential problems in the material composition. Molding compound after Temperature Cycling (TC), High Temperature Storage (HTS), and other reliability tests become much more resistant to acid etching because epoxy is fully cross-linked and hardened. As a result, acid decapsulation of thermally stressed packages is much more difficult compared to fresh packages. Longer acid etching time is needed, which makes preservation of Cu/Al bonds during decapsulation becoming extremely difficult [24]. The situation becomes even worse when dealing with one-of-a-kind field return failed components. The history of the failed component is often unknown and the acid etching recipes developed on unstressed sample are often not suitable for decapsulating the failed sample.

1.4.2 Conventional Plasma Decapsulation

Conventional oxygen plasma etchers that use a vacuum chamber and a Radio Frequency (usually 13.56 MHz) power source are capable of etching organic materials so in principle they can be used for decapsulation [27-29]. However, the plasma etchers are designed for batch wafer fabrication processes and therefore not necessarily suitable for IC package decapsulation.

A common bottleneck with IC package decapsulation by conventional plasma etcher is the extremely low molding compound removal rate (see Fig.1-9), which results in extremely long decapsulation duration ranging from several hours to even days for a single package [21, 22]. The silica filler in the molding compound cannot be easily removed and forms a residue layer on the molding compound surface that hinders further plasma etching. Adding fluorine into plasma gas does help to remove the silica filler residues [22, 28, 29]. However, the formed fluorine radicals attack Si_3N_4 and Si at the same time, which cause unwanted over-etching damage to the die.

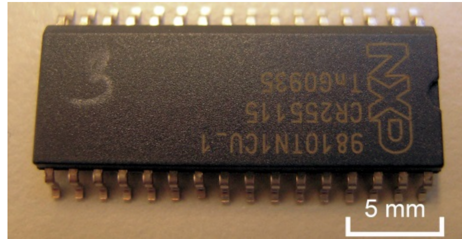

Fig.1-9 Left: Plastic IC package before decapsulation. Right: Package after 30 minutes etching in conventional reduced pressure oxygen RF plasma at 300 W power. Etching is extremely slow, only the surface molding compound layer is being etched.

Another disadvantage is that the IC packages are normally immersed in the plasma during etching. The RF electric field and the ions in the plasma pose potential damage to the die inside the package. Grounding the pins on the package only helps to reduce the damage but does not prevent it. This makes retaining full functionality of the die difficult after decapsulation. The drawbacks of conventional plasma etchers therefore make it not practical for IC package decapsulation.

1.4.3 Laser-ablation

Laser-ablation [30-33] is a commonly adopted process in IC industry to remove bulk layer of molding compound in plastic IC packages. Laser-ablation has the advantage of high precision and high molding compound removal rate, while the disadvantages are unavoidable damage to Si die, Si_3N_4 passivation layer, and bond wire surface. Thus laser-ablation is usually used as a pre-decapsulation process to remove bulk molding compound until the bond wire loop is exposed, then acid etching is performed to fully decapsulate the IC package [26, 34].

1.4.4 The Urgent Need for a New Decapsulation Technology

Clearly, a new decapsulation technique has to be developed for fast, selective and safe decapsulation of copper wire bonded IC packages. The approach in this thesis is to combine the selectivity of a plasma with the speed and absence of RF fields of acid decapsulation by designing a novel Microwave Induced Plasma (MIP) system characterized by high power density, atmospheric pressure operation and absence of exposure of the samples to ions. The performance of this MIP system should outperform acid decapsulation in preservation of fine surface details on the copper wire bonds. Compared to conventional plasma etchers, the MIP system should be at least 20 times faster and does not damage the functionality of the chip.

1.5 Outline of the Thesis

The outline of the thesis is shown schematically in Fig. 1-10. Chapter 2 describes the prototype setup of the Microwave Induced Plasma decapsulation system designed for copper wire package decapsulation. Chapter 3 investigates problems when using the original Beenakker cavity as the source of the plasma. Modifications are proposed that enable generation of an atmospheric pressure high-power density stable $Ar/O_2/CF_4$ plasma. Based on the plasma chemistry, MIP afterglow etching recipes for a variety of materials are developed in Chapter 4. The optimal recipes for high etching rates as well as the rate-limiting factors of etching each material are given, the results provide reference to plasma etching selectivity and preservation of certain materials during MIP decapsulation of IC packages. Chapter 5 focuses on the application of MIP afterglow etching in IC package decapsulation. Four different processes are proposed and their pros & cons are analyzed. Case studies on typical copper wire package decapsulation tasks are given and comparisons with conventional acid decapsulation are made. Chapter 6 explores the application of MIP afterglow etching in LED package decapsulation. Chapter 7 describes the business development of the MIP system and commercialization of the product. Main conclusions and recommendations for future work are given in Chapter 8.

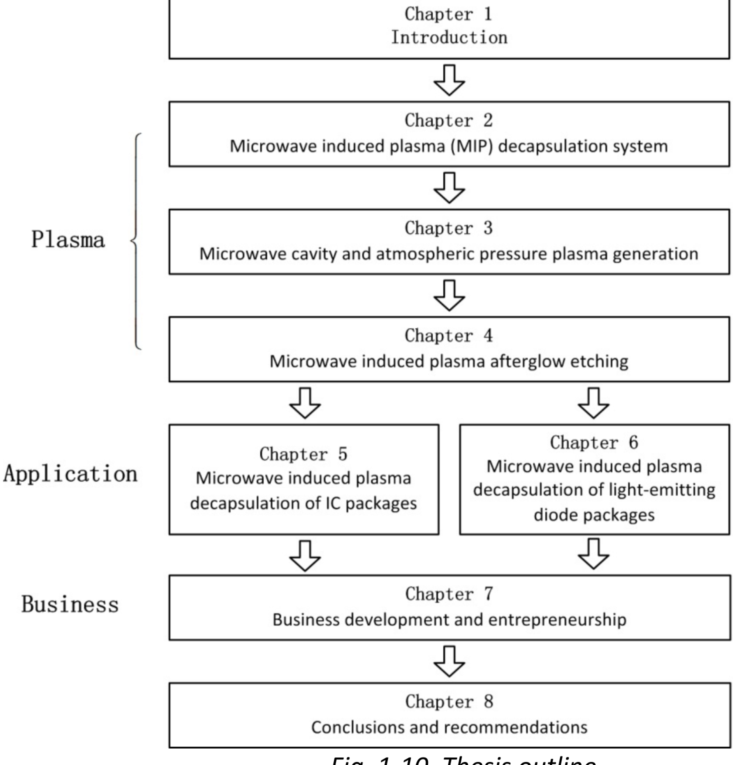

Fig. 1-10. Thesis outline

Chapter 2
Microwave Induced Plasma Decapsulation System

2.1 System Setup

For our plasma etching and IC package decapsulation experiments, a Microwave Induced Plasma (MIP) decapsulation system was built. The MIP system should be able to generate a stable plasma, preferably under atmospheric pressure. Localization control and process monitoring during plasma etching should be enabled, thus IC package decapsulation process can be well-controlled with high reproducibility.

Through four years of development, a prototype MIP system was built and the schematic representation of system setup is shown in Fig.2.1. The system consists of a microwave generator (Sairem solid-state, f=2450+-20 MHz, P=0~180 W), a lab-built Beenakker type microwave resonant cavity, a gas discharge tube, three mass flow controllers, a CCD camera, a programmable XYZ-stage, and a computer to control the components.

For safety consideration, the MIP system is placed in a chemical fume hood for exhaust treatment. Health regulation limits the radiation leakage at 5 cm from the instrument outer frame to be lower than 1.0 mW/cm^2. By careful engineering of the microwave plasma, leakage radiation measured at 5 cm from the instrument outer frame is 0.0 mW/cm^2 (will be elaborated in Section 3.5). Thus the MIP instrument is safe to use according to regulations.

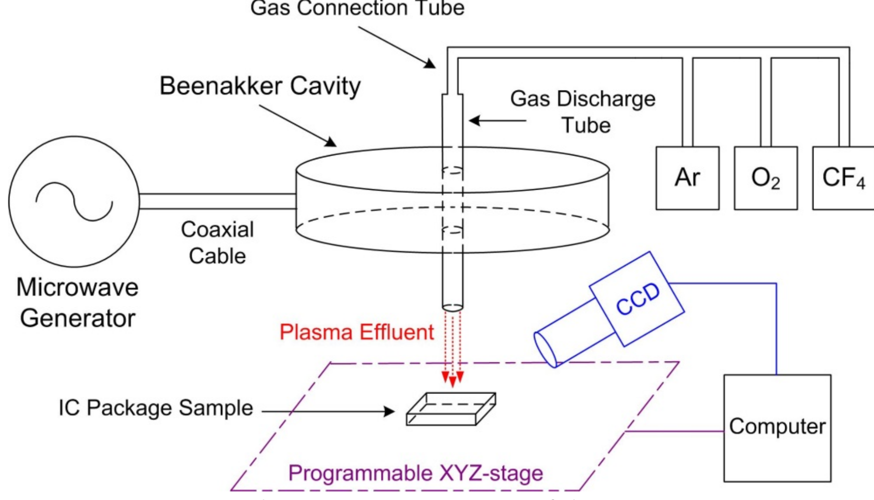

Fig.2.1 Schematic representation of the MIP system

The microwave power from the generator is delivered to the Beenakker cavity via a coaxial cable. The cavity has the shape of a pill box with an outer diameter of about 12 cm and a height of 2 cm. It is designed to resonate at 2.45 GHz in the TM_{010} mode. In this mode the electric field amplitude inside the cavity is zero at the periphery and maximum in the center. A quartz or alumina gas discharge tube (1.2 mm i.d., 6 mm o.d.) is inserted through the center of the cavity to sustain the plasma. Argon is the plasma carrier gas. O_2 and CF_4 are added as etchant gas.

IC package sample heating in conventional plasma etchers is normally achieved by placing a hotplate beneath the IC package. In the MIP system, sample heating is made through direct heating by the plasma effluent. Heating by plasma effluent gas gives the advantage of maintaining a low IC package bulk temperature, while having a localized heating on the plasma etching site.

The plasma source is carefully engineered such that plasma etching is done by radicals in the plasma afterglow, rather than ion bombardment. The prevention of ions and microwave leakage fields on the IC package sample is crucial to avoid damage to the device inside the package. It will be demonstrated in Chapter 5&6 that semiconductor devices remain functional after their packages have been decapsulated by this MIP system.

A programmable XYZ-stage is used as the IC package sample stage. The movement of the stage is controlled by a computer and programs are written to define customized scan routes. There are basically two approaches to etch a defined area by plasma. The conventional approach is to put the IC sample in a chamber filled with plasma and use a mask to define the area for etching. The alternative approach is to make a very confined plasma and scan the plasma beam across the area that is intended for etching. The advantage of the later process is not only the convenience of defining the etching area, but also the possibility to vary the scan speed at different regions to achieve variable etching profiles across the IC package sample.

A CCD camera is integrated into the MIP system to enable real-time monitoring of the plasma etching process. The position of the CCD camera and the plasma recipe is adjusted so that the camera focuses on the surface of the IC package that is under plasma etching. Effluent of the plasma afterglow has a circular effective etching area with a diameter of 4 mm. The camera captures real-time image on a 1.6 mm by 1.2 mm rectangular area on the IC package. Because the stray field generated from the plasma is low, there is no influence on the CCD camera due to electromagnetic interference and clear images can be received throughout the etching process.

Table 2.1 Images of the IC package during MIP decapsulation

Etching stage	Etching time	Images from CCD
Stage 1: Etching just begun. Viewing area: 1.6 x 1.2 mm Thickness of molding compound: 1000 um	40 sec	
Stage 2: Top part of bond wires exposed. Cu bond wires have a diameter of 38 um.	2 min	
Stage 3: Si die exposed. More copper bond wires exposed.	4 min	
Stage 4: Cu bond wires clearly exposed. Structures on the Si die over-etched.	5 min	

The stable high-efficiency plasma and the good process control of this MIP system provides unique added value for IC package failure analysis. Table 2.1 illustrates real-time images taken by the CCD camera at different stages during decapsulation of a copper wire bonded plastic IC package. The plasma conditions are not altered during etching and images at different time spans are recorded. At stage 1, the thick molding compound on top of the bond wires is etched. The sparkling particles in the image are silica filler particles. At stage 2, the copper bond wires appear. At stage 3, after etching for four minutes the Si die appears. At stage 4, further exposure of the Si die to the plasma caused over-etching of the Si_3N_4 passivation layer. The damaged structures on the die can be seen under the CCD camera. After five minutes plasma etching, plasma removes 1000 um thick molding compound and the copper bond wires are clearly exposed.

2.2 Conclusions

A prototype MIP system is built. Major components in the system include microwave generator, Beenakker-type resonant cavity, discharge tube, mass flow controller, programmable XYZ-stage, and CCD camera. The system works under atmospheric pressure thus vacuum components are not needed. The system is placed inside a chemical fume hood for exhaust treatment. Safety issues on microwave leakage hazards are taken care of by careful engineering on the microwave induced plasma. The role of each component in the system and how the MIP system as a whole works during IC package decapsulation applications are explained.

The core component in the MIP system is the Beenakker cavity, which is the plasma source that determines the plasma etching performance. The following chapters will cover modifications of the original Beenakker cavity, plasma etching recipe development, and semiconductor decapsulation applications. The MIP system described in this chapter is used in all microwave induced plasma etching and decapsulation experiments in this thesis.

Chapter 3

Microwave Cavity and Atmospheric Pressure Plasma Generation

3.1 Introduction

Sustaining a stable plasma at atmospheric pressure usually is more difficult than in vacuum. Due to the high pressure, electrons cannot gain sufficient energy by elastic collisions and collisions between ions and radicals in plasma are more frequent resulting in higher recombination rate. Because the dissociation energy of polyatomic gas is lower than its ionization energy, gases like O_2 or CF_4 cannot successfully generate plasma with existing plasma sources under atmospheric pressure at power levels below 100 W.

Noble gases that are monatomic are used as carrier gas to generate atmospheric pressure plasma. Argon and helium gases both can be used with the MIP system. Due to the difference in ionization energy and atomic mass, more power is needed to sustain a plasma with helium (24.59 eV) than with argon (15.76 eV) under the same operation conditions. Moreover, as the typical gas flow in the plasma is around 1400 sccm, argon having a lower running cost is more suitable than helium to be used as the plasma carrier gas in day-to-day operations. In addition, the thermal conductivity of helium ($0.1513\, W \cdot m^{-1} \cdot K^{-1}$) is much higher than that of argon ($17.72 \times 10^{-3}\, W \cdot m^{-1} \cdot K^{-1}$), increasing the risk of too high temperatures of the IC package during decapsulation.

There are several existing designs of microwave induced plasma cavities [35-37], for example Beenakker cavity, microstrip, plasma torch, surfatron, etc. Each apparatus employs a distinct wave propagation phenomenon thus has different plasma characteristics. For the application in plasma decapsulation of IC packages, Beenakker cavity is selected due to its high power density and low stray field.

The original Beenakker cavity is designed for sustaining atmospheric pressure helium plasma and is a breakthrough in gas chromatography [36-38]. The cavity is one of the very few designs that can sustain atmospheric pressure helium plasma. However, when sustaining argon plasmas there turns out to be a severe impedance mismatch in the microwave plasma system. The resulting high power reflection (>50%) induces instability during plasma etching and damage to the magnetron source. More problems emerged when using the original cavity for semiconductor package decapsulation applications. Apparently, modifications to the original Beenakker cavity are needed for plasma etching applications.

The problems that are investigated and solved in this chapter are:

- How to reduce the high power reflection due to impedance mismatch with the original cavity when sustaining atmospheric pressure argon plasma.
  Section 3.2.2, 3.2.3, and 3.2.4
- How to reduce the high power reflection and instability of argon plasma due to the addition of etchant gas.
  Section 3.2.5 and 3.2.6
- How to fine tune the microwave system during plasma operations.
  Section 3.3
- How to improve the plasma stability by mastering filamentation of the argon plasma.
  Section 3.4
- How to improve the system energy efficiency by managing power loss in the microwave system.
  Section 3.5

The goal is to design a modified Beenakker cavity that enables good impedance matching of the microwave system, such that low power reflection (0% with argon plasma, <10% for mixture plasma) is maintained during plasma operations. Meanwhile, the plasma sustained by the system should have high stability and large operation window, which allows a variety of etching recipes to be used in further materials etching and semiconductor package decapsulation applications. At the same time, the overall power efficiency of the microwave system and the volumetric power density of the plasma should be high, which enables high radical density in the afterglow.

To reach the above mentioned goal, several modifications are proposed. The microwave characteristics of the Beenakker cavity before and after two major modifications are analyzed by both simulation results from microwave circuit measurements and experimental results during real plasma operations.

3.2 Beenakker Cavity Modification Design

3.2.1 Microwave Properties of the Beenakker Cavity

The original Beenakker cavity [38-40] is designed to sustain atmospheric pressure helium plasma for gas chromatography applications. A lab-built original design Beenakker cavity is shown in Fig.3-1-left. The cavity has a cylindrical shape with outer diameter around 12 cm and height around 2 cm. A coaxial connector located at the radial periphery of the cavity can be connected to a 50 Ohm coaxial cable or external tuners. The opening in the radial center of the cavity allows insertion of a gas discharge tube. Two metal tuning screws are located near the

center and periphery of the cavity, respectively. Insertion of the tuning screws varies the electromagnetic field pattern inside the cavity, thus they can be used for fine tuning of the cavity's microwave property. Another opening on the cavity (not visible in Fig.3-1-left) allows insertion of a quartz rod into the cavity, providing another tool to tune the cavity resonance frequency. The inside structure of original design Beenakker cavity is shown in Fig.3-1-right, where the original coupling loop that connects external coaxial connector to the cavity inner surface can be seen.

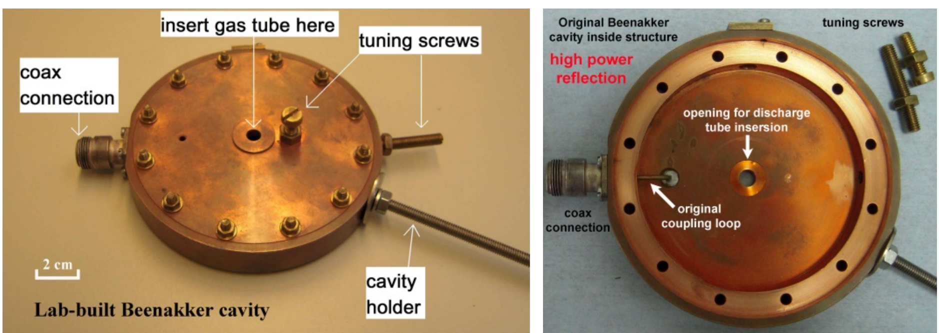

Fig.3-1 Lab-built original Beenakker cavity outside (left) and inside (right) structure. This original design suffers from high power reflection (>50%) when sustaining atmospheric pressure argon plasmas, but works well with helium plasmas.

A. Resonance structure

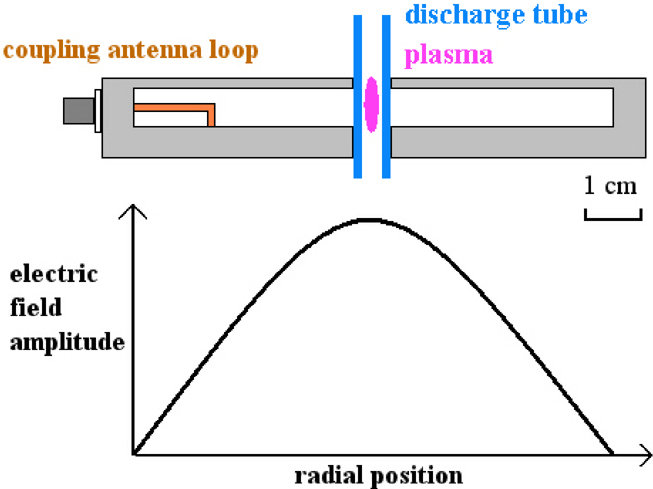

Fig. 3-2 Cross sectional view of the original Beenakker cavity and the electric field amplitude distribution along radial direction

The Beenakker cavity has a hollow structure (see Fig. 3-2). A bent copper coupling loop located at the radial periphery inside the cavity couples microwave power from the outside coaxial connector into the cavity. Due to its design, the electric field amplitude distribution inside the Beenakker cavity follows a zero order Bessel function distribution along the radial direction. Electric field strength reaches maximum value in the center and zero at the periphery. A gas discharge tube is inserted through the center of the cavity to utilize the high power density electric field to sustain an atmospheric pressure plasma.

For a cavity to resonate at 2.45 GHz in TM_{010} mode we can calculate the resonant frequency. The resonant frequency f_R of the cavity is related to the inside diameter D of the cavity by formula [39]:

$$D = \frac{c(ka)_{mn}}{\pi f_R}, \tag{3-1}$$

where c is the speed of light in vacuum, $(ka)_{mn}$ is the nth root of the mth order Bessel function $J_m(kr)$, where k is the wavenumber and r is the radial coordinate of the cavity . The smallest diameter and hence the largest energy density is obtained when $m = 0$ and $n = 1$, thus $(ka)_{mn} = 2.405$ [39]. For 2.45 GHz resonant frequency, the inside diameter of the cavity is calculated to be 93.7 mm.

B. Cavity material

At high frequencies, electric power transmission becomes completely different from a DC circuit. Skin effect describes the tendency of an alternating electric current to become unevenly distributed within a conductor, where the current density is largest near the surface of the conductor, and decreases with greater depth in the conductor. This indicates electric current is mostly conducted in the surface layer of the conductor, while most part of the bulk conductor does not contribute to current conduction. Skin depth σ can be calculated by equation:

$$\sigma = \sqrt{\frac{2\rho}{\omega\mu}}, \tag{3-2}$$

where ρ is the resistivity of the conductor, ω is the angular frequency of the current, and μ is the absolute magnetic permeability of the conductor. Skin depth value of commonly used metals at 2.45 GHz can be calculated:

Aluminum $\rho = 2.82 \times 10^{-8}\Omega \cdot \mathrm{m}$ thus $\sigma = 1.71\ \mu m$
Gold $\rho = 2.44 \times 10^{-8}\Omega \cdot \mathrm{m}$ thus $\sigma = 1.59\ \mu m$
Copper $\rho = 1.68 \times 10^{-8}\Omega \cdot \mathrm{m}$ thus $\sigma = 1.32\ \mu m$
Silver $\rho = 1.59 \times 10^{-8}\Omega \cdot \mathrm{m}$ thus $\sigma = 1.28\ \mu m$

By definition, the current density at the skin depth below the surface of the conductor falls to about 37% of total current density. Thus at microwave

frequencies, most of the current flows in an extremely thin layer in the conductor surface with only a few micrometers thick. A material that has smaller skin depth value results in less electric energy loss, thus the bulk cavity is made of copper taking also the cost and manufacturability issue into account. Plating a thin layer of silver on the bulk copper surface can further decrease the energy loss. Because scratches and abrupt structures might cause distortion of local electromagnetic field distribution, the surface of the cavity should be polished smoothly and care has to be taken when inserting tuning elements into the cavity.

3.2.2 Impedance Mismatch When Sustaining Argon Plasma

In microwave theory, the components in a transmission line have a certain impedance value at a certain signal frequency. When the impedance of every component is of the same value, high frequency signal can be transmitted from the source to the load without any reflection. Such zero reflection condition is called impedance well-matched, or a well-tuned microwave system.

In the case of the MIP system at 2.45 GHz frequency, the output impedance of the microwave generator and the characteristic impedance of coaxial connection cable are 50 Ohm. The Beenakker cavity with a burning argon plasma inside has to have 50 Ohm input impedance in order to meet impedance match requirement. Otherwise microwave power will be reflected back to the generator and the degree of reflection depends on the deviation of cavity impedance from 50 Ohm.

The microwave property of an empty resonant cavity is very different to a cavity with a burning plasma inside. The plasma filament inside the cavity absorbs microwave power and change the input impedance of a resonant cavity. A plasma filament in the cavity can be treated as a dielectric material with losses. Plasma characteristic properties like electron density and plasma frequency can be related to the relative permittivity of the plasma [41], which is a complex value. The real part of the relative permittivity causes frequency shift of the resonant cavity. The imaginary part causes dissipation of energy in the plasma medium.

The original Beenakker cavity becomes severely impedance mismatched when there is a burning argon plasma inside, therefore high power reflection takes place thus causing instability in the plasma system.

To understand the influence of a plasma to the microwave characteristics of the Beenakker cavity, a measurement setup is built (see Fig.3-3). The signal generator delivers 2~3 GHz microwave frequency signal to the cavity. A quartz discharge tube with 6 mm outside diameter and 2 mm inside diameter is inserted through the radial center. For ideal measurements, a plasma should be located in the discharge tube and act as the load to the microwave system. However, high power is needed to sustain an atmospheric pressure argon plasma thus it is

impossible to feed the plasma only with the output power from the signal generator. Experimentally we found that a stainless steel metal wire with 1.5 mm diameter and 82 mm length has a microwave absorption behavior, which is similar to that of a real argon plasma under low power conditions. Therefore, this metal wire is used to simulate an argon plasma in microwave characterization measurements. The reflected signal from the Beenakker cavity passes through a circulator and is collected by a network analyzer. The measurement instrument used is a Rohde&Schwarz (ZVL 6, 9 kHz ~ 6 GHz) network analyzer, which incorporates a signal generator, a circulator, and a network analyzer in one instrument.

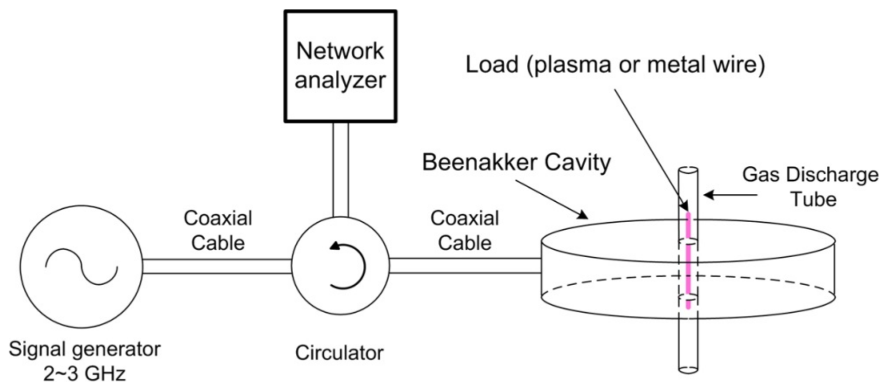

Fig.3-3 Test setup for microwave property characterization of the Beenakker cavity

Because the cavity is designed to resonate at near 2.45 GHz, the network analyzer is expected to detect a resonant characteristic curve when the signal is scanned from 2 GHz to 3 GHz. The scattering parameter S_{11} is plotted to study the resonant behavior of the cavity. By definition,

$$S_{11} = V_{re}/V_{in}, \tag{3-3}$$

where V_{in} and V_{re} are the input and reflected voltage waves, respectively. S_{11} is a complex number that represents the input port voltage refection coefficient. By definition, $|S_{11}| \leq 1$. When $|S_{11}| = 1$, the input signal is totally reflected. When $|S_{11}| = 0$, the input signal is totally transmitted. The unit used to describe $|S_{11}|$ is mU, which stands for milli-units or 1/1000. Power reflection P_{re} as in percentage is related to $|S_{11}|$ through formula,

$$P_{re} = |S_{11}|^2 \times 100, \tag{3-4}$$

Voltage standing wave ratio VSWR_{in} can be used as an efficiency measure for transmission lines in high frequencies. It is related to S_{11} by formula

$$\mathrm{VSWR}_{in} = \frac{1+|S_{11}|}{1-|S_{11}|}, \tag{3-5}$$

where $\mathrm{VSWR}_{in} = 1$ denotes critical matching and $\mathrm{VSWR}_{in} = \infty$ represents complete reflection. In this thesis, $|S_{11}|$ and power reflection will be used to describe the coupling condition of the microwave system. Table 3-1 shows some representative P_{re} values according to different $|S_{11}|$ values.

Table 3-1 S_{11} values and corresponding power reflection values

$\|S_{11}\|$ value (mU)	1000	700	500	300	100	70	0
Power reflection (%)	100	49	25	9	1	0.49	0

A. Influence of the coupling loop inside an empty original Beenakker cavity

The coupling loop that connects the coaxial connector to the inside of Beenakker cavity couples microwave signal from outside into the cavity. (For reference of coupling loop location, refer to Fig.3.1-right.) The position where this coupling loop is connected to the bottom lid of cavity may influence the microwave property of the cavity. Experiments are conducted to evaluate the influence of the coupling loop location to $|S_{11}|$ parameter of an empty Beenakker cavity. An original Beenakker cavity without load (no metal wire or plasma inside) is measured as in Fig.3-3 configuration.

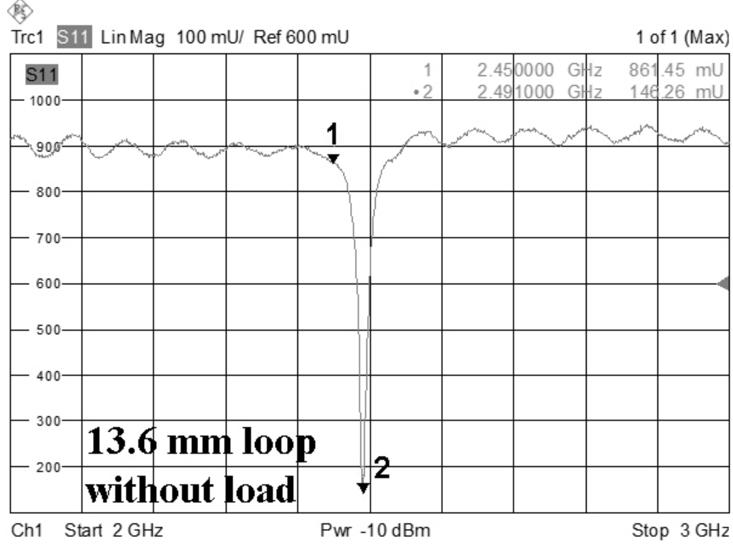

Fig.3-4 S_{11} parameter of an empty original Beenakker cavity with a 13.6 mm coupling loop (Marker 1 & 2 pointing at 2.45 GHz & 2.491 GHz, respectively)

The first measurement is when the coupling loop is connected at 13.6 mm far from the radial edge of the cavity. Fig.3-4 shows the $|S_{11}|$ parameter measured. The horizontal axis is the signal frequency, which is scanned from 2 GHz to 3 GHz. The vertical axis is the S_{11} scattering parameter. The cavity has an inner diameter of 92.5 mm, which corresponds to a resonant frequency of 2.484 GHz through calculation. The measured $|S_{11}|$ parameter shows a sharp resonance curve that centers at 2.491 GHz (Marker 2 in the graph). The calculated resonant frequency differs from the measured value by 0.007 GHz. This difference is most likely due to the influence of coupling loop insertion inside the empty cavity, which makes the effective inside diameter of the cavity smaller. The corresponding Smith chart measured under the same condition is plotted in Fig.3-5.

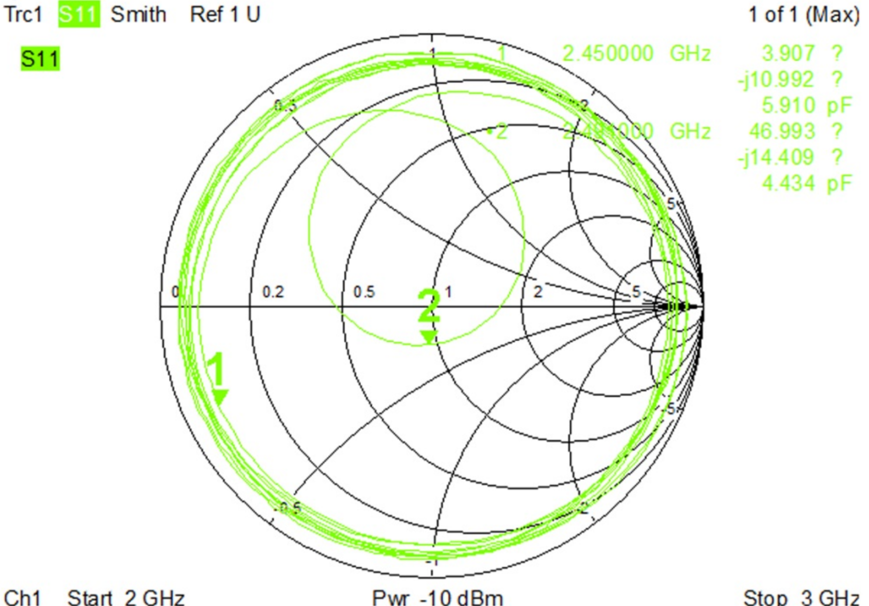

Fig.3-5 Smith chart of an empty Beenakker cavity with a 13.6 mm coupling loop (Marker 1 & 2 pointing at 2.45 GHz & 2.491 GHz, respectively)

When the coupling loop connection location is varied, the resonant frequency of the cavity shifts accordingly. When the loop location is at 14.7 mm and 16 mm far from the radial edge of the cavity, the resonant frequency decreased to 2.488 GHz and 2.481 GHz respectively (see Fig.3-6 and Fig.3-7).

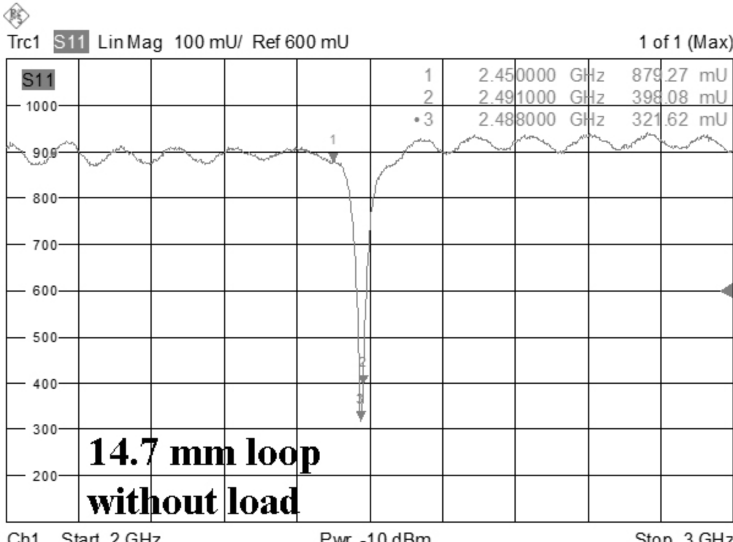

Fig.3-6 S_{11} parameter of an empty original Beenakker cavity with a 14.7 mm coupling loop (Marker 3 pointing at 2.488 GHz)

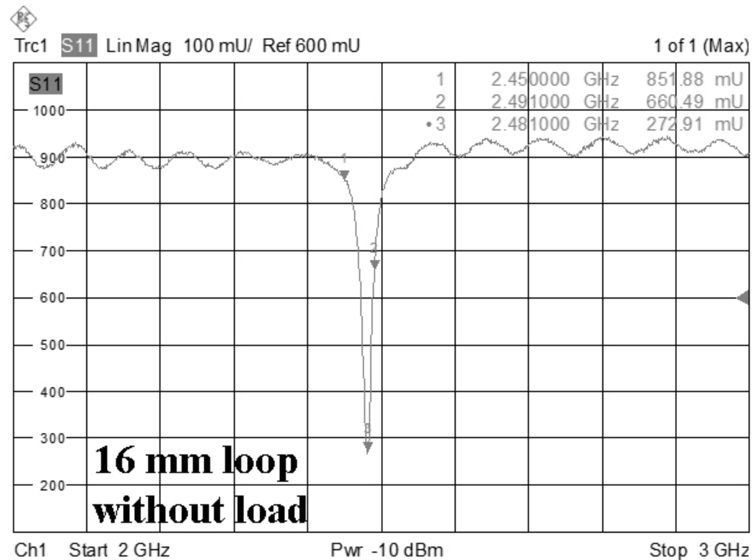

Fig.3-7 S_{11} parameter of an empty original Beenakker cavity with a 16 mm coupling loop (Marker 3 pointing at 2.481 GHz)

The position where the coupling loop connects with the cavity determines the inductive coupling area, therefore influences the microwave property of the Beenakker cavity. Experimentally we found that increasing the coupling loop location from the radial edge of the cavity result in a decrease in empty cavity resonant frequency.

B. Influence of plasma loading to an empty Beenakker cavity

Electrons in the plasma influence the electromagnetic field distribution inside a resonant cavity. Therefore, the presence of a plasma filament distorts an empty cavity's resonant structure. Depending on the electron density n_e and electron collision frequency ω_p of a specific plasma, the resonant frequency of a cavity with a plasma inside may shift away from the empty cavity scenario and the quality factor Q of the cavity is also expected to change. The perturbation theory relates the shift in resonant frequency $\Delta\omega$ of a resonant cavity to the complex plasma conductivity σ through equation [42, 43]:

$$\frac{\Delta\omega}{\omega} = \frac{j}{2\omega\epsilon_0}\left(\frac{\int \sigma {E_0}^2 dv}{\int {E_0}^2 dv}\right), \tag{3-6}$$

where E_0 is the electric field in the absence of a plasma, ω is the resonant frequency of an empty cavity. The real part of Eq. (3-3) gives the change in the resonant frequency of the cavity caused by plasma, while twice the imaginary part of Eq. (3-3) gives the change in the $1/Q$ value of the cavity. Solving Maxwell's equations with boundary conditions yield solutions to TM_{010} mode cavity with plasma conditions, thus the resonant frequency, quality factor, and electromagnetic field distribution of the TM_{010} mode cavity can be estimated [44-47]. A limitation of using perturbation theory for measurement is that the plasma to be measured has to be inside the cavity, otherwise the leakage fields near the opening holes in the radial center of the cavity will cause invalid calculations.

In general, the presence of a plasma inside a resonant cavity will increase the resonant frequency of the cavity because the dielectric coefficient of plasma is less than unity [48]. In the meantime, the presence of a plasma absorbs microwave signals around the resonant frequency, thus reduces the quality factor of the cavity (see Fig.3-8).

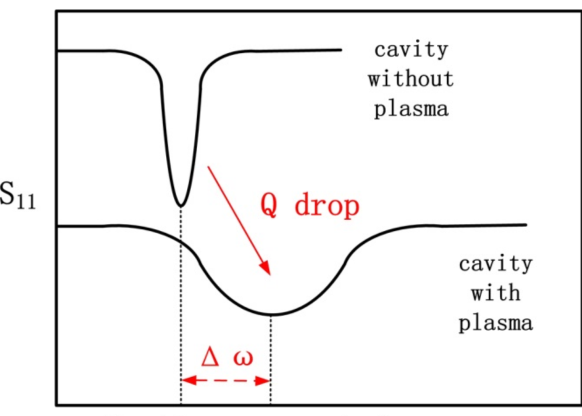

Fig.3-8 Schematic representation of the effect of plasma on cavity microwave characteristics

Load (atmospheric pressure argon plasma)
>50% power reflection
Original Beenakker Cavity
Gas Discharge Tube
Coaxial Cable
Power generator 2.45 GHz

Fig.3-9 Schematic representation of the MIP setup with original Beenakker cavity that results in high power refection under argon plasma operations

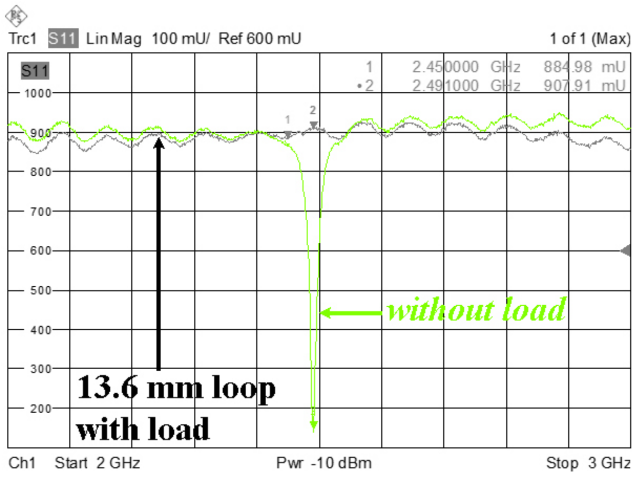

Fig.3-10 S_{11} parameter of an original Beenakker cavity with a metal wire as load, the resonance feature disappeared. (S_{11} curve measured when no load is present in the empty cavity as shown in Fig.3-4 is replotted here for comparison.)

Experimentally (see Fig.3-9 for test setup), we found that the MIP system suffers from more than 50% power reflection when directly connecting the microwave power generator to the original Beenakker cavity with a burning argon plasma inside, which is due to the severe impedance mismatch at 2.45 GHz.

Characterization measurements of the original Beenakker cavity with a metal wire inside are made to simulate the influence of a plasma (measurement setup shown in Fig.3-3 is used). The resonance characteristic curve once a metal wire is inserted into the cavity is entirely different (see Fig.3-10). Although the metal wire (1.5 mm diameter, 80 mm long, steel) insertion does not represent the exact condition of an argon plasma insertion, it does give an idea from spectrum analysis that the original Beenakker cavity becomes severely detuned when an atmospheric pressure argon plasma is present inside the cavity.

3.2.3 Solutions to Impedance Mismatch and Literature Study

In microwave power coupling, the MIP system can be considered as a high frequency circuit. In order to reach good impedance matching in which 0% of power is reflected, there are two parameters that need to meet the requirement.

The first requirement relates to frequency, which requires the resonant frequency of the cavity with an argon plasma has to be equal to the output frequency of the power generator (2.45 GHz). To tune the resonant frequency of the Beenakker cavity, one method is to insert dielectric materials with low loss into the cavity. The resonant frequency of the cavity decreases when dielectric material is inserted, thus this one-direction tuning method requires the cavity to be designed to have a higher resonant frequency. An alternative method is to use a frequency-variable generator. By changing the output frequency of the generator, frequency tuning can be achieved. Such kind of variable frequency generator is only available recently on the market and the tuning range is still limited.

The second requirement relates to impedance, which requires the input impedance of the Beenakker cavity with an argon plasma has to be equal to the characteristic impedance of the coaxial cable (50 Ohm at 2.45 GHz). Impedance matching of the Beenakker cavity can be achieved by two ways. One is external tuning, which is to use external tuners to match the system. Another way is internal tuning, which is redesigning the coupling antenna. Internal tuning in principle is to incorporate a tuner into the cavity, it gives better tuning range and much more stable plasma compared to external tuning. Tuning is often done experimentally and once an optimal condition is reached, the tuning parts are fixed. Both external and internal tuning are in theory the same principle, which is varying the corresponding capacitance and/or inductance values of the load impedance by changing the physical position of the tuning elements [49].

Different modifications of the original Beenakker cavity have been proposed by several researchers. Deutsch et al.[50], Zander et al.[51], and Bollo-Kamara et al.[52] placed an external double stub tuner between the microwave power generator and the original Beenakker cavity. Microwave coupling is made by tuning the stubs on the external tuner, while the metal tuning screws on the Beenakker cavity were not used. Such configuration is comparatively easier to implement as double stub tuners are commercially available. Because external tuning is used, there is expected to be power loss in the double stub tuners thus reducing the amount of actual power that is delivered to the plasma. Overheating damage to double stub tuners may take place, which shortens the lifetime of tuners and makes tuning erratic [53, 54]. Modern industrial plasma etchers normally adopt computer controlled self-adjusting external tuning and special cooling elements to maintain good microwave coupling of the system.

Rait et al.[53] replaced the fixed coupling loop in the original cavity with a movable one. Optimal loop position is determined experimentally and dielectric material tubes are used to tune the resonant frequency of the cavity. Power reflection can be reduced to 6-8 W under 50 W forward power level.

Haas el al.[54] and Michlewicz el al.[55] connected two adjustable tuning stubs with the original inductive coupling loop inside the cavity. Such configuration is like adding an internal double stub tuner onto the original Beenakker cavity. They claim 0 W power reflection can be achieved by varying the tuning stub positions.

Van Dalen et al.[56] and Forbes et al.[37] removed the original inductive coupling loop and connected a side arm taken from the ¼ wave Evenson cavity to the upper lid of the original Beenakker cavity. Variable capacitive coupling can be achieved by adjusting the penetration depth of the antenna rod. Quartz tuning rods are inserted into the cavity to tune the resonant frequency. Reflected power can be maintained below 1 W under experimental conditions.

Matus et al.[57] adopted a different approach in capacitive coupling, where a sliding antenna coupling probe is clamped on to the lid of the original Beenakker cavity. Quartz tuning rods are also used to tune the resonant frequency. Low power reflection is achieved under 13-15 W forward power level.

From literature study, the impedance mismatch problem when using the original Beenakker cavity is well recognized and can be solved by adding either external or internal tuning elements. However, all the proposed redesigns need complex engineering and addition of bulk microwave components into the system. Although microwave power reflection can be decreased, the additional components are likely to consume microwave power thus the increase in overall power efficiency of the modified MIP systems is limited.

3.2.4 Modifications to Solve Impedance Mismatch

In order to achieve good impedance matching when an atmospheric pressure argon plasma is present inside the Beenakker cavity, the empty cavity must be intentionally designed detuned. To find the optimal solution to the microwave coupling problem by making the slightest change to the original cavity, great effort has been made on modifying the internal structures of the original Beenakker cavity.

The coupling loop that connects the coaxial connector on the cavity to the inner surface of the cavity is found to be the most critical. The structure and position of the loop determines local electromagnetic field distribution, hence influences the field interaction with the argon plasma filament. Modifications of the original

coupling loop significantly change the cavity's resonant behavior with and without the presence of a burning plasma.

We achieved the best results by a redesigned coupling loop by adding a variable antenna onto the original coupling loop inside the cavity. With the modification, power reflection in the MIP system is decreased from originally 50% to almost 0% when sustaining argon plasma. Characterization measurements of the redesigned coupling loop are made under different conditions. Measurements with empty cavity and cavity with metal wire insertion used the setup as displayed in Fig.3-3. Measurements with argon plasma present used the microwave power generator.

A. Spectrum analysis

The empty Beenakker cavity with a redesigned coupling loop behaves completely different to the original cavity with original coupling loop (see Fig.3-14). The resonant peak near 2.49 GHz is missing when coupling loop modification is adopted, which indicates the empty cavity becomes significantly detuned from its original resonant characteristics.

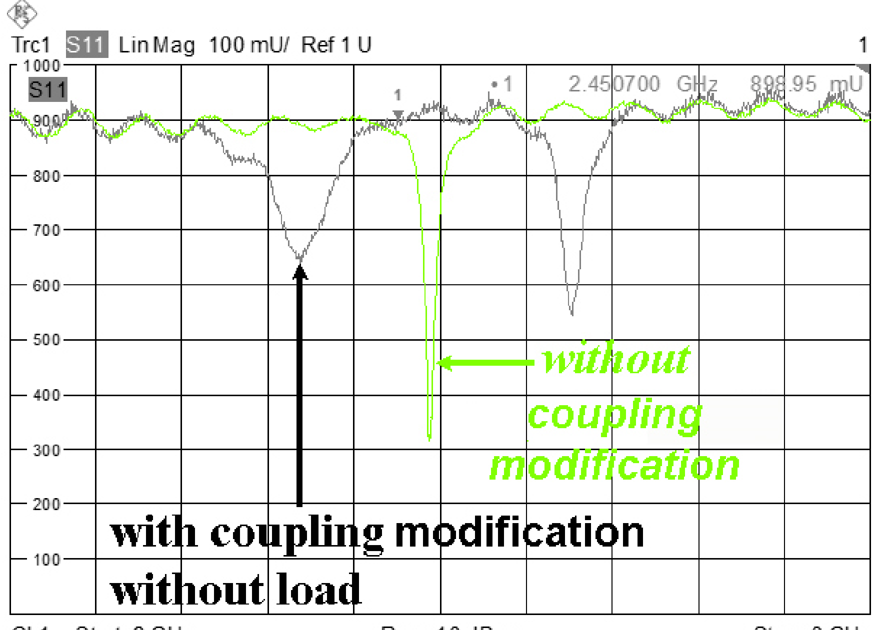

Fig. 3-14 S_{11} parameter of an empty Beenakker cavity with coupling modification. (S_{11} curve measured without coupling modification as shown in Fig.3-4 is re-plotted here for comparison. Without coupling modification, empty cavity resonates at 2.49 GHz)

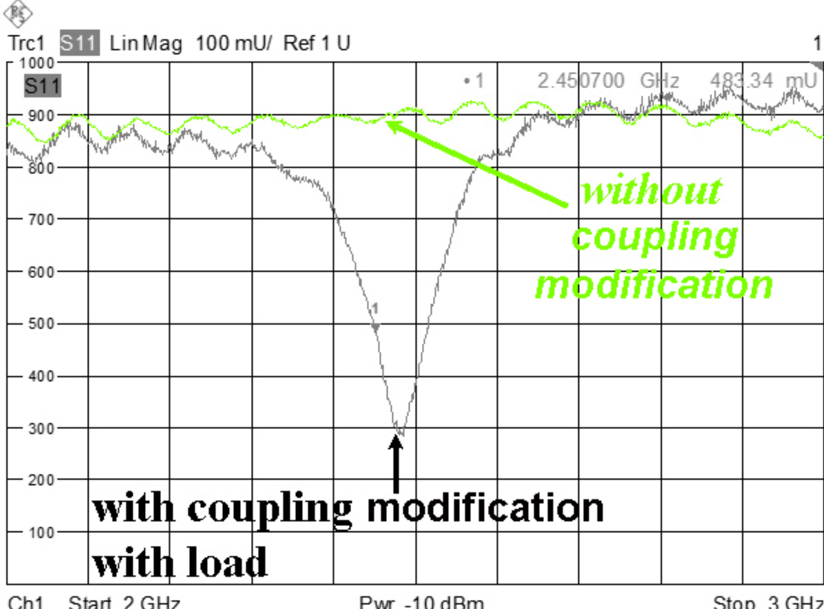

Fig. 3-15 S_{11} parameter of a Beenakker cavity with coupling modification and a metal wire inserted as load. Cavity show strong resonance near 2.45 GHz. (S_{11} curve measured without coupling modification as shown in Fig.3-10 is re-plotted here for comparison.)

With a metal wire inserted as loading material in the cavity, the characteristic of the Beenakker cavity with coupling loop modification is shown in Fig.3-15. The loaded cavity with coupling modification showed a strong resonance near 2.45 GHz, with a peak S_{11} value of 300 mU that translates to 9 % power reflection. Although metal wire does not fully represent the condition of a plasma, it clearly shows the coupling efficiency has been significantly improved by redesigning the original coupling loop.

The original Beenakker cavity is well-tuned for empty and helium plasma condition, but it becomes detuned for argon plasma condition. The coupling modification leads to a detuned cavity under empty condition, but a well-tuned cavity under argon plasma condition.

B. Reflection power analysis under plasma loading

Experiments are also performed under burning plasma conditions (see Fig.3-16 for setup), with constant 50 W input microwave power and 1400 sccm argon gas flow rate. Power reflection in watts is measured by the microwave generator and the percentage of power reflection is calculated. Fig.3-17 shows the coupling loop modification structure variation in one direction and the resulting change in power reflection percentage. A slight change in coupling modification structure results in dramatic variation in the overall power reflection in the microwave system. It is possible to achieve 0 % power reflection by fine tuning the variable antenna that we added onto the original coupling loop.

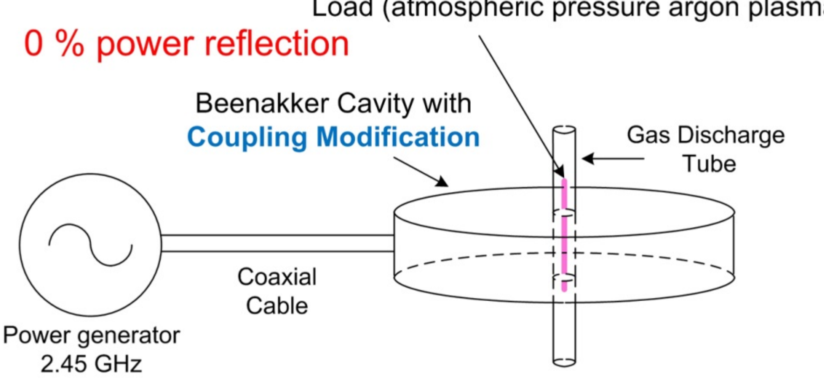

Fig.3-16 Schematic representation of the MIP setup with coupling modification that results in low power refection when sustaining argon plasma

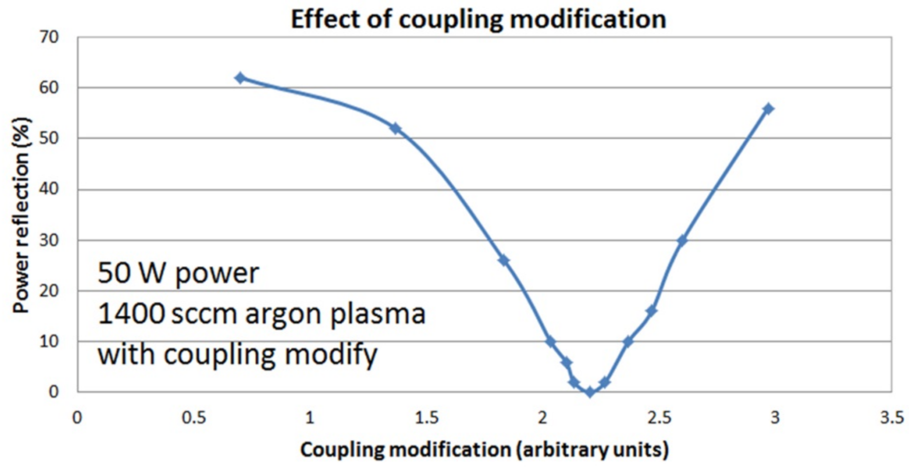

Fig.3-17 Power reflection versus the variable antenna position

The variable antenna that works as modification element on the original coupling loop acts as a tuner inside the resonant cavity, the structure and position of the variable antenna varies the equivalent impedance of the Beenakker cavity with a burning atmospheric pressure argon plasma inside. On the Smith Chart, a well-designed coupling modification should bring the input impedance as seen by the microwave generator from an off-center point to the 50 Ohm pure resistive center point, where impedance matching is achieved. The effect of the variable antenna is equivalent to the tuning stubs in an external stub tuner, which is seen as an LC tuning element in a microwave circuit.

The efficiency of the coupling modification design is further evaluated through comparison experiments with burning argon plasma conditions (see Table 3-2). Three different microwave system configurations are tested and compared. When directly connecting the original Beenakker cavity to the power generator, high power reflection (60%) is observed due to the severe impedance mismatch. When adding an external double slug tuner between the original Beenakker cavity and the power generator, tuning can be improved and power reflection is reduced to 10%. However, at higher power levels the external tuner becomes heated and tuning becomes erratic. When directly connecting the Beenakker cavity after coupling modification to the power generator, the 0% power reflection can be achieved. The plasma filament length is a good indicator of the absorbed microwave power in plasma, where the filament is longest under the modified cavity condition.

Table 3-2 Effect of coupling modification in the original Beenakker cavity

	Original cavity	Original cavity +external tuner	Cavity after coupling modification
External tuner	No	Yes	No
Coupling modification	No	No	Yes
Power input (W)	20	20	20
Power reflection (W)	12	2	0
Power reflection (%)	60	10	0
Filament length (cm)	0.3	1.0	1.4
Image of argon plasma (1400 sccm)			

Once tuning is made by the coupling modification element inside the cavity, no further adjustments are needed. The argon plasma is stable in all power ranges with a suitable-sized discharge tube (see Table 3-3). Power reflection can be maintained at less than 5% with input power levels from 10 to 100 W.

Compared to the internal coupling solutions proposed by other researchers as discussed in Section 3.2.3, the internal coupling antenna modification we proposed provides even better impedance matching performance by making the slightest change to the original cavity. As the tuning element used in our solution is comparatively much smaller in dimensions and does not contain tuning stubs, higher overall system power efficiency is expected.

A limitation of our coupling solution is the inconvenience to tune the cavity during plasma operation, for example when adding etchant gas into the argon plasma which will be discussed in Section 3.2.5. A further improvement that solves this tuning problem by widening the cavity's process window will be proposed in Section 3.2.6.

Table 3-3 Plasma sustained by the Beenakker cavity with coupling modification

	Condition 1	Condition 2	Condition 3	Condition 4
Input power (W)	20	30	40	50
Power reflection (W)	0	1	2	2
Filament length (cm)	1.4	2.3	2.8	3.2
Image of argon plasma (1400 sccm)				

3.2.5 Influence of Etchant Gas Addition

The addition of etchant gas like O_2 and CF_4 containing electronegative elements into the argon plasma consumes free electrons in the plasma, therefore reducing the electron density and change the microwave property of the plasma. A well-matched Beenakker cavity with argon plasma becomes mismatched once etchant

gas is added. When more etchant gas is added, the plasma dims and power reflection increases. Upon reaching the upper limit of etchant gas addition amount, the plasma extinguishes as the electrons generated are less in number than the electrons consumed at the same time. The dimming and extinguishing of the plasma is probably due to low threshold for the dissociation of O_2 and CF_4 and the electron negative character of its constituents.

A set of experiments is conducted to evaluate the effect of etchant gas addition to the degree of detuning of the cavity. A Beenakker cavity with coupling modification as discussed in Section 3.2.4 is used. The cavity is well-matched for argon plasma conditions and results in 0 W power reflection under 40 W input power with 1400 sccm argon gas flow rate at 2.45 GHz (see Fig.3-18.a).

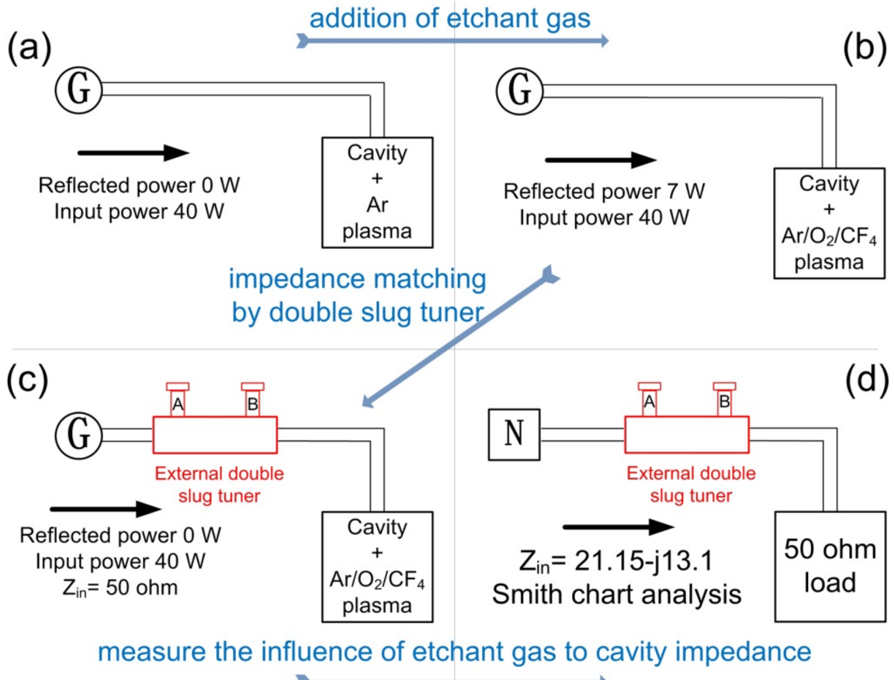

Fig.3-18 Schematic representation of the measurement of etchant gas influence to the microwave property of Beenakker cavity. (a) generator connected to cavity with Ar plasma (b) generator connected to cavity with $Ar/O_2/CF_4$ plasma, (c) an external tuner is added between generator and cavity to correct the impedance mismatch, (d) Network analyzer is connected to the tuner terminated by a 50 Ohm load for Smith chart analysis (block letters G and N denote microwave power generator and network analyzer, respectively)

The addition of etchant gas detunes the cavity and causes a power reflection increase to 7 W just before that the plasma extinguishes (see Fig.3-18.b). An external double slug tuner is added to correct the impedance mismatch caused by O_2/CF_4 etchant gas and to retune the microwave system back to impedance matching with 0 W power reflection (see Fig.3-18.c). Thus, the detuning of cavity caused by etchant gas addition is compensated by the external tuner. A network analyzer is then connected to measure the tuner, which is terminated by a 50 Ohm load (see Fig.3-18.d). The S_{11} parameter and Smith chart are then measured by the network analyzer.

The Smith chart analysis is shown in Fig.3-19. After modification on the original coupling loop, the Beenakker cavity with a burning argon plasma results in 50 Ohm input impedance as seen by the power generator (central point on Smith chart). The addition of etchant gas in the argon plasma shifts this point to an off-center point causing impedance mismatch. The insertion and tuning of the double slug tuner corrects this mismatch caused by etchant gas addition, and brings the cavity impedance back to the central 50 Ohm point. The tuning effect of the double slug tuner to a 50 Ohm load changes the equivalent impedance to $Z_t = 21.3 - j12.54$ and is marked by the arrow in Fig.3-19. The input impedance when etchant gas detunes the cavity $Z_{etchant}$ equals to the conjugate value of Z_t, $Z_{etchant} = Z_t^* = 21.3 + j12.54$. The addition of etchant gas shifts the input impedance of the cavity with a burning plasma from 50 Ohm to 21.3+j12.54 Ohm, thus causing impedance mismatch and high power reflection.

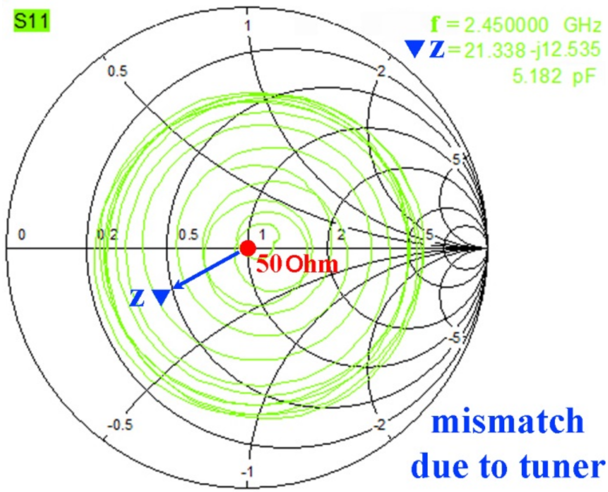

Fig.3-19 Smith chart of the double slug tuner terminated by 50 Ohm load. Marker Z is the measured impedance value of the tuner with load, where impedance Z is 21.3-j12.54 Ohm at 2.45 GHz. Numbers on the chart denotes normalized impedance values. Central point represents 50 Ohm impedance where impedance matching position is located.

3.2.6 Modifications to Broaden the Stable Plasma Operation Range

When etchant gas is added to the argon plasma, the reflected power increases drastically and the plasma in the Beenakker cavity becomes unstable. This phenomena result in a narrow process window that allows only a very limited amount of etchant gas to be added in the argon plasma. In MIP etching experiments, it is found that the amount of etchant gas has to exceed certain values to achieve satisfying etching rates under low input power levels. Thus, the challenge is to broaden the process window or to reduce the susceptibility of the Beenakker cavity sustained argon plasma to etchant gas addition.

In microwave engineering, the quality factor Q describes the resonant cavity's bandwidth relative to its center frequency. Higher Q value indicates that the cavity has more selectivity, but would be more difficult to tune. The original Beenakker cavity has a high Q value and thus has high susceptibility to detuning by etchant gas addition. The presence of an argon plasma decrease the Q value of the cavity, yet obviously, the Q value is still too high for etching applications.

The solution to decrease the Q value of the Beenakker cavity without jeopardizing the cavity's microwave power efficiency is achieved by adding another modification component. The process window can be dramatically enlarged, which enables stable plasma operation with high amount of etchant gas addition under low input microwave power levels. The Beenakker cavity after process window modification can be directly connected to the power generator and no external microwave components are needed (see Fig.3-20). The Beenakker cavity with both coupling modification and process window modification results in 0~10% low power reflection with a large process window, while no further tuning is needed during different plasma operation conditions.

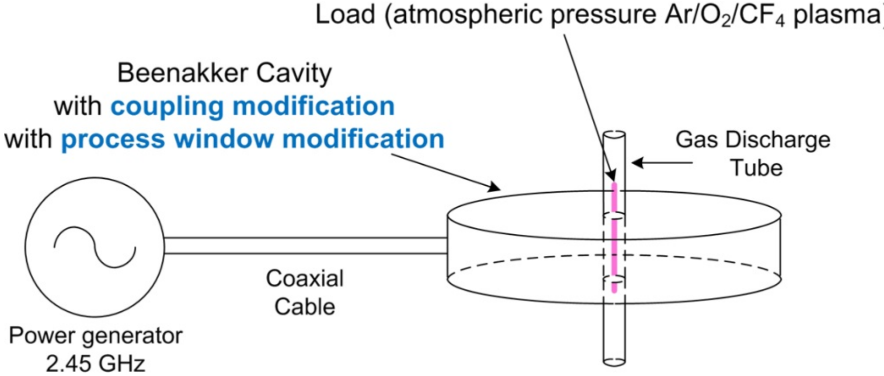

Fig.3-20 Schematic representation of the MIP setup with coupling modification and process window modification.

A. Spectrum analysis

The effect of the process window modification can be explained through analyzing the S_{11} parameter. Fig.3-21 shows for an empty Beenakker cavity, the resonance spectrum broadened when process window modification is applied. Similarly, a loaded Beenakker cavity that adopted the process window modification shows a broadening in the original resonant spectrum (see Fig.3-22). The cavity's bandwidth increased, resulting in a decreasing *Q* value thus indicates a reduction in susceptibility to frequency variation. The detuning effect when etchant gas is added into argon plasma becomes less influential after implementing the process window modification inside the Beenakker cavity.

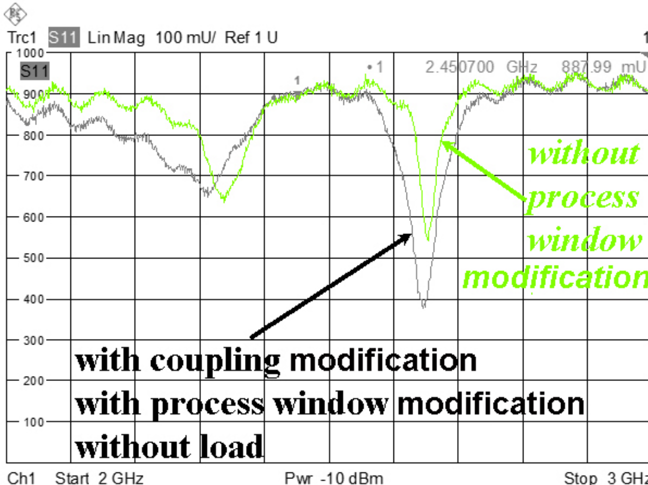

Fig.3-21 S_{11} parameter of an empty Beenakker cavity with process window modification. (S_{11} curve measured without process window modification as shown in Fig.3-14 is re-plotted here for comparison.)

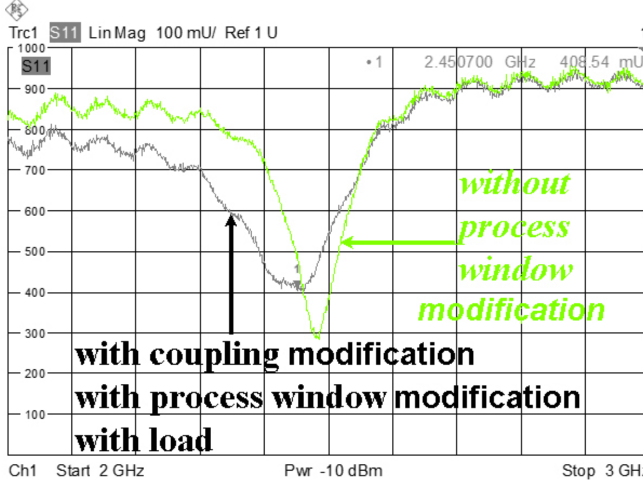

Fig.3-22 S_{11} parameter of a Beenakker cavity with process window modification and with metal wire as load. (S_{11} curve measured without process window modification as shown in Fig.3-15 is re-plotted here for comparison.)

B. Plasma operation process window analysis

In macroscopic analysis, the change in process window is evaluated by measuring the power reflection due to etchant gas addition before and after process window modification is implemented. A microwave power generator is directly connected to the Beenakker cavity, delivering constant 40 W microwave power at 2.45 GHz. Argon plasma with constant 1400 sccm gas flow is generated in an alumina discharge tube through the cavity. O_2 and CF_4 etchant gas are added into the argon plasma with increasing amount, causing an increase in power reflection due to their detuning effect. The plasma becomes unstable when power reflection reaches 20%. At more than 25% power reflection, plasma will extinguish.

The Beenakker cavity without process window modification shows a narrow process window (see Fig.3-23), allowing a maximum of 24 sccm pure O_2 addition or 10 sccm pure CF_4 addition before plasma extinguishes. The stable plasma operation area is defined as the area that power reflection value is less than 25 %, the area is in arbitrary unites (a.u.). The larger the stable operation area value the larger the plasma process window. The same amount of CF_4 addition induces more detuning of the cavity compared to O_2 addition. This difference is most likely due to the fact that fluorine is more electron negative than oxygen.

The process window of the Beenakker cavity can be greatly broadened after adopting the process window modification design (see Fig.3-24), allowing more than 48 sccm pure O_2 addition or 18 sccm pure CF_4 addition without extinguishing the plasma. This improvement in process window is correlated to the broadening effect of the cavity's resonance spectrum, which is principally accredited to the modification design. The stable and large process window allows a variety of etching recipes with different etchant gas combinations to be developed for later plasma etching applications. At 40 W input power, a plasma can be operated stably with an argon flux of 1400 sccm and with 4% molecular oxygen admixture.

For comparison, the process window of a different type of plasma generator, named Surfatron [58-60], is also evaluated under the same operation condition. Fig.3-25 shows the process window of Surfatron. By comparing the stable plasma operation area, the process window of the Beenakker cavity with process window modification (512 a.u.) outperforms that of the Surfatron (352 a.u.) and the original cavity (120 a.u.).

Therefore, the Beenakker cavity with both coupling modification (proposed in section 3.2.4) and process window modification is used as the plasma generator in MIP decapsulation system due to its superior performance and suitability for this application.

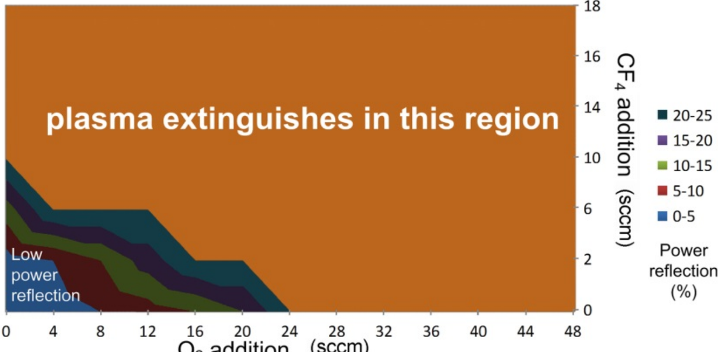

Fig.3-23 Process window of the Beenakker cavity without process window modification (stable operation area = 120 arbitrary unit)

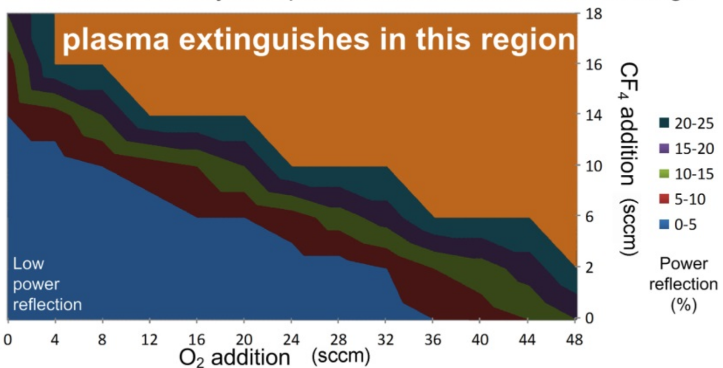

Fig.3-24 Process window of the Beenakker cavity with process window modification (stable operation area = 512 arbitrary unit)

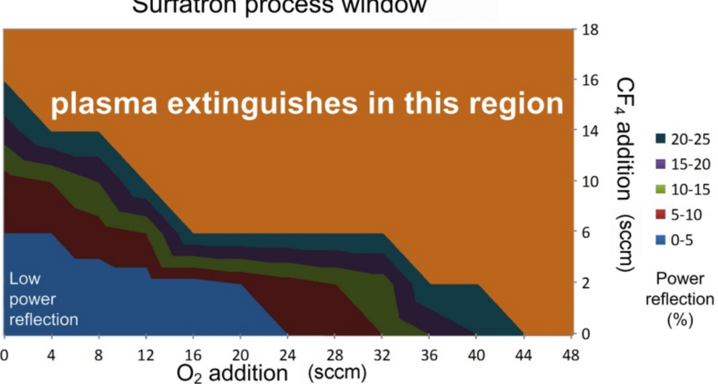

Fig.3-25 Process window of a surfatron plasma source (stable operation area = 352 arbitrary unit)

3.3 Frequency Tuning

A. Influence of dielectric material insertion

The insertion of dielectric materials varies the resonant behavior of the Beenakker cavity. Literature has shown that the volume of inserted dielectric material as well as its position in the cavity causes a shift in the cavity's resonant frequency [52, 56]. From microwave measurements on an empty original design Beenakker cavity, it is found that the complete insertion of a quartz rod (4 mm o.d., 10 cm long) from radial direction induces a -48 MHz shift to the cavity's resonant frequency (see Fig.3-26). Because dielectric materials do not absorb microwave power, quartz rods can be used as a tuning element to aid the impedance matching of the Beenakker cavity. However, tuning by dielectric material can only be done in one direction as no dielectric materials with dielectric constant less than one are available. In practice, it is found that frequency tuning by quartz rods provides only a limited influence thus cannot solve the impedance mismatch problem with the original cavity.

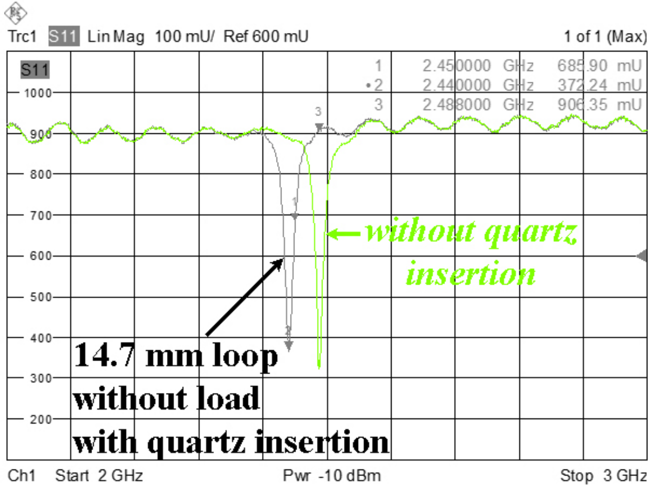

Fig.3-26 S_{11} parameter of an empty original Beenakker cavity with and without quartz rod (4 mm diameter, 10 cm long) insertion

B. Frequency tuning by the power generator

An alternative way to tune the frequency of the microwave system is to change its power source frequency. Instead of changing the resonant frequency of the Beenakker cavity, the output frequency of the microwave power generator may be changed so it could be equal to the cavity's resonant frequency. However, such types of variable frequency microwave power generator are only available on market very recently and their frequency tuning range is limited.

The capability of frequency tuning by the generator is demonstrated by the measurement graph shown in Fig.3-27. In this experiment, a Beenakker cavity with coupling modification is used. Process window modification is not used in order to demonstrate the influence of frequency tuning. An argon plasma is generated and CF_4 etchant gas is then added into the plasma to cause detuning of the cavity. The intensity of detuning is measured by the percentage of input power that gets reflected. The output frequency of the generator (Sairem solid-state) is varied from 2430 MHz to 2470 MHz, while the power level is kept at constant. The power reflection surface in the graph varies with both CF_4 amount and generator frequency. In practice it is possible to use a variable frequency generator to aid the impedance matching of the original Beenakker cavity. However, the tuning range and the magnitude of tuning effect are still limited.

For stable $Ar/O_2/CF_4$ plasma operations, the best solution is to use the original Beenakker cavity with both coupling modification and process window modification. Frequency tuning by the microwave generator is only used as a fine tuning method with a maximum influence of 5% power reflection.

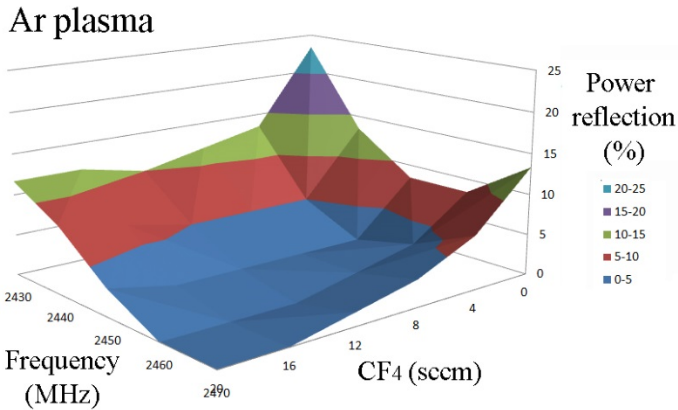

Fig.3-27 Influence of frequency tuning by the microwave power generator to an Ar/CF_4-plasma-containing Beenakker cavity without process window modification.

3.4 Filamentation of Plasma

The atmospheric pressure argon plasma generated in MIP setup appears as a long filament inside the discharge tube. There is an upper limit on the radius of a plasma filament generated by microwave power under atmospheric pressure due to skin effect. The skin effect limits the penetration of radio frequency electric field in a conductor. The penetration depth of electric field in the plasma is given by [61]

$$\delta_c = \sqrt{\frac{2}{\sigma\omega\mu_0}}\,, \tag{3-7}$$

where μ_0 is the permittivity of vacuum, ω is the wave angular frequency, and σ is the conductivity of plasma. At atmospheric pressure, the conductivity of plasma can be expressed as [62]

$$\sigma = \frac{n_e e^2}{m_e}\frac{1}{v_m^{eff} + j\omega}, \tag{3-8}$$

where n_e is the electron density, m_e is the electron rest mass, v_m^{eff} is the effective collision frequency. The tendency of filament formation is increased with higher field frequency, higher absorbed microwave power level, and larger discharge tube inner diameter [63].

The appearance of the filament of an argon plasma sustained by 2.45 GHz microwave with different input power levels is summarized in Table 3-4. The argon gas flow rate is kept at 800 sccm. A quartz tube with 6 mm outer diameter and 4 mm inner diameter is used as the discharge tube. At stage 1, the plasma is sustained at low input power level. Only one stable plasma filament is present in the tube. The filament does not fill up the whole tube, instead it is located close to the tube wall filling up half of the tube. At stage 2, with increasing input power level to 47 W, the plasma becomes unstable and transition from one filament to two filaments takes place. At stage 3, plasma splits into two stable filaments when input power levels become higher than the transition power. The length of the two filaments could be the same or different under different input power levels, indicating the power dissipation in each of the filaments. Both filaments are located close to the tube wall, rather than in the center of the tube.

Table 3-4. Filament formation in argon plasma

	Stage 1	Stage 2	Stage 3
Description	One stable filament	Transition to two filaments	Two stable filaments
Input power	Low, < 40 W	Mid, 47 W	High, > 55 W
Image of the plasma filament			

For optimum control of the plasma etching process, it is advisable to have only one stable plasma filament located in the center of the tube. In order to achieve this, experiments on filament formation under different conditions are conducted. It is found that a discharge tube with larger inner diameter sustaining a plasma with lower argon flow rate tends to have multiple plasma filaments more easily under the same input power level. A discharge tube with 1.2 mm inner diameter is chosen at last to ensure there is only one stable plasma filament present in the center of the discharge tube at input power levels below 100 W. Discharge tubes with inner diameters smaller than 1.2 mm can still sustain stable single-filament argon plasma. However, using a discharge tube with a smaller inner diameter will result in a smaller plasma etching area and higher heat dissipation from the plasma to tube. Both effects hinder the efficiency of plasma etching.

Large area uniform plasma etching does not necessarily require a uniform plasma. An alternative solution to generate large area stable MIP in one gas discharge tube is to have multiple holes in the tube each with 1.2 mm inner diameter. Multiple separately confined stable MIP filaments could induce multiplication of the overall MIP afterglow etching efficiency. However, through experiments it is found that no matter how many holes are there in the discharge tube, there is only one single stable plasma filament in a certain hole. It seems impossible to generate multiple plasma filaments in each and every hole under the current MIP system configuration. The major reason is difficulty to uniformly distribute power in each plasma filament.

3.5 Power Efficiency of the MIP System

In the MIP system, microwave power is delivered from the power generator through several microwave components to feed the plasma. Although many researchers have investigated how to reduce power reflection in the MIP system, no one has evaluated the power efficiency of the MIP system. However, it is important to analyze the power dissipation path to evaluate the overall efficiency of the MIP system. In other words, what is the percentage of output power from the generator that is actually consumed by the plasma itself?

A well-matched MIP system results in almost 0% power reflection when a plasma is present inside the modified Beenakker cavity. However, this only indicates that no microwave power is reflected back to the generator, and does not mean that all the microwave power from the power generator is absorbed by the plasma. Several paths of power dissipation have to be examined: loss in coaxial cable, loss in Beenakker cavity, loss in microwave stray field, and loss in plasma.

The aims of analyzing the power efficiency of the MIP system are:

1. Maximize the percentage of microwave power delivered to the plasma.
2. Suggest requirements on microwave components for commercial product MIP instrument manufacturing. So that each instrument built will have the same power efficiency and consistent etching performance.

A. Power loss in transmission line

To evaluate the power loss in coaxial cable, double slug tuner, and empty Beenakker cavity, several measurements are performed under different connection configurations (see Table 3-5). Output power is the amount of microwave power that is delivered from the microwave generator. Reflected power is the amount of power that is reflected due to impedance mismatching and reflects back to the generator. Both values are monitored by the power meter on the generator.

Under Test 1, the generator is not connected to any external components. Due to impedance mismatch with an open circuit terminal, 100% power gets reflected back to the generator.

Under Test 2, the generator is connected to a 1.5 meter coaxial cable. The 1.5 m cable is found to be lossy through network analyzer measurements, which means the cable dissipates electromagnetic energy. The data on reflected power confirms power loss, 9 W is lost due to the coaxial cable and connectors.

Under Test 3, the generator is connected to a 1 meter coaxial cable. The 1 m cable has excellent quality at 2.45 GHz and is confirmed by network analyzer measurements, thus the loss in this 1 m cable is expected to be lower than that in the 1.5 m lossy cable. Reflected power data shows 5 W is lost due to the coaxial cable and connectors. Compared to the 1.5 m lossy cable, power lost reduced from 9 W to 5 W, which clearly shows the quality of coaxial cable has apparent effect on the efficiency of the MIP system.

Table 3-5 Power loss measurements

Test #	Connection configuration	Output power (W)	Reflected power (W)
Test 1	No coaxial cable or cavity connected	**40**	**40**
Test 2	1.5 m lossy coaxial cable, open end	**40**	**31**
Test 3	1 m excellent quality coaxial cable, open end	**40**	**35**
Test 4	1 m excellent quality coaxial cable, Beenakker cavity, no plasma	**40**	**33**
Test 5	1 m excellent quality coaxial cable. Beenakker cavity, with plasma	**40**	**0**

Under Test 4, the generator is connected to a 1 meter coaxial cable and terminated by a well-matched modified Beenakker cavity. There is no plasma in the cavity, thus the measurement only shows power loss in the MIP system. The addition of an empty Beenakker cavity further reduced reflected power by 2 W, indicating power dissipation inside the cavity and connectors. Because the cavity is made of copper and has polished inside surfaces, microwave power loss in the bulk cavity is expected to be low.

Under Test 5, the connection configuration is the same as in Test 4, except that an argon plasma is ignited in the Beenakker cavity. The plasma tunes the MIP system into an impedance well-matched condition. No measurable power is reflected back to the generator.

Based on these 5 tests, estimation on power dissipation in the transmission line of the MIP system is made. Out of 40 W output power from the generator, 7 W power is lost in the transmission line.

B. Power loss in the Beenakker cavity under plasma operations

From power loss measurements based on no-plasma condition, it is found the power loss in a well-matched modified empty Beenakker cavity is around 5% under 40 W input power. When there is a plasma present inside the cavity, the temperature of the cavity increases and it is worthwhile to investigate the heating process.

The experiment is conducted at 50 W output power at 2.45 GHz with 1400 sccm Ar gas flow rate. An alumina discharge tube with 6 mm outer diameter and 1.2 mm inner diameter is used to contain the plasma. After ignition of the plasma, the MIP system goes into well-matched condition with 0 W power reflections back to the generator. Measurement configuration is shown in Fig.3-28. Two thermal couple sensors (one near the center and one near the periphery of the cavity) are attached by thermal glue and fixed by plastic tapes. As the cavity has a much larger dimension compared to the size of the plasma, temperature gradient is expected to take place across the lid.

When a burning plasma is present, the temperature of a Beenakker cavity rises with increasing operation time (see Fig.3-29). Thermal equilibrium of the MIP system is reached after sustaining a plasma for 40 minutes. The cavity temperature measured by both thermal couples gives similar values. Cavity is heated up to around 45°C under 50 W output power from generator with 0 W reflected power.

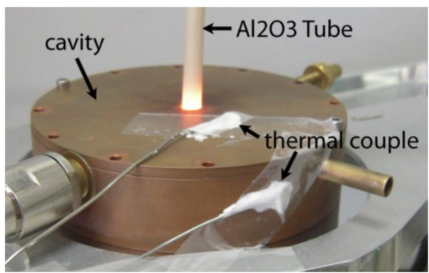

Fig.3-28 Temperature measurement setup (plasma ignited)

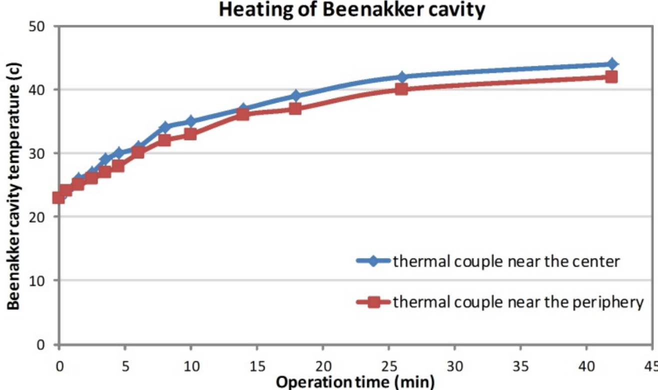

Fig.3-29 Cavity temperature increase measured by the two thermal couples

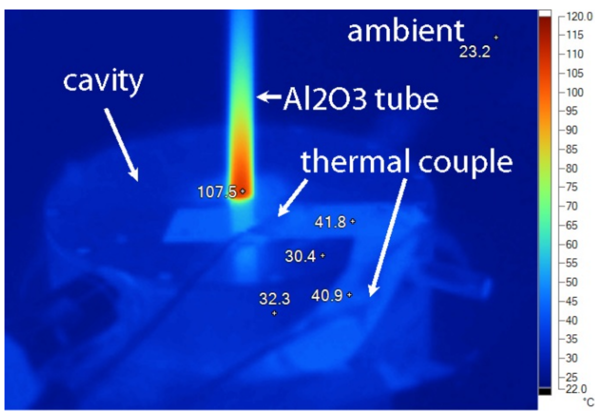

Fig.3-30 Infrared camera image of cavity (10 sec after the plasma is turned off)

Besides thermal couple measurements, infrared camera photos are taken to investigate the temperature distribution (see Fig.3-30). Although the cavity outer surface is rough, the emissivity coefficient is not 1. Direct infrared measurement on the cavity copper surface results in wrong readings due to the reflection of light on metal surface. An engineering solution is to cover the copper surface with

a layer of plastic tape with coarse surface. The tape results in almost 100% emissivity coefficient on the cavity surface thus provides a correct measurement. In order to avoid possible RF interference due to the plasma, an infrared image is taken 10 seconds after the plasma is turned off. The cavity temperature stabilizes around 41°C under 50 W output power from generator with a burning plasma present, which is consistent with thermal couple measurements. The infrared measurement value of the Al_2O_3 discharge tube temperature is not correct due to the drastic cooling of tube in the 10 seconds time span, yet the infrared camera image illustrates how heat is dissipated on the cavity and discharge tube.

The most possible reason for cavity temperature increase is heating by plasma. The plasma filament that is located through the axis of the cavity has high power density. Although exact temperature value of the plasma gas where ionization takes place cannot be measured due to its small physical dimensions, the temperature of Al_2O_3 discharge tube outside the cavity is around 250°C, which is much higher than the bulk cavity temperature. It should be noted that the temperature of the Al_2O_3 discharge tube inside the cavity where ionization takes place is much higher. Heat is most likely transferred from the Al_2O_3 discharge tube surface to the Beenakker cavity through radiation, convection and conduction.

C. Power loss due to microwave leakage field

Plasmas are formed by ionized gas and electrons thus they normally have excellent electrical conductivity. Microwave frequency electromagnetic waves interact with the plasma filament and feed power majorly to the free electrons in the plasma. Plasma filaments act as antennas with high conductivity that readily carry and emit microwave signals. Inside the cavity, the emitted electromagnetic waves are reflected back to the plasma when reaching the polished copper inner surfaces. If the plasma filament extends outside the cavity, electromagnetic waves will be emitted to the environment thus inducing microwave leakage field.

To measure this leakage field is extremely difficult. The generator output frequency is 2.45 GHz, thus the wave length λ is 12.2 cm. By definition, near field is 0-1 λ from the source, transition zone is 1-2 λ, and far field is >2 λ. The field distribution in near field is extremely complex and it is not possible to get correct measurement by using a microwave leakage detector. Under 20 W power levels and 1400 sccm Ar plasma condition, the maximum reading on the microwave leakage detector (Sairem IFP5C) is 2.0 mW/cm^2 when the detector is placed at 6 cm away from the plasma. The leakage field demonstrates a high degree of polarization and the measured field strength may decrease to 0.0 mW/cm^2 if the angle of the detector is varied. Therefore, the near field measurement values by a leakage detector should not be trusted. Reliable measurements should be made in far field. However, at far field the leakage field power density is so low that the detector was not able to pick up.

A rough estimation can be made by the leakage detector measurements assuming a uniformly dissipated leakage field with a spherical shape surrounding the plasma filament. An averaged field strength of 2.0 mW/cm^2 on the surface of a sphere with 6 cm radius results in a power dissipation in leakage field to be 1 W.

With the addition of O_2 or CF_4 etchant gas in the plasma, the argon plasma filament shrinks inside the cavity thus reducing the antenna effect of the plasma filament. Therefore the microwave leakage field strength at 6 cm from the plasma is kept below 1.0 mW/cm^2 during normal plasma etching processes. Human operator of the MIP instrument is normally at the outer frame of the MIP instrument, which is >20 cm from the plasma source. At this distance the leakage field is 0.0 mW/cm^2 measured by the leakage detector. Health regulation limits the leakage radiation at 5 cm from the instrument outer frame to be lower than 1.0 mW/cm^2, thus the MIP instrument is safe to use according to regulations.

D. Power loss in plasma

The power consumption in plasma is dissipated by excitation, dissociation and ionization of the plasma gas. One major objective when designing the MIP system is to provide as high power efficiency as possible, that is why efforts have been made to decrease power loss in the microwave components.

Several points attribute to the overall high system power efficiency: a good quality coaxial cable, well-polished cavity inner surfaces, elimination of the need to use an external tuner, and a good recipe that keeps the plasma filament inside the cavity.

To estimate the power efficiency of the MIP system, consider the 40 W generator output power and 1400 sccm Ar plasma condition. A 1 meter coaxial cable consumes 5 W power; an empty Beenakker cavity consumes 2 W power; the leakage field emits 1 W power; reflected power is 0 W; subtracting these amounts results in a power consumption in plasma to be 32 W. Counted from the output port of the microwave generator, the power efficiency of the MIP system is estimated to be 80%.

Comparison of MIP with conventional reduced pressure plasma can be estimated in power absorbed per unit volume. For a typical reduced pressure plasma etcher at 1 kW, the volume of plasma is about 3 cm^3, which results in power density of 300 W/cm^3 [58]. For MIP generated with Beenakker cavity with coupling modification, the volume of plasma is about 0.02 cm^3 at 32 W absorbed power levels, which corresponds to a power density of 1600 W/cm^3. Thus, compared to a conventional plasma etcher used in wafer fabrication, an MIP sustained by a Beenakker cavity generates a plasma with much higher power density while consuming a much lower power.

3.6 Conclusions

The impedance mismatch problem when sustaining an atmospheric pressure argon plasma by the original Beenakker cavity is solved by adding a variable antenna to the original coupling loop inside the cavity. Microwave power reflection of the system is reduced from 50% to 0% when sustaining argon plasma. The proposed modification avoids the addition of bulk microwave tuning components, while the performance is even better.

The addition of O_2 or CF_4 etchant gas into the argon plasma detunes the impedance of the original Beenakker cavity, thus inducing instability to plasma. The proposed solution is to add an modification element that broadens the process window of the cavity by decreasing the cavity's quality factor. The outcome is a wide process window that allows as much as 4% molecular oxygen admixture in argon plasma gas under low input power level at 40 W. Microwave power reflection of the MIP system can be maintained under 10% when sustaining $Ar/O_2/CF_4$ plasma with input power levels lower than 100 W.

Fine tuning of the MIP system during plasma operation can be done by either varying the resonance frequency of the cavity or varying the output frequency of the generator. After implementing both the coupling loop and process window modifications on the original Beenakker cavity, fine tuning by varying the output frequency of the generator is found to be the preferred solution.

Power dissipation paths in the MIP system are evaluated. Efforts are made to minimize the power loss in transmission line, resonant cavity, and leakage field. Counted from the output port of the microwave generator, the power efficiency of the MIP system is estimated to be 80%. The volume power density of MIP sustained by modified Beenakker cavity is 1600 W/cm^3 under 40 W input power, which is much higher than the case with a conventional ICP at 300 W/cm^3 under 1000 W input power. The high power density of MIP contributes to high radical concentration in plasma afterglow.

Beenakker cavity adopting both the coupling loop and process window modifications is found to be the most suitable plasma source for semiconductor package plasma decapsulation applications due to its high power density, power efficiency, plasma stability, wide plasma operation range, and low stray field.

Chapter 4

Microwave Induced Plasma Afterglow Etching

4.1 Introduction

In this chapter we investigate plasma etching recipes for different inorganic, organic and compound materials, as well as the key elements that enable etching of these materials. The high etching rate of different materials under low input power will demonstrate the high efficiency of the MIP instrument. The findings from this chapter build the foundation for plasma decapsulation applications, which will be described in Chapters 5&6.

Temperature during plasma etching is a crucial element. In section 4.2, the temperature of the plasma afterglow and the bulk IC package is studied by numerical modeling, thermal couple measurements, and in-situ temperature monitoring during plasma decapsulation. The goal is to find a suitable operation range that allows a sufficiently high plasma etching rate, while at the same time maintaining a moderate bulk IC package temperature to minimize potential thermal mechanical stress.

The efficiency of the MIP is evaluated by the etching rate of different materials. Section 4.3 addresses the lifetime and flux of radicals in plasma afterglow that enables high material etching rate. Sections 4.4~4.8 cover the plasma etching rate of epoxy molding compound, Si, SiO_2, Si_3N_4, silicone, copper, aluminum, palladium, and gold. Those materials are of special interest because they are commonly used in semiconductor packages. Optimal etching recipes for each material will be given, while comparison between recipes and chemistry behind the difference will be proposed.

Decapsulation of semiconductor packages requires certain components in the package to be removed, while other components have to remain undamaged throughout the plasma etching process. A list of materials that may appear in semiconductor packages is listed in Table 4-1, while their functions and requirements after decapsulation are also described. This chapter investigate under what condition can a certain material be etched, at what speed, and what is the etching selectively over other materials.

The pool of data on $Ar/O_2/CF_4$ plasma etching provides insight to the etching rate and selectivity of multiple materials. After knowing the chemistry and key elements in each reaction, fast and safe decapsulation of semiconductor packages is achievable by choosing the correct recipe and designing a suitable process.

Table 4-1. Materials in semiconductor package

Material	Function in semiconductor package	Material to be removed or preserved during plasma decapsulation?
Si	Chip or die material	Preserve
SiO_2	Filler particles in epoxy molding compound	Remove
Si_3N_4	Passivation layer on Si die	Preserve
Epoxy	Matrix in epoxy molding compound	Remove
Epoxy Mold Compound	Encapsulation material in plastic IC packages	Remove
Silicone	Encapsulation material in LED packages	Remove
Copper	Bond wire material	Preserve
Aluminum	Bond pad material	Preserve
Palladium	Protection layer on Pd/Cu type bond wires	Preserve
Gold	Bond wire material	Preserve

4.2 MIP Afterglow Etching Temperature

Heat can be transferred via three paths: conduction, convection and radiation. The flow of plasma effluent onto the IC package sample surface causes the sample temperature to increase. Heat can be transferred from the effluent to the package by convection. Inside the package, heat is transferred by conduction. Radiation takes place on the surface of the package.

To get an overview of temperature distribution inside an IC package and its surrounding environment during plasma decapsulation, a thermal model is built and verified by thermal couple measurements.

To investigate the temperature on the interface where plasma etching takes place, in-situ temperature measurement on localized area (1 mm × 1 mm) is conducted.

4.2.1 Numerical Thermal Model

The thermal model is built in Fluent software [64] A better understanding of the etching process can help to choose suitable recipes for different etching steps from a thermal point of view.

A. Model definition

The schematic diagram of the IC package sample under the plasma effluent in the thermal model is depicted in Fig.4-1. This graph is not drawn to scale in order to show all components. An alumina gas discharge tube is placed on top of the package. The plasma effluent flows downwards to the surface of the IC package. The package with a size of 20.7 mm in length, 7.6 mm in width, and 2.45 mm in height has three components. The bulk material is molding compound. Inside the package a silicon die with a size of 3.4 mm in length, 2.0 mm in width, and 0.4 mm in height is located in the center. The copper lead frame inside the package is located beneath the die and is simplified to a strip in the model. Two simplified copper lead fingers extend out of the package. The parameters used in the model are set up according to a real Small Outline (SO32) IC package sample that will be further tested in thermal couple temperature measurements. The package structure in the model is simplified to only containing lead frame, Si die and epoxy molding compound.

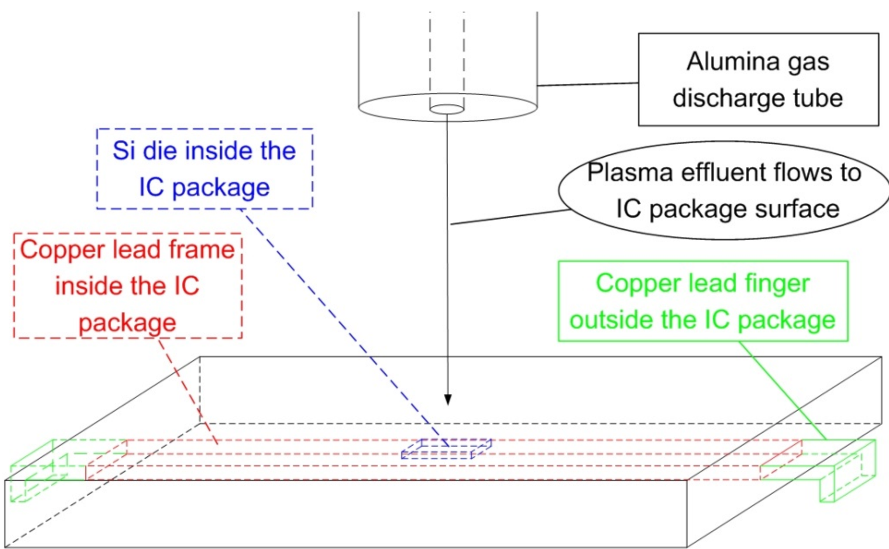

Fig.4-1 Schematic diagram of the thermal model

B. Simulation results

The temperature distribution along a cross section through the center of the 3D thermal model is depicted in Fig.4-2. Plasma effluent flows to the surface of the IC package. The temperature of the effluent on top of the package is influenced by the total gas flow and the initial gas temperature. As shown in the graph, under this configuration the effluent temperature at 1 cm on top of the package is 688 K (415°C). The temperature of the IC package is 372 K (99°C) near the edge, which is much lower than the effluent temperature.

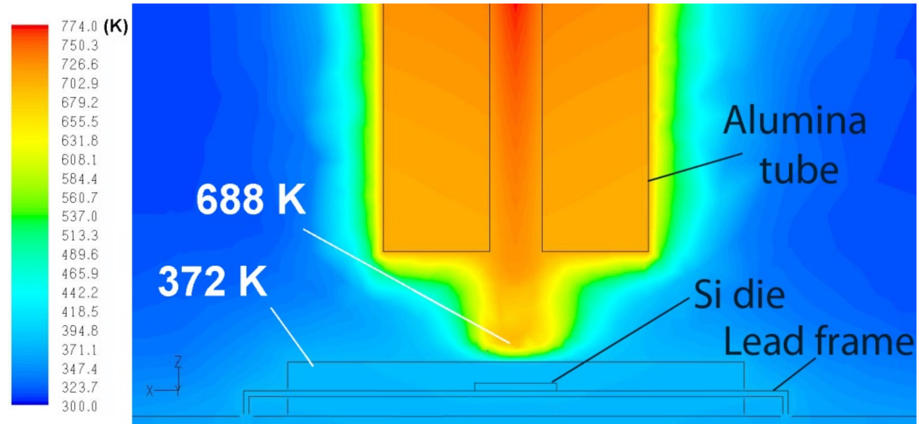

Fig.4-2 Cross sectional view of temperature distribution

The simulation results show that heat transfer from gas to solid is not efficient. The temperature inside the IC package is increased from around 100°C to 150°C when the effluent temperature at 1 cm from the top of the package is increased from around 400°C to 700°C. In etching experiments, it is found that without changing plasma gas recipes a higher molding compound etching rate always associates with a higher plasma effluent temperature. At effluent temperature below 300°C the etching rate is low. At effluent temperature around 600°C the volumetric etching rate can be as high as 2.5 mm^3/min. When etching the thick molding compound, a recipe with a high plasma effluent temperature can be used to achieve high etching rate. In the meantime the plasma effluent does not raise the temperature inside the IC package to above 150°C.

4.2.2 Temperature Measurement

The temperature of the plasma effluent and an IC package is measured by a thermal couple. To measure the effluent temperature, a thermal couple is placed in the center of the effluent flow path from the alumina tube, 1 cm above the IC package. To measure the package sample temperature, a thermal couple is glued

by thermal glue to the left and right corner, and bottom of the package where the gas flow velocity is comparatively low.

Temperature of the plasma effluent and the corresponding package temperature under different input microwave power levels are measured. During the measurements, gas flow and gas composition are kept constant. Ar is used as plasma carrier gas, sufficient O_2 is added into the plasma so that the plasma filament does not extend out of the gas discharge tube and the microwave leakage remained low. Absorbed microwave power is calculated from the output power and reflected power readings from the microwave generator.

As it is shown in Fig.4-3, the plasma effluent temperature increases from 380°C to 670°C when absorbed microwave power is increased from 40 W to 90 W. The corresponding package temperature is much lower than the effluent temperature. Temperature at the corner of the package increases from 85°C at 40 W to 150°C at 90 W. These values are in good agreement with the simulation results. Package temperature on the right corner and left corner are almost the same. Package temperature on the bottom side is 10°C to 20°C lower than temperature on either side of the corners.

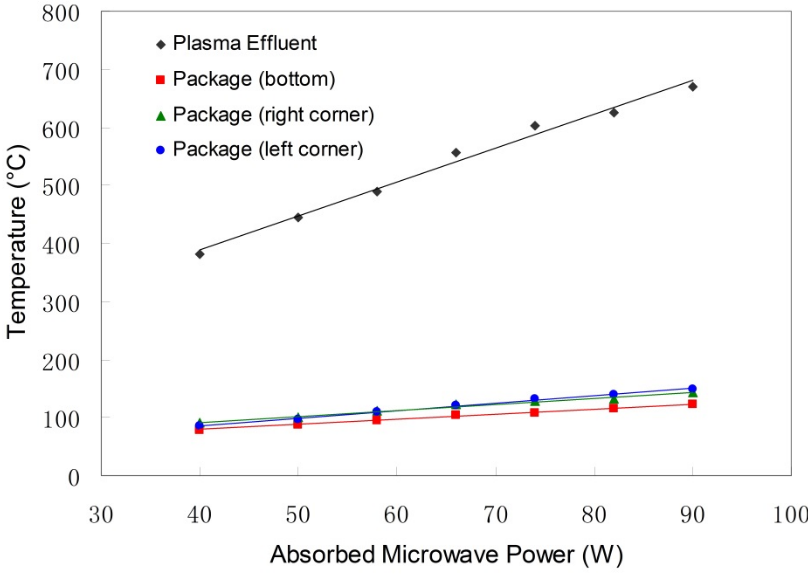

Fig.4-3 Effluent and package temperature versus absorbed microwave power

4.2.3 In-situ Temperature Monitoring

Higher processing temperature increases molding compound etching rate but also increase the potential to damage the bond wires and die inside the IC package. To fully evaluate the MIP etching process, in-situ temperature measurement is conducted by decapsulation of a discrete diode device in a Small-outline Transistor (SOT23) package while monitoring the forward voltage variation. A constant current source is built by serial connection of a direct current power supply that delivers constant 31 V output, a 56 kΩ resistor, and a SOT23 diode device. The forward voltage of the diode is monitored by a multimeter.

A. Calibration of the diode temperature sensor

The voltage versus temperature correlation of the diode sensor under constant current is first calibrated. The diode package is glued to a thermal couple and heated in a furnace. Fig.4-4 shows the measured forward voltage of the diode with respect to different temperature values.

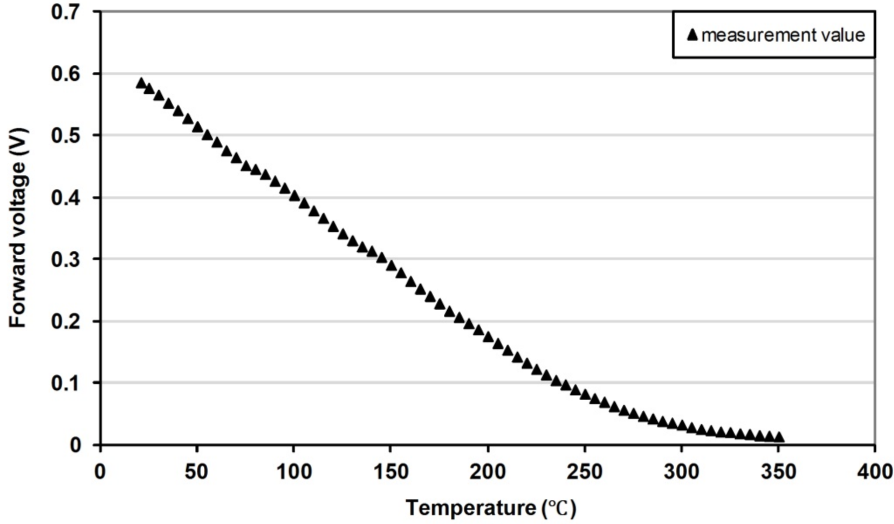

Fig.4-4 Forward voltage drop with respect to temperature

B. Temperature monitoring during MIP decapsulation

The forward voltage of a diode device in a SOT23 plastic package during $Ar/O_2/CF_4$ MIP afterglow etching is measured and calculated into temperature value according to the calibration curve. Plasma etching recipe with 40 W input power levels, 1400 sccm Ar, 5 sccm O_2, and 5 sccm CF_4 is used.

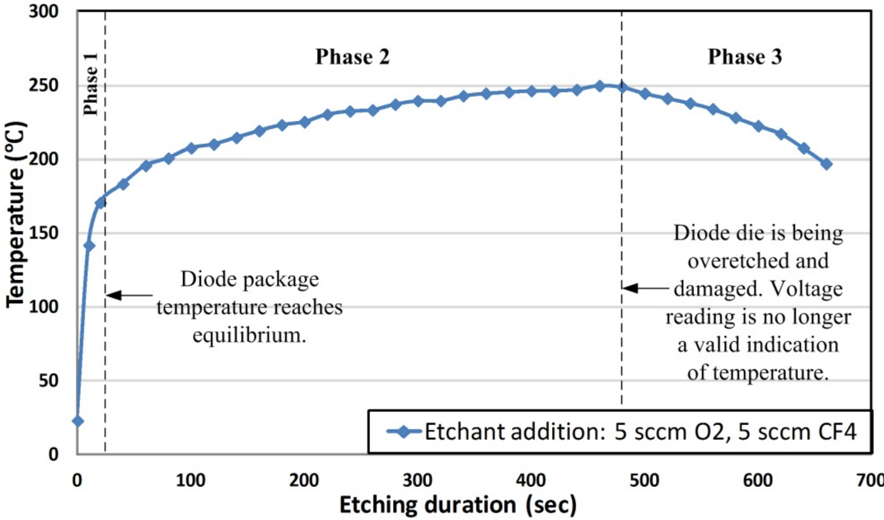

Fig.4-5 Temperature monitoring during MIP decapsulation

The diode die temperature variation during 660 seconds of MIP etching is plotted in Fig.4-5. The temperature curve can be divided into three sections each representing a different phase during decapsulation.

Phase1 is the heating process where the die temperature increases drastically from room temperature to 170°C in 20 seconds, reaching thermal equilibrium.

In Phase2, the die temperature increases linearly from 170°C to 250°C in 450 seconds. During this period, the molding compound on the SOT23 package is being removed by the oxygen and fluorine radicals in the plasma effluent. The thickness of molding compound on top of the die decreases from 350 µm to 0 µm. Because the die is becoming in closer contact to the heated effluent, the die temperature increases.

In Phase3, an unexpected sudden decrease in temperature reading takes place. This does not mean the decrease of diode temperature in reality. The diode die is now being over-etched by the plasma and the functional silicon structures beneath the Si_3N_4 passivation layer are damaged. The forward voltage values are no longer a valid indication of the temperature that the die measures, instead it is a signal of over-etching damage. The over-etching phenomenon is confirmed by the real-time monitoring of the IC package surface under the CCD camera. Such damage is irreversible and the diode I-V characteristics measured after cooled down to room temperature behave differently to an undamaged device.

C. Influence of etchant gas addition to process temperature

The addition of O_2 and CF_4 etchant gas into Ar plasma decreases the number of free electrons due to the consumption in excitation and dissociation reactions of etchant molecules. The result is a decrease in the plasma effluent temperature. Fig. 4-6 shows the influence of O_2 etchant gas addition into a 1400 sccm Ar plasma under 30 W and 40 W input microwave power conditions. The measurement is made by directing the effluent of the plasma to the surface of an undamaged diode die in a SOT23 package.

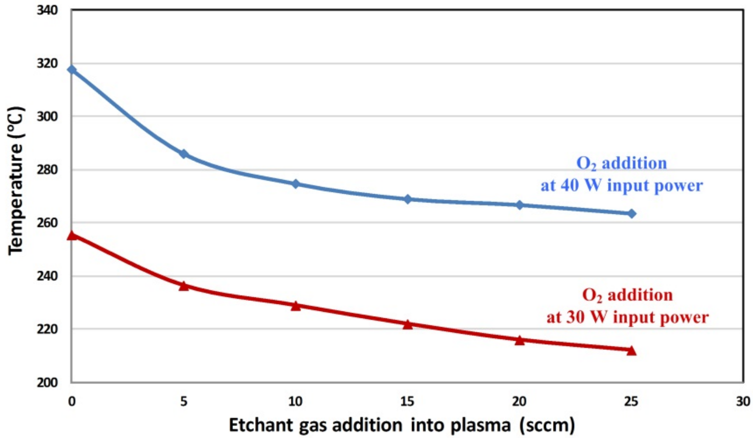

Fig.4-6 Influence of O_2 addition and power to diode die temperature

4.3 Species and Their Lifetimes in the Plasma Afterglow

At atmospheric pressure, reactive neutral species will dominate plasma chemistry while ions become relatively insignificant. The electron density n_e of a microwave induced atmospheric pressure argon plasma is in the order of 10^{13}~10^{14} cm^{-3} [58, 65-67], while average electron temperatures T_e range from 1.5~2 eV ($1\,eV = 11600K \times k_B$, where k_B is Boltzmann constant) [65, 67]. The recombination coefficient for ions and electrons at atmospheric pressure is 10^{-6} cm^3/s yielding after 10 µs a charged particle density of only 10^{11} cm^{-3} [68], which is orders of magnitudes lower than reactive neutral species concentration.

Addition of O_2 etchant gas will reduce electron density. The free electrons that have high enough energy to induce excitation and dissociation of ground state triplet oxygen. Active species in the plasma afterglow can be atomic oxygen $O(^3P)$, metastable molecular oxygen, and ozone O_3. It has been reported that oxygen atoms were the active species involved in oxygen plasma afterglow etching of polymer materials [68, 69], while in an atmospheric pressure Ar/O_2 or He/O_2 plasma the concentration of oxygen atoms was 10^{14}~10^{16} cm^{-3} [69-73] with a lifetime of approximate 2 ms [68].

In the case of the Ar/O_2 MIP afterglow, 1400 sccm plasma gas flows through a hole with 0.6 mm diameter, which yields the linear velocity of gas is 2050 cm/s inside the discharge tube. IC package sample is placed at 0.6~2 cm below the plasma filament, which means oxygen atoms travel 0.3~1 ms to reach the package surface. Given the oxygen atom lifetime of 2 ms, the concentration of oxygen atoms that reach the reaction site does not decrease dramatically. Table 4-2 shows the Ar/O_2 MIP afterglow with 1400 sccm Ar, 40 W absorbed microwave power and 0~50 sccm O_2 gas addition. Glow in the plasma effluent is observed when O_2 gas is added into argon plasma, while the light might come from excited state oxygen and recombination of oxygen atoms. The long tail of glow that is observed in low power Ar/O_2 MIP afterglow demonstrates the high radical flux that can be generated by the Beenakker cavity.

The Ar/CF_4 MIP afterglow generates fluorine atoms. It has been reported that in an atmospheric pressure He/CF_4 plasma, the concentration of fluorine atoms was 10^{15} cm^{-3} and after 2 ms traveling time the F concentration is not expected to decrease dramatically [74].

In the application of using MIP afterglow to decapsulate IC packages, the 2 cm distance from plasma source to package surface is short enough to ensure that both O and F atom concentrations remain at high value. The concentration of O and F atoms in atmospheric pressure plasma is normally around 10^{14}~10^{16} cm^{-3} [69-73], and 10^{15} cm^{-3} [74], respectively. O and F atoms concentration in atmospheric pressure MIP afterglow are in general at least two orders of magnitude higher than that found in low-pressure plasmas. The high flux of radical contributes to high etching rates that are achieved with this MIP system.

Table 4-2. Plasma afterglow in Ar/O_2 MIP at 40 W power (O_2:0~50 sccm)

O_2 (sccm)	0	5	10	20	50
Image of plasm a after glow	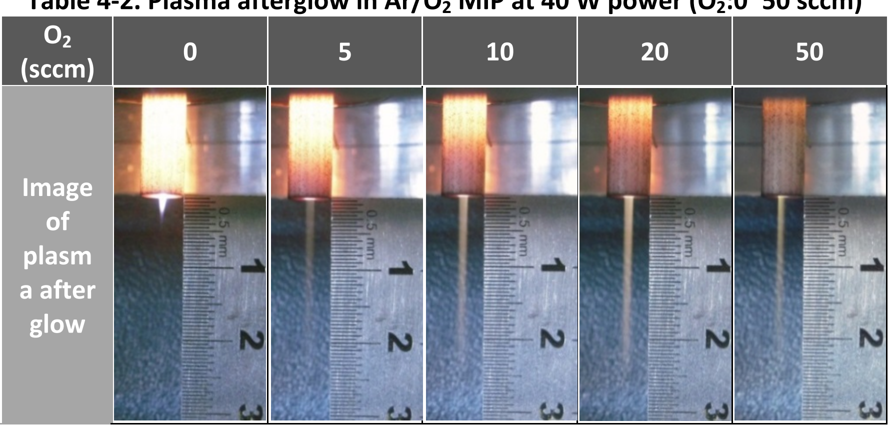				

4.4 MIP Afterglow Etching of Epoxy Molding Compound

The two major components in Epoxy Molding Compound used in plastic semiconductor packages are epoxy (10~30 %Wt) and silica fillers (70~90 %Wt). Cured epoxy forms the backbone in molding compound, while silica fillers are added to correct the thermal expansion coefficient mismatch between epoxy and silicon die (see Fig.4-7). Other additives in molding compound are hardener, carbon black, flame retardant, etc.

For removal of compound material that contains both organic and inorganic material, plasma etching recipe has to be developed that enables etching of both materials and optimize the combined etching rate of the two.

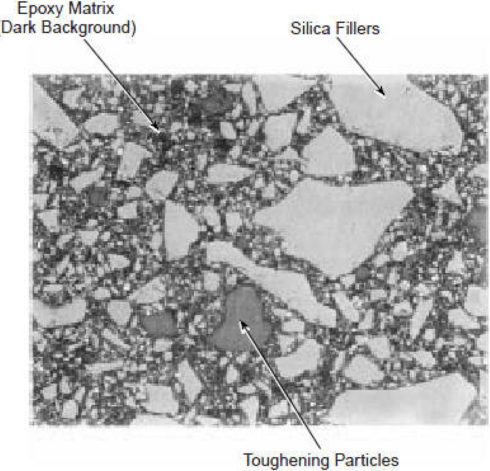

Fig.4-7 Cross section view of molding compound material [3]

4.4.1 Ar/O_2 Plasma Etching

Oxygen radicals in the plasma effluent react with epoxy in molding compound. It has been reported that oxygen atoms were the active species involved in oxygen plasma afterglow etching of polymer materials [68, 69]. When only oxygen plasma is used, etching leaves a layer of silica agglomerate residue on the molding compound surface (see Fig.4-8a). This silica layer blocks further etching of molding compound by the plasma effluent. The most possible reason that may cause the agglomeration of silica particles is the silane coupling agent [75, 76], which is added to the molding compound to improve the adhesion between silica fillers and epoxy chains. The hydroxyl groups on the surface of silica can form hydrogen bond with the hydroxyl groups on the organosilane. After the following curing process, Si-O covalent bonds can be formed at the interface connecting silica filler with epoxy. The agglomeration of silica fillers after long time exposure under Ar/O_2 plasma is most likely due to Si-O covalent bond between the silica particles.

Exposure of the silica agglomerate under Ar/CF_4 plasma results in etching of Si containing material by fluorine radicals, thus efficiently breaks the Si-O bond on the interface and dissociates the agglomerate into separate particles. However, the introduction of fluorine causes over-etching damage to Si die.

An alternative way to efficiently remove this SiO_2 residue layer is to put the sample into ultrasonic cleaning for 5 seconds. The cavitation force readily breaks the SiO_2 agglomerate and removes the residue layer. This Ar/O_2 etching and ultrasonic cleaning combination proved to be a crucial process to maintain undamaged Si die after plasma decapsulation, which will be further discussed in Section 5.3.

4.4.2 Ar/CF_4 Plasma Etching

Fluorine radicals in the plasma effluent react with silica filler in Epoxy Molding Compound. Since Ar/CF_4 plasma does not readily etch epoxy in molding compound, overall molding compound etching rate is extremely low. Etching leaves very shallow spherical cap profile on the molding compound surface, with a diameter of 2.5 mm and a depth too little for efficient etching (see Fig.4-8b).

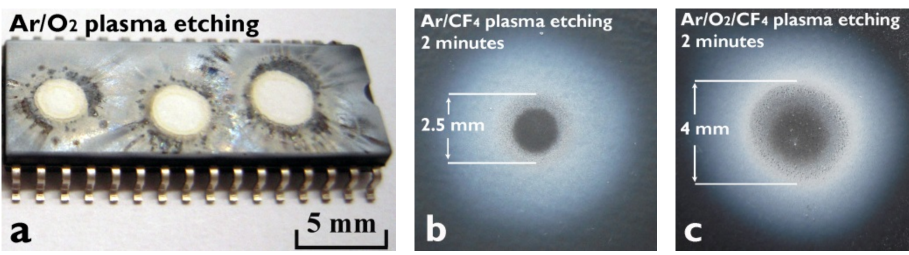

Fig.4-8 Epoxy molding compound after (a) Ar/O_2 plasma etching, (b) Ar/CF_4 plasma etching at 60 W for 2 minutes, (c) $Ar/O_2/CF_4$ plasma etching at 60 W for 2 minutes

4.4.3 $Ar/O_2/CF_4$ Plasma Etching

Only when both O_2 and CF_4 are added into the plasma can a high molding compound etching rate be achieved. The epoxy in molding compound is completely etched by oxygen radicals forming H_2O, CO_2. At the same time, the silica filler is etched at a low rate by fluorine radicals forming SiF_4, so that the silica filler becomes smaller and the filler agglomerate structure become loose. The gas flow from the plasma effluent blows off the etched silica filler. Etching leaves deep spherical cap profile on molding compound surface, with a diameter of 4 mm and a depth of 180 µm after just 2 minutes etching (see Fig.4-8c).

It should be noted that molding compound etching by $Ar/O_2/CF_4$ plasma requires epoxy to be fully etched, while SiO_2 fillers are only partly etched by plasma and mostly blown off by gas flow of the plasma effluent.

To find the optimal O_2 and CF_4 etchant gas percentage, etching of plastic encapsulated Small Outline Transistor (SOT23) packages with 350 µm thick molding compound on top of the die is conducted. Due to the small size of the sample, the molding compound etching rate is measured indirectly. The etching time needed to expose the die is measured and the etching rate is calculated by dividing the thickness of molding compound by the etching time.

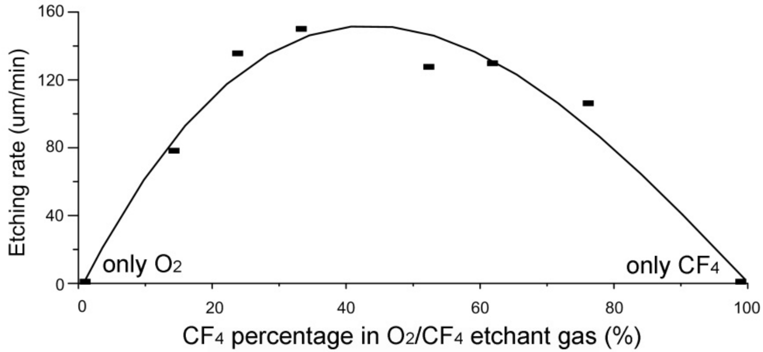

Fig.4-9 Mold compound etch rate versus percentage of CF_4 in O_2/CF_4 etchant gas

During plasma etching experiments, Ar is used as the plasma carrier gas and its flow rate is kept constant at 1400 sccm, input power is 60 W. O_2 and CF_4 are the plasma etchant gas and their combined flow rate is kept at constant 21 sccm. The only variable is the percentage of CF_4 in the O_2/CF_4 etchant gas.

Maximum molding compound etching rate is found to be between 30-60% CF_4 addition (see Fig.4-9). A higher or lower CF_4 addition from this optimal range results in lower etching rate. A low CF_4 addition favors epoxy etching while a high CF_4 addition favors SiO_2 filler etching. As the molding compound is a mixture material, both epoxy and silica filler have to be etched simultaneously to achieve a high combined etching rate. When adding small amount of O_2 into a CF_4 plasma, reactions between CF_3 and O_2 produce COF_2 and increase the concentration of free F atoms [77, 78]. The effect that the addition of CF_4 into O_2 plasmas increases epoxy etching rate due to the catalytic role of F [79-81] may also facilitates molding compound etching by the $Ar/O_2/CF_4$ mixture plasma.

4.4.4 Influence of the Epoxy Molding Compound Composition

The composition of Epoxy Molding Compound may be different from one to another. As a result, the etching rate of different types of molding compound by the same plasma recipe may differ. Thus, it is worthwhile to investigate the influential factors. Three types of molding compound after curing are chosen for etching experiments (see Table 4-3). X84179 differs from X83563 in filler sieving size, where the former one used finer SiO_2 filler particles. G750 used different epoxy and has the coarsest SiO_2 filler particles.

Table 4-3. Three types of molding compound and their composition

	X84179	X83563	G750
Filler content (wt.%)	86	86	88
Filler shape	Spherical	Spherical	Spherical
Filler sieving size (µm)	20	55	75
Epoxy	Biphenyl OCN	Biphenyl OCN	Biphenyl MAR6
Hardener	PN	PN	PN
Catalyst system	A	A	B

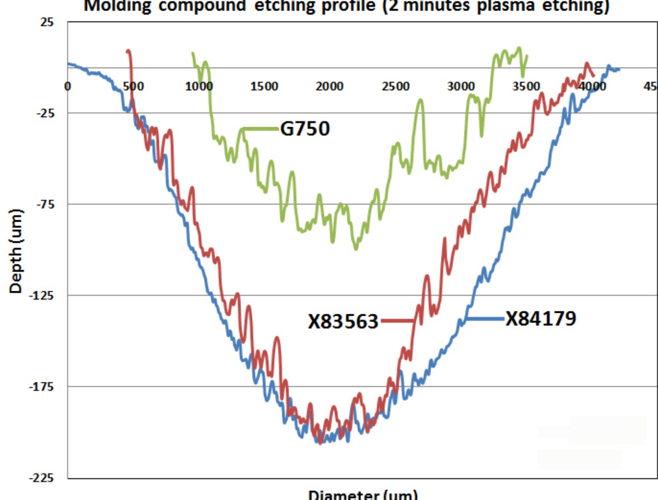

Fig.4-10 Cross-section profile of three types of molding compound after same recipe Ar/O_2/CF_4 plasma etching under 60 W power for 2 minutes

Plasma etching leaves a deep spherical cap profile on all three molding compound surfaces. Fig.4-10 shows the cross-section profile of the three molding compound, each after 2 minutes etching under the same plasma. A Veeco Dektak150 surface profiler is used for the measurement. The surface roughness of the three molding compounds is clearly shown in the profile curves, whereas X84179 is the finest, X83563 is in between, and G750 is the roughest. It is found that the profile shape (both diameter and depth of the spherical cap) of X84179 and X83563 are almost the same, while G750 shows a smaller spherical cap after etching by the same plasma recipe for the same duration.

To find the optimal O_2 and CF_4 etchant gas percentage, the three molding compound are etched with $Ar/O_2/CF_4$ plasma with different CF_4 percentage in the O_2/CF_4 etchant gas. The only variable is the percentage of CF_4 in the O_2/CF_4 etchant gas. The vertical etching rate measured at the deepest point of the etching profile is plotted in Fig.4-11a. Because the etching profile is a spherical cap, it is more suitable to describe the etching rate in volume of material being removed in a certain amount of time. The radius (r) and depth (d) of the spherical-cap-shaped etching profile is measured and the volume (V) of molding compound removed is calculated through equation: $V = \frac{\pi d}{6}(3r^2 + d^2)$. The volumetric etching rate of three types of molding compound is plotted in Fig.4-11b.

The etching rate curve (depth and volume) of X84179 and X83563 almost overlap under every recipe tested, which indicates the difference in filler sieving size does not have apparent influence on the molding compound etching rate by $Ar/O_2/CF_4$ plasma. The sieving size determines the surface-bulk ratio and dimension of filler particles, which may influence molding compound etching rate by plasma. However, variation in etching rate is not observed in the sieving range tested in this experiment.

Another factor that may influence molding compound etching rate is the Weight Percentage (wt.%) of filler. The porosity of filler agglomerate structure could influence the flow pattern of radical gas and thus affect the molding compound etching rate. A high filler wt.% is expected to reduce molding compound etching rate because SiO_2 etches comparatively slower than epoxy with similar plasma etching recipes. In this experiment, filler wt.% difference between the three molding compound is small thus the influence of filler wt.% to etching rate is not likely to be dominating.

The volumetric etching rate of G750 is fivefold lower than that of X84179 and X83563 under most recipes tested (see Fig.11b). The differences of G750 compared to the other two molding compound are filler sieving size, filler wt.%, and epoxy type. Given the similarity in etching rate curve of X84179 and X83563, sieving size should not be influential. The filler wt.% of G750 is only 2% higher than that of X84179 and X83563, which is small thus not likely to cause a fivefold reduction in etching rate.
The different epoxy type in G750 is the most possible reason to the much lower molding compound etching rate. The presence of aromatic and polar functional groups [82], nitrogen and oxygen atoms in the polymer [83], and saturation of polymer [80, 84] all affect the polymer etching rate by O_2/CF_4 plasma. Reported polymer etching rates by plasma are normally in the range of 0.5~1.5 µm/min with optimal CF_4 percentage of 20~50 % in the CF_4/O_2 etchant gas, depending on the reactor type and polymer composition [79-85].

Despite that the etching rate of different molding compound may differ due to composition, the shape of molding compound etching rate curves and the optimal range of CF_4 percentage in O_2/CF_4 etchant gas are similar. CF_4 addition of 30~60% results in maximum molding compound volumetric etching rate.

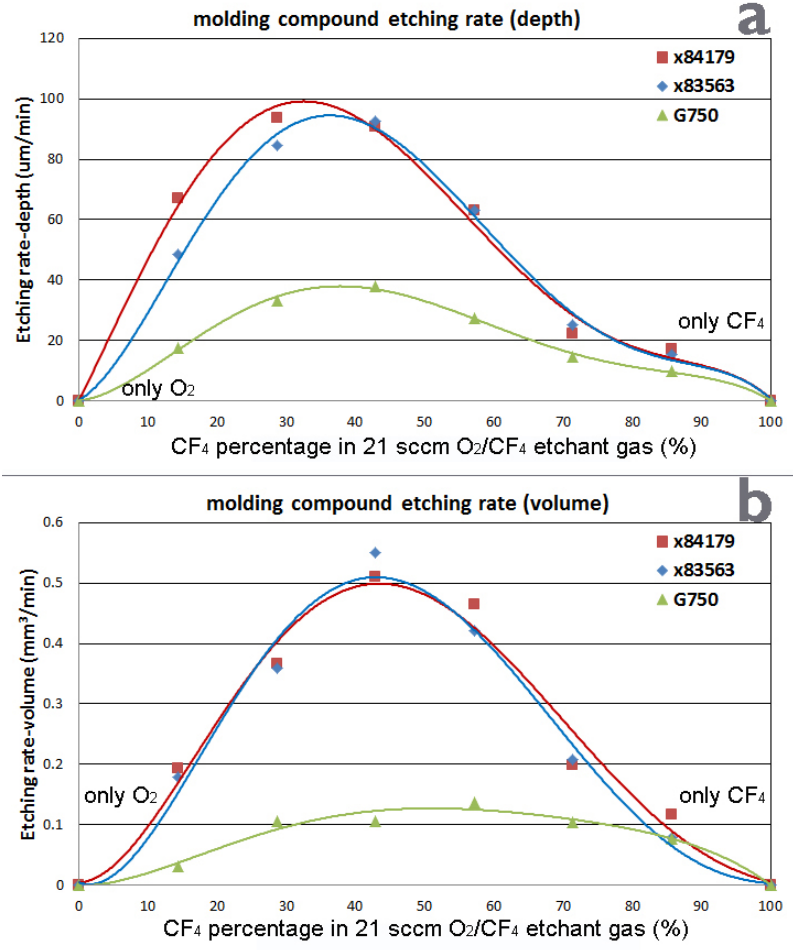

Fig.4-11 Molding compound (X84179, X83563, G750) etching rate versus percentage of CF_4 in O_2/CF_4 etchant gas. Argon gas flow: 1400 sccm, O_2/CF_4 combined gas flow: 21 sccm, input microwave power: 60 W. (a) vertical etching rate in µm/min; (b) volumetric etching rate in mm^3/min.

4.5 MIP Afterglow Etching of Si and SiO_2

During the decapsulation process, silicon is the chip material that must be preserved, in the meantime silicon oxide being the filler material in Epoxy Molding Compound must be removed. The etching rate of Si and SiO_2 are measured under

the exact same plasma conditions used in molding compound etching experiments. Si wafer and quartz plate are etched under plasma afterglow for 10 minutes under each plasma recipe. Fig.4-12 shows the cross-section profile of Si and SiO_2, each after 10 minutes etching under the same plasma recipe. The surface is smooth, while the diameter and depth of spherical-cap-shaped etching result are different.

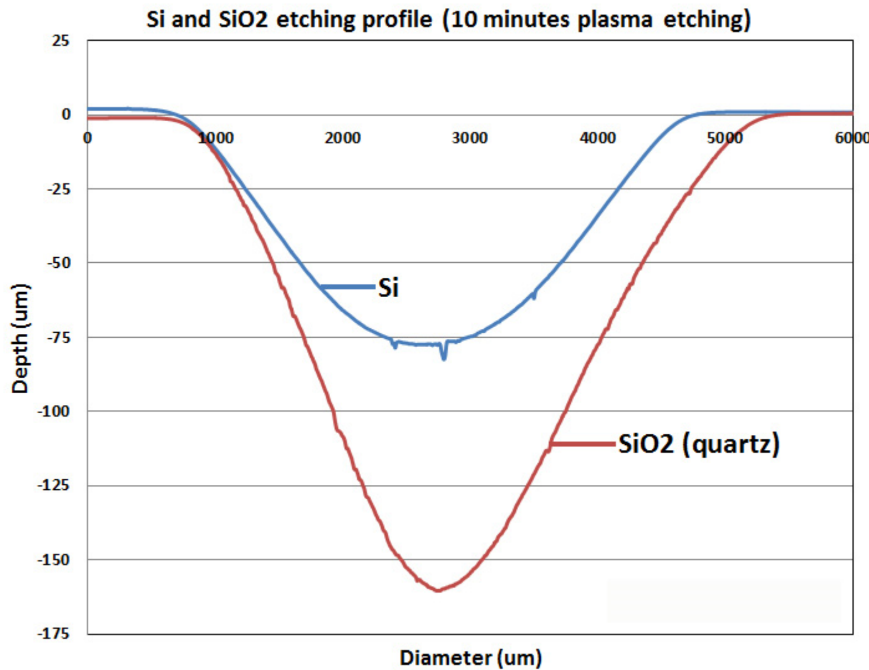

Fig.4-12 Cross-section profile of Si and SiO_2 after same recipe $Ar/O_2/CF_4$ plasma etching under 60 W power for 10 minutes

Si and SiO_2 etching under variable CF_4 percentage in O_2/CF_4 etchant gas is conducted. Etching reaction generates volatile SiF_4 thus bulk material etching can be achieved. The vertical and volumetric etching rates are calculated and plotted in Fig.4-13a and 13b, respectively. Maximum Si and SiO_2 etching rate evaluated by volumetric removal rate occurs at 70~80% CF_4 addition in the O_2/CF_4 etchant gas, where etching rate of Si is 0.13 mm^3/min and SiO_2 is 0.22 mm^3/min.

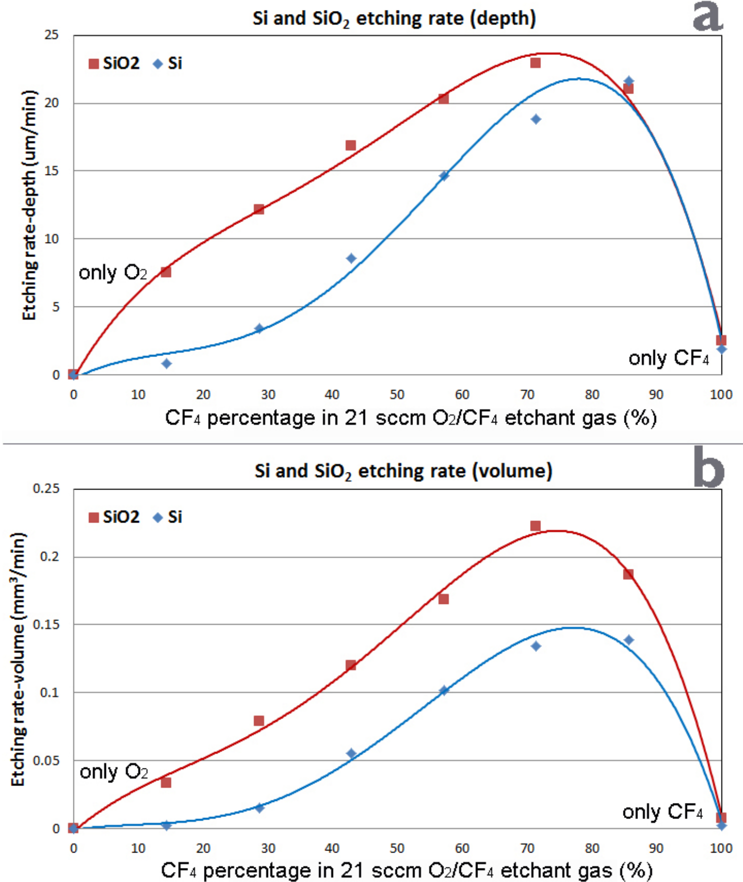

Fig.4-13 Si and SiO_2 etching rate versus percentage of CF_4 in O_2/CF_4 etchant gas. Argon gas flow: 1400 sccm, O_2/CF_4 combined gas flow: 21 sccm, input microwave power: 60 W. (a) vertical etching rate in µm/min; (b) volumetric etching rate in mm^3/min.

When 50~90% CF_4 is added, etching rate of SiO_2 is about 1.7 times of Si (see Fig. 4-14), implying similar etching mechanisms. Atomic fluorine in the plasma afterglow reacts with Si and SiO_2 forming volatile SiF_4. The molar volume of SiO_2 (22.69 cm^3/mol) is 1.88 times of molar volume of Si (12.06 cm^3/mol). It is highly possible that the difference in SiO_2 and Si etching rate is majorly due to the difference in their molar volume values. The reaction rate of fluorine radicals with Si element in both materials is the same, which implies that etching is dominated by the fluorine flux that reaches the reaction site.

When 15% CF_4 is added, etching selectivity of SiO_2 over Si reaches maximum value. Under this etching recipe, SiO_2 etching rate is 0.03 mm^3/min and is high enough to provide efficient etching.

It is reported that fluorocarbon film deposition during plasma etching plays a major role in determining Si and SiO_2 etching rates [86, 87] in RIE, the ion bombardment significantly influence the etching rate and selectivity of SiO_2 and Si. However, it is not possible to use ions in MIP afterglow etching as there are no ions involved in plasma etching. Conventional plasma etchers are built for large area uniform thin film etching, the etching rate of SiO_2 and Si is normally in the range of 0.3~1 µm/min [77, 86-89]. Our MIP instrument is built for localized high speed etching, the etching rate on 12 mm^3 area under 60 W power can reach a maximum 23 µm/min for SiO_2 and of 20 µm/min for Si, which is best suitable for bulk material etching like back-side thinning applications.

The effect of adding O_2 in Ar/CF_4 plasma to increase Si etching rate is demonstrated in Fig. 4-15. The surface image of Si after $Ar/CF_4/O_2$ plasma etching shows grain-like structures and the surface is much rougher than the Ar/CF_4 plasma etched comparison (see Fig. 4-16).

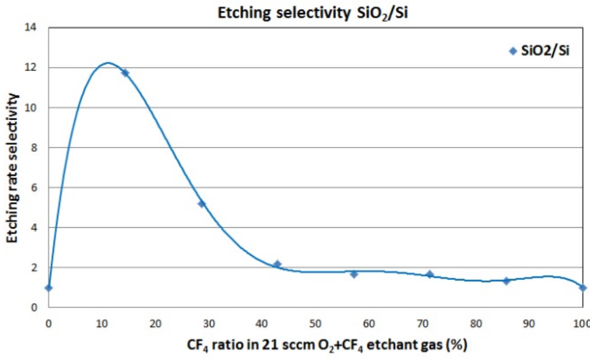

Fig.4-14 SiO_2/Si etching selectivity under varies percentage of CF_4 in O_2/CF_4 etchant gas

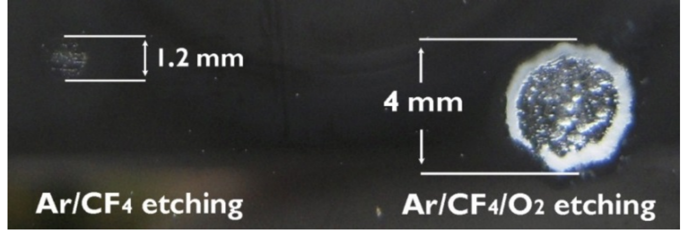

Fig.4-15 Si etching for 10 minutes under 60 W power with Ar/CF_4 plasma (left); $Ar/CF_4/O_2$ plasma (right)

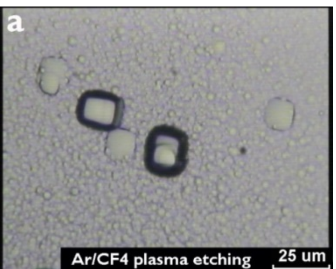

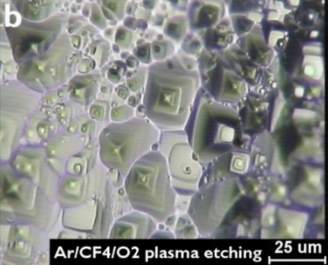

Fig.4-16 Optical microscope images of Si after 10 minutes etching with (a) Ar/CF_4 plasma; (b) $Ar/CF_4/O_2$ plasma

4.6 MIP Afterglow Etching of Si_3N_4

In the decapsulation process, Si_3N_4 passivation layer on the Si die has to be preserved. After non-destructive analysis of the die, removal of Si_3N_4 passivation layer is often performed to gain physical access to the metal layers beneath [22]. Such process is normally conducted by using Reactive Ion Etching (RIE) in a vacuum chamber [90]. RIE uses a combined effect of ion bombardment and chemical etching to remove materials selectively. RIE has the advantage of large area uniform etching, while the drawback is high potential to damage the die due to ion bombardment and exposure under electromagnetic field. Reported works on reduced pressure plasma etching show etching selectivity of SiO_2 over Si_3N_4 is correlated to the fluorocarbon film deposition on the reaction surface, while the selectivity value is in the range of 10~30 under optimal plasma recipe [91-93].

The afterglow generated by our MIP system etches isotropic due to the lack of ion bombardment. Removal of Si_3N_4 passivation layer can be achieved by etching with a fluorine-containing plasma to generate volatile SiF_4. Fig.4-17a shows the device before Si_3N_4 removal. The edge of the Si_3N_4 passivation layer can be clearly seen and it is indicated by the black arrow. The left and lower part of the die is covered by Si_3N_4 passivation. Fig. 4-17b shows the device during Si_3N_4 etching by Ar/CF_4 MIP afterglow. The edge of the Si_3N_4 passivation layer becomes less sharp but still can be observed. The die surface becomes colorful due to light interference caused by the reduction of Si_3N_4 layer thickness. The Si die is still covered by a thin layer of passivation. Fig. 4-17c shows the device after Si_3N_4 removal by Ar/CF_4 MIP afterglow etching. The edge of the Si_3N_4 layer disappeared and the Si die is completely exposed.

The CCD camera which provides real-time imaging of the sample surface under MIP afterglow etching is helpful to control the Si_3N_4 layer removal process and for endpoint detection. Changes in light interference due to the Si_3N_4 thickness reduction can be clearly captured by the CCD camera. In real-time monitoring, the color of the die first change rapidly as the Si_3N_4 layer is being etched quickly. Then the rate of color change slows down dramatically once the Si_3N_4 layer is almost removed.

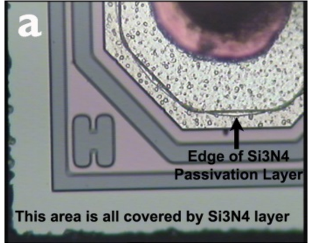

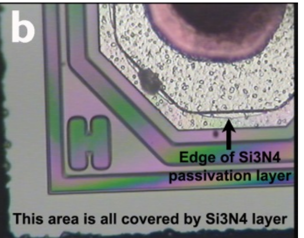

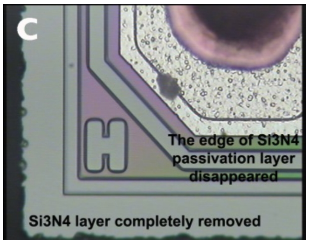

Fig.4-17 Device (a) before (b) during (c) after Si_3N_4 removal

Parameters that influence Si_3N_4 removal by using the MIP system are investigated. SOT23 copper wire bonded package with one diode device inside is used in the experiment. Firstly, the diode dies are cleanly exposed while the Si_3N_4 passivation layer and Si die remain undamaged. Then, different plasma etching recipes are used to remove the Si_3N_4 layer and photos of the die after different etching duration are taken to compare the results.

A. The effect of CF_4 amount in an Ar/CF_4 plasma

The variation of CF_4 amount in the plasma does not play a major role in Si_3N_4 etching. Under the 1400 sccm Ar plasma carrier gas flow, and constant 35 W absorbed power level, variation in CF_4 etchant gas addition from 4 sccm to 16 sccm does not seems to strongly influence the atomic fluorine flux because the free electrons with enough energy to dissociate CF_4 are about the same amount. Since the etching results are similar, atomic F flux should be similar.

B. The effect of absorbed power levels in an Ar/CF_4 plasma

The variation of absorbed microwave power in the plasma plays a major role in Si_3N_4 etching under the same CF_4 addition amount. Higher absorbed power level may increase the amount of free electrons with enough energy to dissociate CF_4 to atomic fluorine. The combined effect of higher fluorine flux and higher effluent temperature contributes to the increase of Si_3N_4 etching rate.

C. The effect of oxygen addition into an Ar/CF_4 plasma

The addition of O_2 into an Ar/CF_4 plasma significantly increases the Si_3N_4 etching rate (see Table 4-5). During the experiment, absorbed power level is kept at 35 W and CF_4 addition is kept at 8 sccm. Comparing horizontally in step 1 after 10 seconds etching, the Si_3N_4 layer in Sample 1 is merely etched while Sample 2 & 3 showed complete removal of Si_3N_4. Comparing horizontally in step 2 after 40 seconds etching, severe over-etching on Si die takes place in Sample 2 & 3 while in Sample 1 the Si_3N_4 layer still has not been completely removed yet. Further etching with an Ar/O_2/CF_4 plasma results in severely damaged silicon die.

Oxygen addition into an Ar/CF_4 plasma induces formation of COF_2 and cause drastic increase in atomic F flux. For this MIP system, the addition of O_2 into CF_4 plasma greatly increases Si, SiO_2, and Si_3N_4 etching rate at the same time.

Table 4-5. Si_3N_4 etching by an $Ar/CF_4/O_2$ plasma

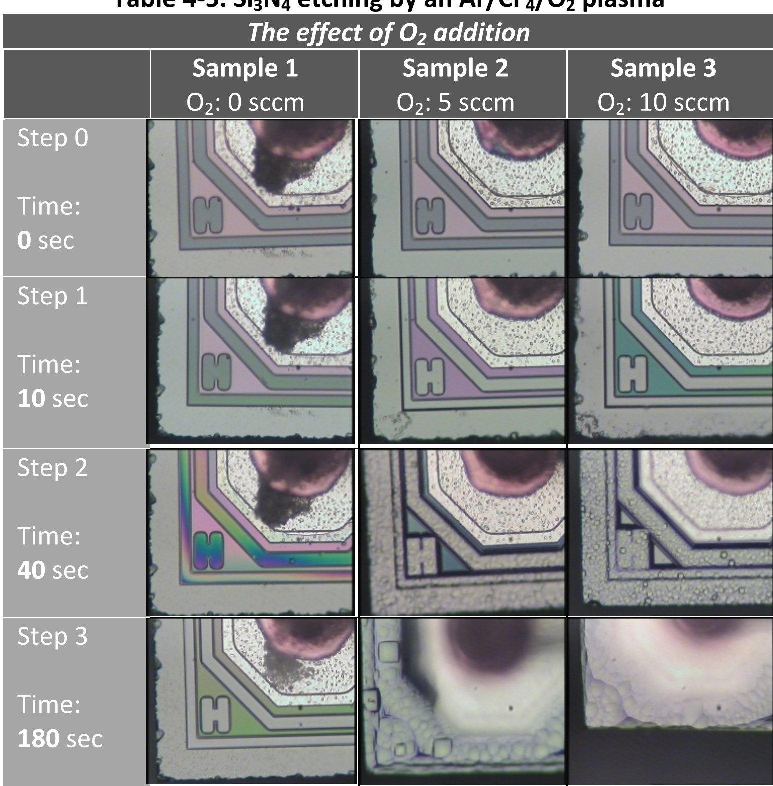

The effect of O_2 addition			
	Sample 1 O_2: 0 sccm	**Sample 2** O_2: 5 sccm	**Sample 3** O_2: 10 sccm
Step 0 Time: **0** sec			
Step 1 Time: **10** sec			
Step 2 Time: **40** sec			
Step 3 Time: **180** sec			

D. Controlled Si_3N_4 passivation layer removal on large die

The degree of influence on the Si_3N_4 etching rate by an Ar/CF_4 plasma is as follows: oxygen addition being the most influential followed by the absorbed microwave power level, while CF_4 variation being the least effective factor. For controlled Si_3N_4 removal, Ar/CF_4 etching at low absorbed power level is more advisable as both fast etching rate and excellent process control can be achieved at the same time.

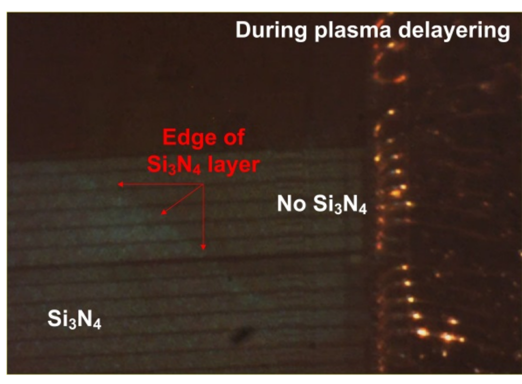

Fig.4-18 Real-time imaging of the plasma etching process demonstrating controlled Si_3N_4 removal

To enable endpoint detection and improve process control, a beam of light from an external light source is directed to the die surface with a certain viewing angle to the imaging path of the CCD camera. When the light path is correctly positioned, the interference of light in the Si_3N_4 passivation layer as well as the difference when no Si_3N_4 layer is on the die surface can be distinguished from the images from the CCD camera (See Fig.4-18). In such a way, the Si_3N_4 layer removal can be monitored real-time and the complete delayering process takes 3 minutes for a die with 4 mm x 4 mm area.

4.7 MIP Afterglow Etching of Silicone

Silicone is commonly used as lens material for high-power Light Emitting Diode (LED) packages and also as chip-coat material for semiconductor packages [21]. Silicone is composed of both organic and inorganic materials, where silicon atoms are chemically bonded to carbon atoms forming Si-O backbone with different functional side-groups.

For silicone etching rate measurements, flip-chipped sapphire substrate GaN-based LED packages without phosphor are used. The silicone lens (1.5 mm thick) on the LED package is etched under the plasma afterglow with different etching recipes. The time needed to remove the silicone lens is measured and the silicone etching rate is calculated from dividing the silicone lens thickness by the total etching time. The volumetric etching rate can be calculated with the diameter and height of the hemispherical silicone lens.

Commercial LED package products are used in order to provide more accurate etching rate measurements. A different approach is to prepare silicone samples by molding commercially available uncured silicone gel and use it for subsequent etching rate measurements. However, it is found that cured silicone with different part numbers have different mechanical and thermal properties compared to the silicone encapsulant used on commercial LED packages. Thus, silicone lens on commercial LED package is chosen as the test vehicle at last to best represent the real case studies.

Silicone etching by an $Ar/O_2/CF_4$ MIP afterglow is evaluated. Ar is used as the plasma carrier gas and its flow rate is kept constant at 1400 sccm. O_2 and CF_4 are the plasma etchant gas and their combined flow rate is kept at constant 21 sccm. The only variable is the percentage of CF_4 in the O_2/CF_4 etchant gas.

The maximum silicone etching rate is found to be between 65% - 85% CF_4 amount in the O_2/CF_4 etchant gas (see Fig.4-19). 200 µm/min silicone etching rate on a confined area under the MIP afterglow corresponds to 0.7 mm^3/min volumetric removal rate. With 0% CF_4 addition and 100% O_2 addition in the etchant gas, atomic oxygen radicals only react with the organic components in silicone leaving

powder-like silicon oxide on the silicone lens surface. The bulk silicone becomes brittle after long time exposure and cracks takes place. With 0% O_2 addition and 100% CF_4 addition in the etchant gas, silicone etching rate is too low to be measured compared to circumstances where both O_2 and CF_4 are added. In silicone materials, Si-O chemical bonds form the backbone structure. Organic groups like methyl and phenyl attach to the side chains to provide different material characteristics. To achieve high plasma etching rate, atomic fluorine is needed to completely break the Si-O chains forming volatile SiF_4, while atomic oxygen is needed to completely remove the organic side chains forming volatile CO_2. The addition of O_2 into CF_4 plasma also enhances the production of fluorine atoms in the effluent that facilitates silicon-containing material etching rate. The optimal mixing percentage of O_2 and CF_4 in the etchant gas is dependent on the silicon and carbon composition in the specific silicone material.

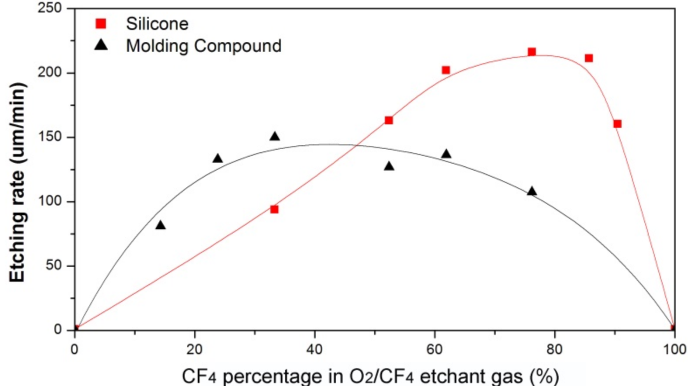

Fig.4-19 Etch rate of silicone under MIP afterglow with different mixing percentage of CF_4 in the O_2/CF_4 etchant gas. Argon gas flow rate = 1400 sccm, O_2/CF_4 total gas flow rate = 21 sccm, absorbed microwave power level = 60 W. For comparison, data on epoxy mold compound etch rate under the same MIP configuration is also plotted here.

Silicone in elemental composition is similar to epoxy molding compound, while in molecular composition or chemical bonds the two are very different. Compared to silicone lens etching, epoxy molding compound etching requires a lower CF_4 percentage where the maximum etching rate is found to be with 30% - 60% CF_4 addition [94] under the same experiment condition (see Fig.4-19). In molding compound, cured epoxy forms the backbone structure with C-C and C-O chemical bonds. Silicon dioxide used as the filler material in plastic molding compound accounts for 70% - 90% weight percentage. During $Ar/O_2/CF_4$ plasma etching, atomic oxygen etches away cured epoxy in the molding compound. Atomic fluorine etches only partly the SiO_2 fillers to cause the silica agglomerate structure become loose. And then the loosened silica fillers are blown away by gas flow.

Thus only a small portion of SiO_2 fillers has to be chemically etched by the MIP effluent, while the majority part of SiO_2 fillers is removed by gas blowing rather than plasma etching. It is highly possible that the amount of Si being chemically etched in silicone lens is much higher than that in epoxy molding compound encapsulant. As a result, maximum silicone etching rate is achieved with higher CF_4 percentage in the O_2/CF_4 etchant gas compared to epoxy molding compound etching under the same MIP etching condition.

The results on silicone lens etching by MIP afterglow are compared with data from literatures on PDMS etching by reduced pressure plasma. PDMS, having different properties to the silicone lens used on LED packages, is a different type of silicone commonly used for microelectromechanical systems fabrication. It is reported that 60~70% of CF_4 amount in the O_2/CF_4 etchant gas in reduced-pressure plasmas results in maximum PDMS etching rates [95-97], which is in the similar CF_4 percentage range in our atmospheric pressure MIP etching results. This indicates although the mechanical and thermal properties of PDMS and silicone lens used on LED packages are different, the chemical composition of the two types of silicone is similar thus their behavior under O_2/CF_4 plasma etching is similar. The PDMS etching rates by vacuum plasma are in the range of 0.3 – 4 µm/min on wafer scale [95-97], while silicone lens etching rates by MIP are in the range of 100 - 200 µm/min on a 12 mm^2 circular area. The higher silicone etching rates in MIP is accredited to the high radical flux generated by the highly confined plasma. With a plasma volume of only 23 mm^3, the power density in an atmospheric pressure MIP is much higher than a reduced pressure RF plasma counterpart.

4.8 MIP Afterglow Etching of Metals

4.8.1 Plasma Etching of Copper

Copper can react with chlorine-based plasma forming porous $CuCl_x$ film that can be removed by a consequent cleaning process [98-100]. Hydrogen-based plasma is also found to etch copper forming possibly CuH [101, 102]. Fluorine based plasma reacts with Cu forming colorless CuF_2 [103], however, copper fluoride is a passivation layer that blocks the diffusion of chemicals [104] and cannot be easily removed.

In a high temperature $Ar/O_2/CF_4$ plasma etching environment, copper bond wires may react with oxygen and fluorine radicals forming CuO_x and CuF_x, respectively. Thus it is important to evaluate the potential damage to copper bond wires under different etching conditions and optimize the process to reduce such reactions.
Bare copper bond wires with 23 µm diameter are used in the experiment. The original copper wire samples have the same initial state showing reddish color and smooth surface. Different plasma recipes are then applied and optical images of copper surface are taken at different time span.

A. Ar/CF_4 plasma etching of copper wires

Examining Sample A1~A3 (see Table 4-7), etching under CF_4 plasma has little effect on the copper wires. The increase of etching duration does not cause observable change in copper surface conditions up to 400 seconds etching. The increase of absorbed microwave power elevates the radical flux as well as the processing temperature. However, in the range of 27 W to 45 W absorbed power levels no observable change on the surface property of copper wires is found. SEM images also confirm the copper wires remain smooth surface after Ar/CF_4 etching.

In a CF_4 plasma at elevated temperature, the atomic fluorine radicals can react with copper and form a colorless copper fluoride thin passivation layer that prohibits further reaction. In the operation range in this experiment copper wires do not suffer obvious surface damage due to CF_4 plasma etching.

Table 4-7. Copper wires etched under CF_4 plasma

	Same CF_4 amount		
	Sample A1 Power: 27 W	**Sample A2** Power: 35 W	**Sample A3** Power: 45 W
Step 0 Time: **0** sec			
Step 1 Time: **30** sec			
Step 2 Time: **100** sec			
Step 3 Time: **400** sec			

B. Ar/O_2 plasma etching of copper wires

Examining Sample B1~B3 (see Table 4-8), etching under O_2 plasma can cause severe damage to the copper wires. Increasing etching duration has obvious impact on the copper wire condition. Comparing vertically Sample B1 for example, the copper wire appears to be smooth and show metallic luster after 100 seconds

etching, while after 400 seconds etching the wires becomes rough and dull indicating oxidization. The increase of absorbed power level also causes significant damage to the copper wires. Comparing horizontally Step 2 for example, the increase of power level causes copper wire to oxidize more readily, where the damage is lowest in Sample B1 and highest in Sample B3.

The atomic oxygen in an O_2 plasma at elevated temperature readily reacts with copper forming Cu_2O and then CuO. Exposure of copper wires under high power for a short time or low power for a long time all cause severe oxidization damage. For decapsulation of plastic semiconductor packages, atomic oxygen is needed to etch epoxy in the molding compound. Under the same system configuration, a lower power plasma requires longer processing time. When developing O_2 containing plasma recipes for decapsulation, care must be taken to balance the etching temperature and duration so that the copper bond wires remain undamaged.

Table 4-8. Copper wires etched under O_2 plasma

Same O_2 amount			
	Sample B1 Power: 27 W	**Sample B2** Power: 35 W	**Sample B3** Power: 45 W
Step 0 Time: **0** sec			
Step 1 Time: **30** sec			
Step 2 Time: **100**sec			
Step 3 Time: **400**sec			

C. Ar/O_2/CF_4 plasma etching of copper wires

When both O_2 and CF_4 gas are added to the plasma, etching damage to copper wire is less severe compared to Ar/O_2 plasma etching but more apparent than Ar/CF_4 plasma etching. Exposure of bare copper wire under 35W Ar/O_2/CF_4 plasma etching for 400 seconds does not cause apparent change on the surface color and smoothness of copper.

4.8.2 Plasma Etching of Aluminum

Aluminum bond pad surface is always covered by a thin layer of native Al_2O_3 film of a few nanometers thick. Fluorine radicals in CF_4 plasma can react with Al_2O_3 and Al, forming AlF_3 [105-108]. Because AlF_3 is a nonvolatile material, it forms a passivation layer on the bulk Al bond pad surface and prevents further etching of Al. Etching experiments with $Ar/O_2/CF_4$ MIP afterglow etching show aluminum bond pad remains intact even after long time exposure under fluorine plasma dry etching (see Fig.4-20).

Hydrogen Fluoride (HF) and Buffered Hydrogen Fluoride (BHF) solution are capable of etching Al and Al_2O_3. Reported etching rate is in the range of 100 nm/min [109, 110], while in our experiment the aluminum bond pad becomes apparently corroded or partially removed after immersion in BHF solution for one hour (see Fig.4-21).

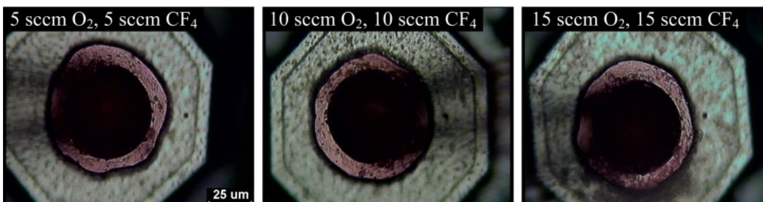

Fig.4-20 Aluminum bond pads beneath copper wire bonds remain intact after long time exposure under different $Ar/O_2/CF_4$ dry plasma etching recipes.

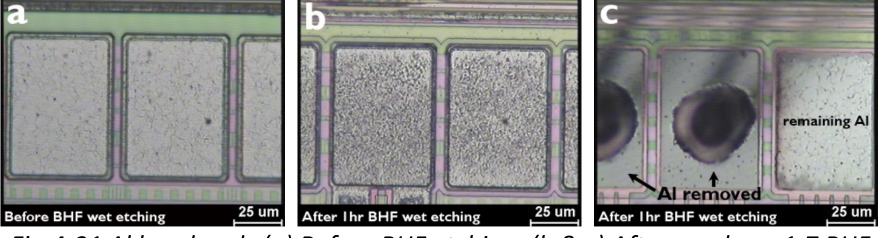

Fig.4-21 Al bond pads (a) Before BHF etching; (b & c) After one hour 1:7 BHF etching at 25°C

The great difference in aluminum etching by dry fluorine-containing plasma and wet HF solution implies the crucial role of water molecules during fluorine-induced corrosion reactions. The effect of water molecule in $Ar/O_2/CF_4$ plasma etching of aluminum bond pad is evaluated by spraying liquid deionized water (H_2O) onto the bond pad during plasma etching (see Fig.4-22). The addition of water molecule dramatically increased the aluminum etching rate by forming $Al(OH)_3$ crystals [111] thus removing the AlF_3 passivation layer. Compared to BHF etching, plasma/water combined etching rate of aluminum is at least 100 times faster, which is most likely due to the presence of highly reactive atomic fluorine in H_2O solution at high temperature (250°C bond pad surface temperature).

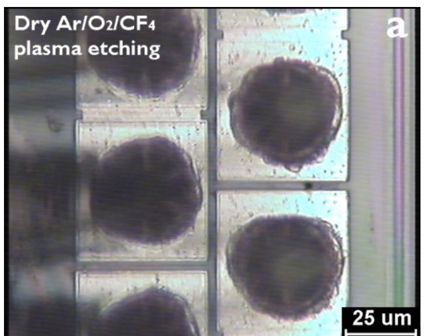

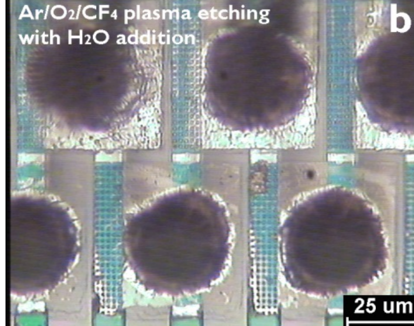

Fig.4-22 Aluminum bond pad (a) After dry Ar/O_2/CF_4 plasma etching; (b) After 30 seconds etching by Ar/O_2/CF_4 plasma with H_2O sprayed on the aluminum surface

There are three possible sources that water molecules may be introduced during plasma etching process or after decapsulation process, while all may result in potential damage to aluminum bond pads thus need to be avoided.

One source of water molecules is from the IC package itself. Especially when the package has gone through temperature humidity qualification tests, moisture can be absorbed into the molding compound material. During Ar/O_2/CF_4 plasma decapsulation, the H_2O molecules that are absorbed inside the epoxy molding compound may aid fluorine radicals in the plasma afterglow to cause rapid etching of aluminum bond pads. This source of water introduction can be avoided by a pre-baking process of the IC package in a furnace to remove moisture, before conducting plasma decapsulation.

The second source is during the ultrasonic cleaning step that is used to remove silica filler agglomerate residue after molding compound removed by plasma. As deionized water is used as the medium in ultrasonic cleaning, moisture may not be removed from the aluminum bond pad area if the sample is not completely dried. This source of water introduction can be avoided by completely drying the sample with N_2 gas blowing.

The third source is moisture from the environment. In one experiment, aluminum bond pads are treated with Ar/O_2/CF_4 MIP etching and then stored in normal air environment for 30 days to evaluate the prolonged corrosion effect (see Fig.4-23). After storage in normal air for 30 days, the aluminum bond pad surface showed corrosion spots that are not found when the same sample is just prepared after Ar/O_2/CF_4 dry plasma etching. Energy-dispersive X-ray spectroscopy (EDX) measurements (see Fig.4-24) of the corroded aluminum bond pad are performed. High concentration of fluorine is found on the corrosion spots. Reported work has shown CF_4/O_2 plasma treated aluminum bond pads may experience corrosion damage when stored in 50% humidity environment, forming $Al(OH)_3$ or $Al(OF)_x$ crystals and show ‘water-lily’ defects [108]. The corrosion effect in our experiment

is likely due to similar reasons. This finding suggests that IC package samples decapsulated by $Ar/O_2/CF_4$ plasma are better to be analyzed quickly. Otherwise the samples must be stored in moisture free environment in order to prevent prolonged corrosion damage to aluminum bond pads.

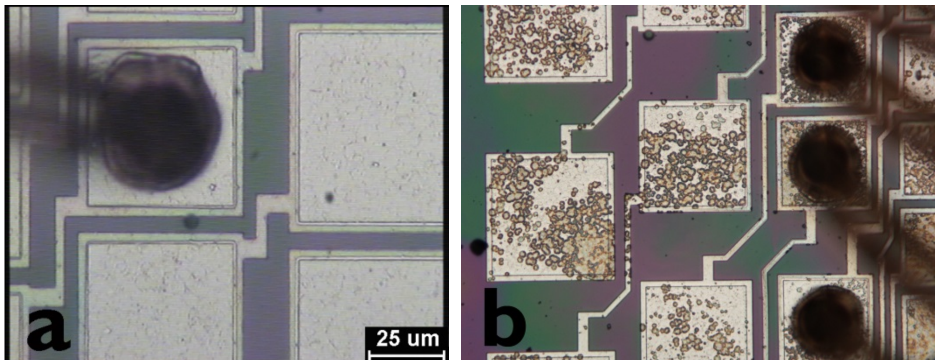

Fig.4-23 Aluminum bond pad (a) Right after dry $Ar/O_2/CF_4$ plasma etching; (b) After storage in normal air environment for 30 days, aluminum bond pads show yellow corrosion spots.

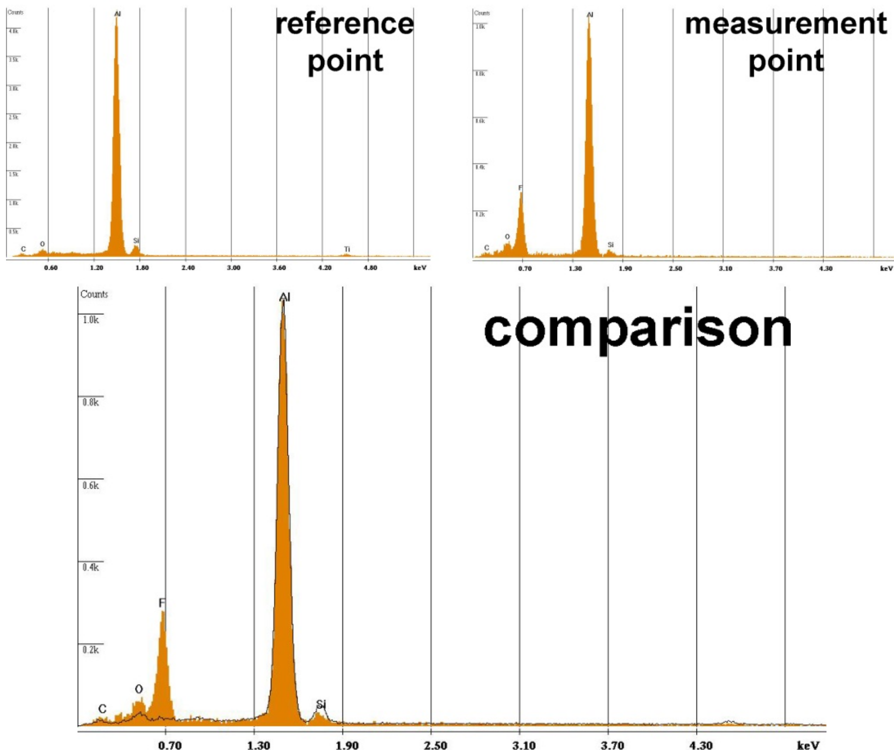

Fig.4-24 EDX on reference point on aluminum pad, corrosion spot, and comparison

4.8.3 Plasma Etching of Palladium

Palladium etching by $Ar/O_2/CF_4$ plasma is extremely difficult because PdF_2 is nonvolatile. Reported works have shown that ion bombardment by argon is needed to remove the PdF_2 passivation to achieve palladium etching, while chemical etching of palladium by fluorine radicals is not possible [112]. Due to this reason, palladium etching is often done by wet etching in concentrated nitric acid or aqua regia [103].

Palladium etching experiments are conducted by placing palladium coated copper bond wires under $Ar/O_2/CF_4$ MIP afterglow etching. The palladium coating layer originally looks silver white and has smooth surface (see Fig.4-26a). The key element in CF_4 plasma etching of palladium is found to be water. PdF_2 is reported to react with water and hydrolyze [103, 113]. When Pd-coated Cu wire is repeatedly etched by dry $Ar/O_2/CF_4$ plasma and then ultrasonic cleaned in water, the palladium layer comes off leaving a rough copper surface (see Fig.4-26b). It is likely that during dry etching fluorine radicals in plasma react with palladium and form PdF_2 passivation layer on the palladium surface, the subsequent ultrasonic cleaning in deionized water cause hydrolysis of PdF_2 and the cavitation force removes this PdF_2 layer. By conducting plasma etching followed by ultrasonic cleaning process, palladium undergoes etching/hydrolysis/removal sequence. Such palladium removal process takes about 30 minutes to completely remove the thin palladium layer on copper wire bond.

The most efficient way to remove palladium is found to be using $Ar/O_2/CF_4$ plasma etching while spraying water on palladium surface. Such process takes only 1 minute to remove palladium coating layer on copper wire. Etching result in Fig.4-26c shows the palladium coating layer on the upper half of copper wire is removed thus the wire looks reddish, while the lower part of copper wire is not exposed to water during etching thus is still covered by palladium and the wire looks silver white. The surface condition of both exposed copper and remaining palladium are smooth and shiny, indicating the high etching selectively of palladium over copper.

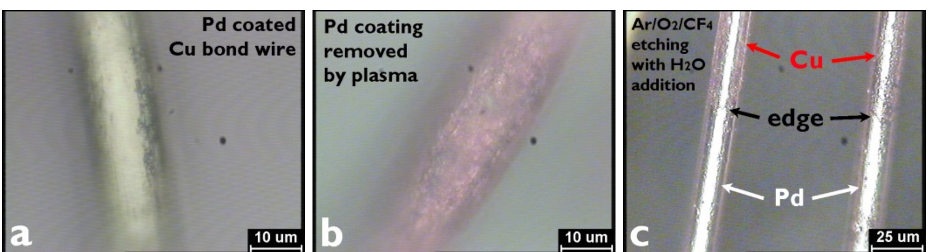

Fig.4-26 Pd coating layer on Cu bond wire (a) Before etching; (b) After 30 min consequently dry $Ar/O_2/CF_4$ plasma etching and ultrasonic cleaning in water; (c) After 1 min $Ar/O_2/CF_4$ plasma etching while spraying water on Pd surface

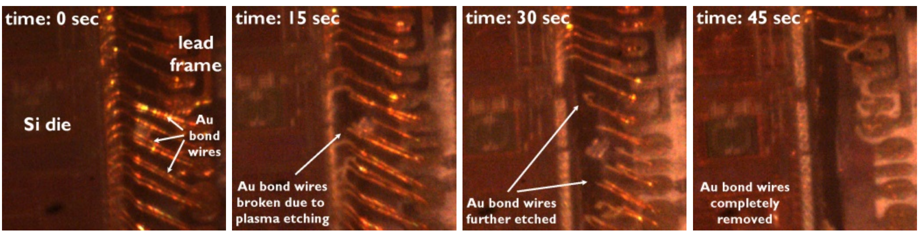

Fig.4-27 Gold bond wires (diameter 18 µm) etched by 35 W $Ar/O_2/CF_4$ plasma afterglow for 0, 15, 30, 45 seconds

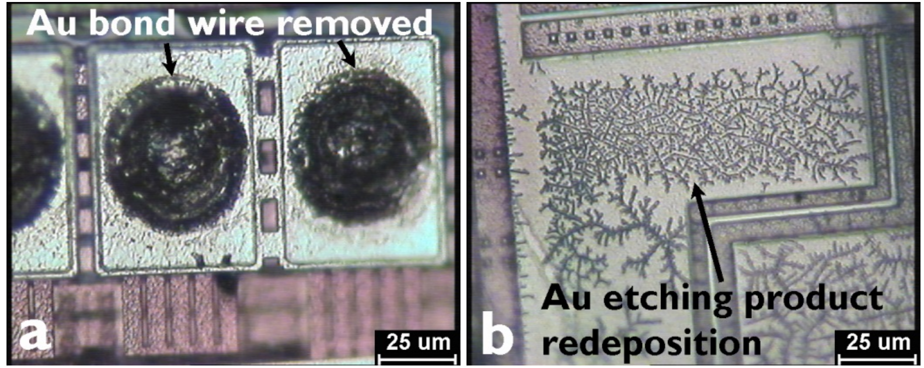

Fig.4-28 (a) Gold ball bond removed on aluminum bond pad after plasma etching, leaving the Au/Al intermetallic compound layer on the bonding surface; (b) Redeposition of gold etching product on aluminum structures on the silicon die surface.

4.8.4 Plasma Etching of Gold

Dry etching of gold in semiconductor devices is normally conducted by Reactive Ion Etching (RIE) with chlorine and/or fluorine radicals, generating $AuCl_x$ and AuF_x etching products. Argon ion bombardment on gold surface is reported to be crucial in the etching process thus RIE is normally used rather than afterglow etching. Typical gold etching rate is in the range of 0.1~1 µm/min [114-116] in the presence of ion bombardment.

The capability of MIP afterglow removal of gold is conducted by placing gold bond wires (non-gold material < 100 ppm) under $Ar/O_2/CF_4$ plasma effluent etching (P=35 W, 1400 sccm Ar, 10 sccm O_2, 10 sccm CF_4). The etching process is monitored by the CCD camera and images of gold bond wires after 0, 15, 30, 45 seconds etching duration are recorded (see Fig.4-27). At 0 seconds, the intact gold wires have smooth surface. After 15 seconds etching, the top part of a few gold wire loops is broken. After 45 seconds etching, all the gold wires in an area of 1 mm × 1 mm are completely removed leaving Au-Al bonding feature on aluminum bond pad (see Fig.4-28a). The estimated gold etching rate is 20 µm/min. A cross-section of the exposed Au/Al bond by Focused Ion Beam (FIB) milling is made,

further EDX analysis showed the Au bond wire on the Au/Al ball bond is removed successfully and the Au-Al Intermetallic Compound (IMC) layer can be observed very well. Such Au bond wire removal ability by MIP afterglow etching gives the possibility to cleanly expose Au-Al IMC layer on an Au/Al ball bond, which is a process not achievable with other techniques thus provides a new approach to analyze the Au-Al IMC layer formation.

It is found that an Ar/O_2 plasma does not etch gold, while an Ar/CF_4 plasma etches gold at a low rate. Aldridge [115], Ranade *et al.* [114] reported adding O_2 in plasma decreases gold etching rate in RIE plasma. However, with our MIP afterglow etcher we observed the opposite effect. When O_2 is added into Ar/CF_4 plasma, gold etching rate drastically increases, which strongly suggests the afterglow etching is governed by fluorine radical flux.

Compounds that can be formed during $Ar/O_2/CF_4$ plasma etching are AuF [117, 118], AuF_3 [113, 116, 119], and AuF_5 [120]. The most likely etching product in this reaction is AuF_3, which is an orange crystalline solid [103] that sublimes at 300°C [113, 119]. The local temperature on the wire surface is likely to cause AuF_3 etching product to sublime thus fluorine radicals can continuously react with freshly exposed gold. Redeposition of yellow-orange solid gold etching product is found on unetched areas on the sample (see Fig.4-28.b). Focused ion beam cross-section of the branch-like structure on the redeposited film is made and EDX on the redeposited material confirms gold is the major composition.

In some semiconductor package decapsulation applications, gold wire bonding is used in the package and must be preserved after decapsulation. It is possible to prevent unwanted over-etching damage to gold wires when using $Ar/O_2/CF_4$ plasma etching. The key element is to reduce plasma afterglow gas temperature below 300°C, thus the etching product AuF_3 does not sublime. One of the application examples is MIP decapsulation of wire-bonded high-power LED packages, which will be discussed in Section 6.3.

4.9 Conclusions

Microwave induced plasma afterglow etching is a highly accelerated chemical reaction that is dominated by the flux of neutral radicals in the plasma effluent. Etching rate of a certain material depend on the volatility of the reaction product and processing temperature. High power density in plasma generates high radical flux, while the long lifetime reactive atoms and metastable molecules in the afterglow contribute to high etching rates.

The temperature distribution inside an IC package during MIP afterglow etching is evaluated. Suitable operation condition has a plasma effluent temperature of 400°C, resulting in an etching reaction interface temperature of 250°C and a bulk

IC package temperature of 100°C. The MIP system use the plasma afterglow to directly control the surface temperature where etching reaction takes place on the IC package sample, rather than using a separate heating element that is adopted in most plasma etchers. This configuration is more power efficient and induces less thermal mechanical stress to the IC package.

The plasma filament generated in the MIP system has extremely high power density (1600 W/cm^3 under 40 W input power) because the space where plasma is generated is very confined. For conventional plasma etchers that use a vacuum chamber, the plasma fills in a large part of the chamber and the power density is relatively low (300 W/cm^3 under 1 kW input power). The long lifetime (~2 ms) high density of oxygen and fluorine atoms (10^{16} cm^{-3}) generated by the high power density atmospheric pressure MIP afterglow ensures a high radical reactant flux and plasma etching rates.

The plasma etching chemical process is investigated and a complete set of MIP afterglow etching recipes are developed for Si, SiO_2, Si_3N_4, epoxy, epoxy molding compound, silicone, copper, aluminum, palladium, and gold, which includes all kinds of materials that may appear in an IC package (see Table 4-9). The optimal etchant gas composition and ratio for different materials are evaluated and compared. During MIP afterglow decapsulation of IC packages, preservation of wire bond and of die material is as crucial as achieving high encapsulation material removal rate. Plasma etching recipe has to be selected according to the decapsulation process and the specific failure analysis task, for instance what material or structure must be preserved while other material or structure can be sacrificed.

The fluorine atoms generated in CF_4-containing MIP afterglow readily reacts with metals and silicon-containing materials, forming metal fluorides and gaseous SiF_4, respectively. Etching rate greatly depends on the volatility of the etching product. Fluoride compounds of copper, aluminum, and palladium are nonvolatile thus forming a thin passivation layer that prohibits further bulk material etching, while gold fluoride is volatile thus causing gold to be rapidly etched in an $Ar/O_2/CF_4$ MIP afterglow.

A key element in CF_4-containing plasma etching of aluminum and palladium is found to be moisture, whereas the H_2O molecules react with aluminum fluoride and palladium fluoride forming easily removable products. Therefore, care must be taken to prevent introduction of moisture during or after $Ar/O_2/CF_4$ MIP afterglow etching, otherwise immediate or prolonged process-induced damage will appear on palladium-coated copper wires or aluminum bond pads.

Comparing to the etching rate values obtained from conventional plasma etchers, materials etching rate of this MIP system is at least 20 times faster. For IC package

decapsulation applications where normally an area of 1 cm^2 needs to be etched, using a confined plasma to scan across the IC package is more suitable than using a large chamber of plasma and a mask to define a small area that is intended to etch.

Table 4-9. MIP afterglow etching recipes & decapsulation process requirements

Material	Optimal plasma etching recipe	Etch rate @60W, vertical (µm/min)	Etch rate @60W, volume (mm^3/min)	Key element to preserve this material during MIP decapsulation
Si	O_2/CF_4 (70~80% CF_4)	21	0.13	No F in afterglow
SiO_2	O_2/CF_4 (70~80% CF_4)	23	0.22	Packaging material No need to preserve
Si_3N_4	O_2/CF_4		Bulk etching	No F in afterglow
Epoxy	O_2/CF_4		Bulk etching	Packaging material No need to preserve
Epoxy Molding Compound	O_2/CF_4 (30~60% CF_4)	40~100	0.14~0.51	Packaging material No need to preserve
Silicone	O_2/CF_4 (65~85% CF_4)	200	0.7	Packaging material No need to preserve
Copper	O_2,	oxidizatio n	~0	Low temperature, low etching duration
Aluminum	O_2/CF_4 with H_2O addition		Thin film etching	No presence of H_2O & F at the same time
Palladium	O_2/CF_4 with H_2O addition		Thin film etching	No presence of H_2O & F at the same time
Gold	O_2/CF_4	20 (@ 35 W)	Bulk etching	Low plasma effluent gas temperature < 300°C

Chapter 5

Microwave Induced Plasma Decapsulation of IC Packages

5.1 Introduction

This chapter focuses on the application of MIP afterglow etching for decapsulation of IC packages with copper or gold wire bonding. 90% of semiconductor packages use wire bonding interconnection [121]. Copper wire bonding being a new technology is gradually but steadily replacing gold wire bonding, about 15% of wire bonded devices use copper in year 2011 [121]. As components in the IC package have different structures and material composition, the plasma etching recipes that have been developed in Chapter 4 need to be combined with tailored processes with respect to the specific IC package structure and analysis objective.

In the early stage of this project, MIP decapsulation results are obtained by manually positioning the IC package under the plasma afterglow for etching. Thus etching process control and monitoring were not possible. As a result, molding compound can be removed effectively but the uniformity of etching was poor. Fig.5-1 shows a decapsulation result in the early stage. Although most part of the die has been exposed, a lot of problems need to be solved (see Fig.5-2): non-uniform etching, severe over-etching damage to the Si die, severe oxidization damage to the copper bond wires, and poor reproducibility, etc.

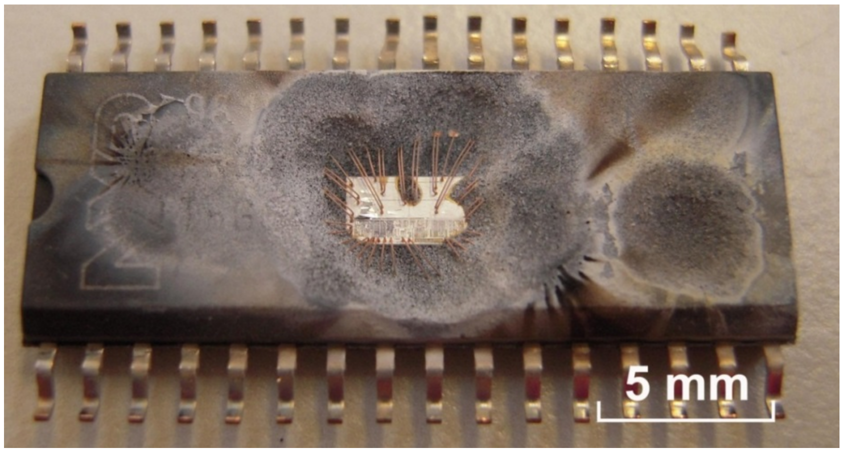

Fig.5-1 Early stage result on MIP decapsulation of a copper wire bonded IC package. Image shows the die is mostly exposed, while the areas on the upper and right edge is still covered by molding compound. Areas on lower-left die show severe over-etching damage. Si_3N_4 passivation layer and Si die are also damaged.

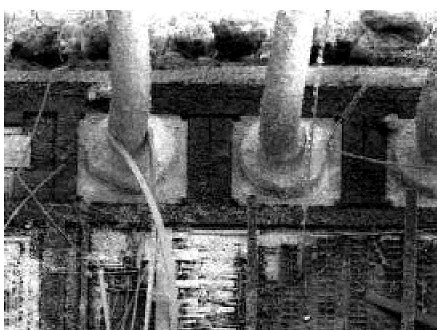
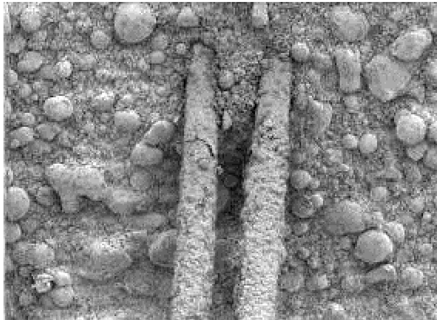

Fig.5-2 SEM images showing magnified details after MIP decapsulation in early stage. Left: severely over-etched die structures. Right: severely oxidized copper bond wires

This Chapter is divided into different sectors (5.2 - 5.5) based on four different decapsulation processes, namely:

- $Ar/O_2/CF_4$ plasma decapsulation
- $Ar/O_2/CF_4$ plasma + Ar/O_2 plasma decapsulation
- Laser-ablation + Ar/O_2 plasma decapsulation
- Laser-ablation + low power $Ar/O_2/CF_4$ plasma decapsulation

Each decapsulation process contains distinct recipes that solve typical types of IC package decapsulation problem, while each process has advantages and disadvantages compared to another process. Examples on decapsulation of commercial IC packages will be given to show why certain process is developed and how this process is useful for a typical type of failure analysis application.

The four decapsulation processes cover mostly all representative IC package decapsulation cases. By selecting a proper process, the following objectives can be achieved after decapsulation:

- Clean exposure of die, bond wires, and bond pads without process-induced damage
- No damage to the device electrical functionality
- Preservation of fine surface details on Cu, Pd-coated Cu, and Au bond wires
- No over-etching damage to Si_3N_4 passivation layer and Si die
- Clean exposure of high-density multi-tier fine-pitch wire bonds

Section 5.6 and 5.7 discuss applications of MIP decapsulation in challenging analysis cases, where the focus includes thermally stressed samples after quality tests, and samples with delamination defects. These typical types of cases are chosen because there are no other suitable decapsulation solutions at the

moment except MIP. And these cases are the typical failure analysis and quality control challenges faced in IC packaging industry due to the switch to copper wire bonding technology and the lack of a suitable decapsulation technology.

Section 5.8 discuss a case in failure analysis that acid decapsulation is not able to tackle due to the unavoidable corrosion damage to the copper wire bonds in samples after HAST quality tests. MIP decapsulation successfully solves this analysis problem and helped a company to accomplish a challenging copper wire reliability evaluation task.

Comparison of MIP decapsulation with the currently used alternative solution of cold acid decapsulation will be made. Section 5.3, 5.4, 5.6, 5.7 will show cold acid decapsulation comparisons that represents the best result one could achieve by wet etching. The superior ability of preserving minute surface features by MIP decapsulation in a reasonable time that facilitates further failure-site analysis will be demonstrated.

5.2 $Ar/O_2/CF_4$ Plasma Decapsulation

High power $Ar/O_2/CF_4$ plasma afterglow etching readily removes molding compound at a high rate, thus it seems to be the ideal solution for IC package decapsulation. However, etching uniformity is often poor and over-etching damage to Si die and Si_3N_4 passivation layer is severe, which makes devices always damaged after plasma decapsulation thus hampers further failure analysis. This section aims to mitigate the drawbacks when using this approach. Investigation on the optimal process and best achievable decapsulation result with $Ar/O_2/CF_4$ plasma will be discussed.

5.2.1 The Scan Etching Process

MIP afterglow etching has a circular effective etching area with 4 mm diameter. Many times the IC package size is larger than the plasma etching area thus the package has to be scanned under the plasma. Manual control of the scan process often leads to poor etching uniformity.

To solve the non-uniform etching and poor process control problem, a programmable XYZ-stage and a CCD camera are integrated in the MIP system. The XYZ-stage allows one to scan the IC package sample beneath the MIP effluent with a certain scan rate and scan path, therefore improving the etching uniformity.

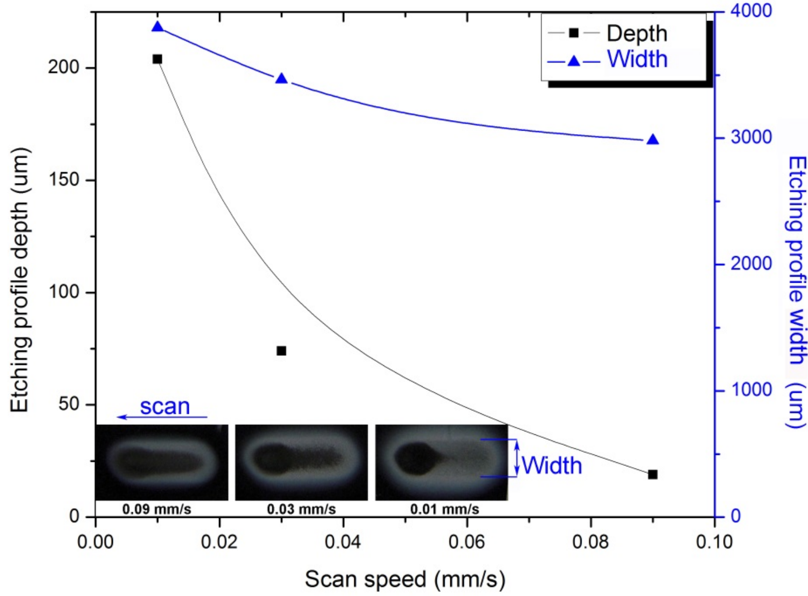

Fig.5-3 Ar/O_2/CF_4 MIP afterglow scan etching epoxy molding compound (from Sumitomo co.). Etching profile measured in depth and width versus scan speed.

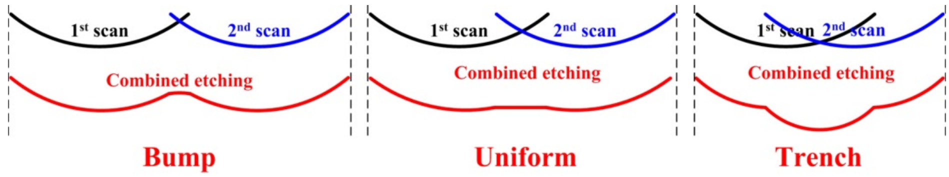

Fig.5-4 Combined etching profile of two scans

Besides the plasma etching recipe, more parameters need to be considered in order to achieve a large area uniform etching when scanning the plasma beam across the IC package. The influence of the scan speed to the etching profile is shown in Fig.5-3. Due to the movement of the XYZ-stage, etching leaves anisotropic trench-like profiles. The three samples are scanned with different speeds from right to left for 8 millimeters distance. The etching profile width and depth values are measured by Veeco Dektak150 surface profiler. Slower scan speed result in larger etching depth and width. The data is then used to design the scan route for real decapsulation applications.

The schematic representation of designing a uniform etching profile by combining multiple scans is shown in Fig.5-4. The scan speeds, the relative position between two scan paths, and the plasma recipe have combined effect on the final etching profile.

MIP afterglow decapsulation of plastic Small Outline (SO32) packages with 38 µm thick copper bond wires and a 3.4 mm * 2.0 mm * 0.4 mm silicon die is conducted. A photo of the package is shown in Fig.5-5 and its X-ray photo is shown in Fig.5-6. The package has 38 bond wires and 32 pins. The cross-section of the package is shown in Fig.5-7. The thickness of molding compound on top of the die is about 1000 µm.

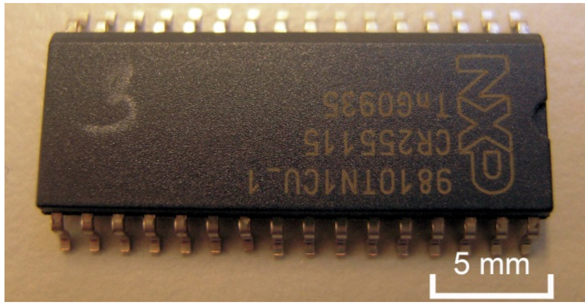

Fig.5-5 Plastic SO32 IC Package

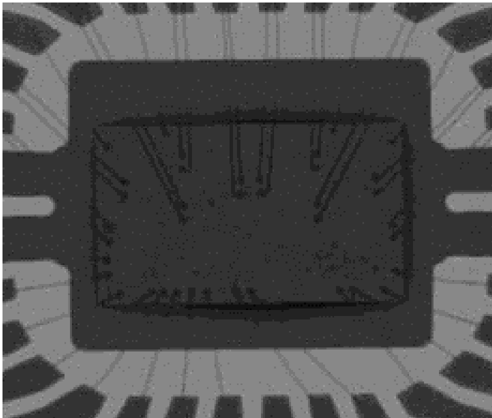

Fig.5-6 X-ray of the package

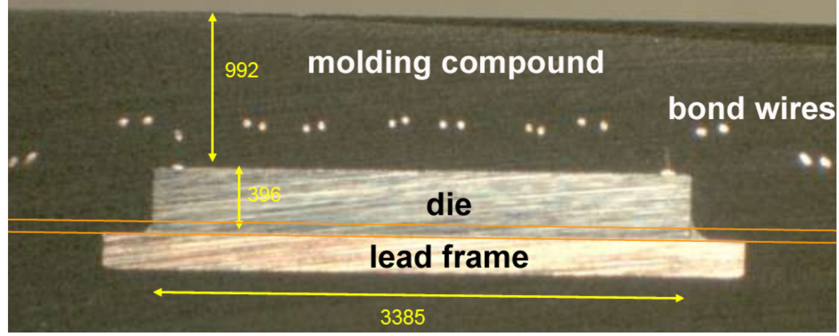

Fig.5-7 Cross section of the package (dimensions in µm)

Varying the scan speed during plasma etching on different regions is a solution to achieve a uniform etching profile. Optimization of the plasma recipe, the number of scans, and the scan routes is made to ensure high plasma etching rate while maintaining a high etching selectivity and uniformity. Table 5-1a lists the operation conditions for etching at varying scan speeds. Table 5-1b illustrates the scan route and etching result for each scan sequence.

Table 5-1a Operation conditions for etching at varying scan speed

	MW power (W)	Duration (min)
Scan sequence 1	100	10
Scan sequence 2	60	6
Scan sequence 3	60	5

Table 5-1b Scan routes under varying scan speed (mm)

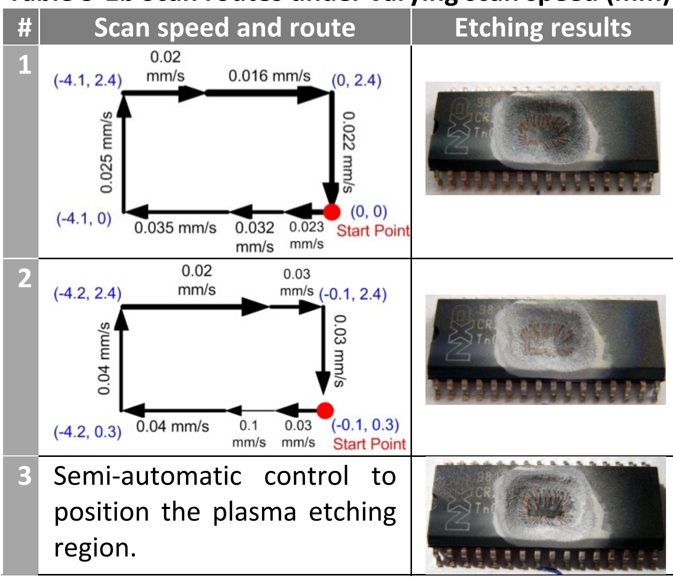

#	Scan speed and route	Etching results
1		
2		
3	Semi-automatic control to position the plasma etching region.	

The first scan is done under high power and varying scan speed with regard to the bond wire distribution under the epoxy molding compound. The positions of the bond wires are easily obtainable from inspection on a decapsulated package under the CCD camera or an X-ray image. The approximate position of the bond wires can be directly read out by the coordinate from the XYZ-stage. The general rule of defining the scan speed is to scan comparatively slower on regions that have bond wires underneath. The masking effect of the scattered bond wires to plasma etching is only a decrease in etching rate rather than a complete blockage. An optimized etching results in a uniform dent exposing the top parts of the bond wires.

The second scan also took the bond wire distribution into consideration and used lower microwave power. An inspection on the etching profiles resulted from the first scan is made in order to help defining the second scan route. Exposure duration of the copper wires under the plasma should be minimized as the oxygen abundant plasma effluent at elevated temperature easily causes oxidization on copper. After six minutes etching, most parts of the bond wires are exposed and a thin layer of molding compound is left on top of the die.

The third scan is done semi-automatically by scanning the package while inspecting the surface being etched through the CCD camera. A compromise is made between the plasma etching rate and etching controllability when exposing the silicon die beneath the molding compound.

The first and second etching processes are 100% reproducible. The third etching step can be replaced by an automatic scan but the algorithm to translate the bond wire positions and the non-uniform etching profile left on the surface is too complex and time consuming. Thus it is more advisable to conduct the final etching step by positioning the package with the help of the images received from the CCD camera.

5.2.2 The Decapsulation Results

The fully decapsulated package is shown in Fig.5-8. Cavity opening is sufficient for circuit access. Further inspection by SEM is shown in Fig.5-9. The copper bond wires and aluminum bond pads are in fair condition and showed no obvious damage. The copper ball bonds and wires suffer surface oxidization but showed no measurable reduction in size compared with the acid decapsulation results. The surface of the silicon die showed minute over-etching damage on the die structures. However, over-etching on the Si_3N_4 passivation layer is inevitable due to the chemical nature of fluorine radicals in the plasma afterglow.

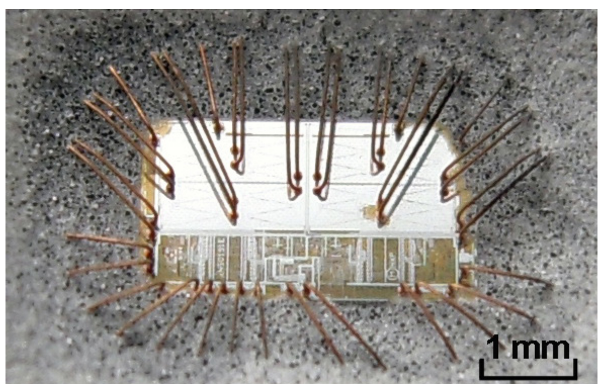

Fig.5-8 SO32 IC package after Decapsulation

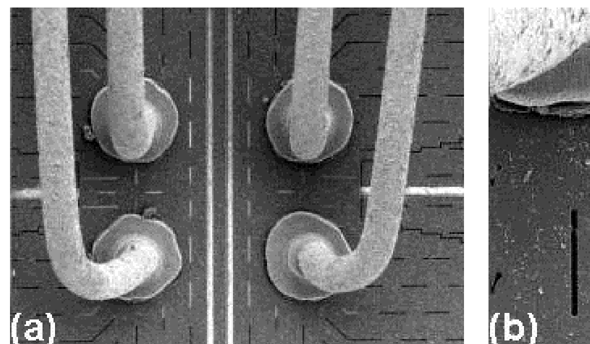

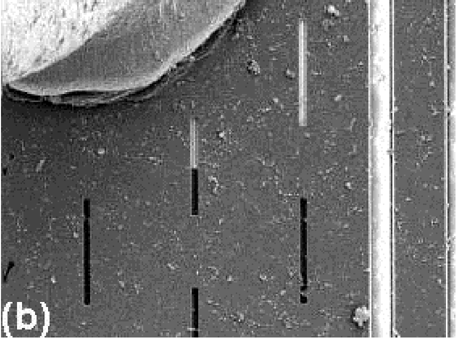

Fig.5-9 SEM pictures on decapsulated SO32 package: (a) bond wires, (b) die structures.

Wire pull and ball shear test on the 38µm-thick copper wire bonds are performed to evaluate the potential mechanical degradation due to plasma etching. The mechanical test data are within the specified range and showed no degradation in bond strength due to plasma etching.

In conclusion, with the help of programmable XYZ-stage and integrated CCD camera, $Ar/O_2/CF_4$ plasma afterglow etching provides fast and uniform decapsulation to expose copper wire bonds without damage. However, the over-etching damage to Si die and Si_3N_4 passivation layer cannot be avoided due to the fluorine atoms in the plasma afterglow. Unwanted etching on Si_3N_4 passivation layer or Si die structures introduces damage to the die, thus jeopardizing successfully finding the failure-site and the following root-cause analysis. The application of this $Ar/O_2/CF_4$ plasma decapsulation process is limited to wire bond analysis only.

5.3 $Ar/O_2/CF_4$ Plasma + Ar/O_2 Plasma Decapsulation

The fluorine atoms in plasma afterglow always cause over-etching damage to Si die and Si_3N_4 passivation layer during IC package decapsulation. Two major reasons that conventional plasma decapsulation is not widely used in industry are because of process-induced over-etching [122] and electrical [29] damage to the die.

The only way to prevent over-etching is to not use fluorine-containing gas and only use oxygen as etchant gas. However, after Ar/O_2 plasma etching, only the epoxy on the surface layer of molding compound is etched, while the silica fillers are not removed at all. As a result, a thick layer of silica agglomerate remains on the molding compound surface that hinders further etching. This residue layer cannot be easily removed by high pressure gas blowing [29].

This section investigates the plasma etching process and proposes a combination of $Ar/O_2/CF_4$ etching and Ar/O_2 etching followed by ultrasonic cleaning. The combined process ensures no damage to the Si_3N_4 passivation layer and Si die after MIP decapsulation. The application of ultrasonic cleaning and using cavitation force [123-125] to dissociate the silica agglomerate residue layer after Ar/O_2 plasma etching is introduced.

5.3.1 $Ar/O_2/CF_4$ Plasma Decapsulation and Over-etch Damage

Decapsulation of a Small Outline Transistor (SOT23) package (see Fig.5-10a and b) with two 23 µm copper wire bonds are performed by using an $Ar/O_2/CF_4$ mixture plasma with 45 W input microwave power. 70% of O_2 and 30% of CF_4 in the etchant gas mixture is used to achieve a high molding compound etching rate. Semiconductor package is etched continuously for 5 minutes by this recipe until the wire bonds and die are all exposed as viewed through the CCD camera.

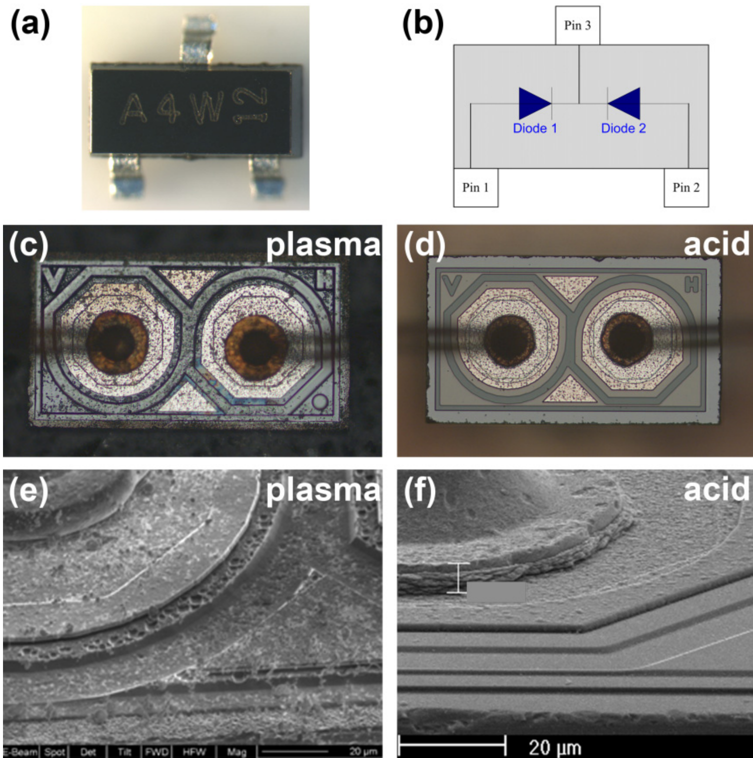

Fig.5-10 (a) Small Outline Transistor (SOT23) semiconductor package before decapsulation; (b) Schematic representation of the circuit inside the package; (c) Optical picture of semiconductor package after $Ar/O_2/CF_4$ MIP afterglow decapsulation; (d) Semiconductor package after acid decapsulation; (e) SEM image of the silicon die after $Ar/O_2/CF_4$ MIP afterglow etching; (f) SEM image of the die after acid etching.

The same type of package is decapsulated by nitric and sulfuric mixture acid as a reference. Comparing Fig.5-10c with Fig.5-10d, the copper bond wires after plasma etching is obviously more reddish in color and larger in diameter. This indicates the copper wire bonds after MIP afterglow etching is in much better condition than after acid etching. However, the surface of the silicon die after plasma etching appears to be more rough and unclean.

Further analysis under SEM showed the Si_3N_4 passivation layer on top of the die is completely removed and over-etching on the silicon die left rough porous structures after MIP afterglow etching (see Fig.5-10e). SEM picture on acid etching result showed the Si_3N_4 passivation and silicon die are in good condition but the copper wire bond suffered shrinkage in size due to acid corrosion (see Fig.5-10f). Although optimization of recipes helps to reduce damage in both decapsulation methods, over-etching of Si_3N_4 passivation by $Ar/O_2/CF_4$ MIP afterglow decapsulation and corrosion on copper wires by acid decapsulation seems inevitable.

5.3.2 $Ar/O_2/CF_4$ + Ar/O_2 Plasma Decapsulation, No Damage to Si_3N_4 and Si

To completely prevent over-etching damage to the Si_3N_4 passivation layer and Si die, an improved plasma decapsulation process is developed by combining $Ar/O_2/CF_4$ plasma etching with Ar/O_2 plasma etching.

In the first step, $Ar/O_2/CF_4$ mixture plasma is used to fast remove thick molding compound (about 300 µm thick) on top of the silicon die in 4 minutes. The bond wires are exposed after this etching step but the ball bonds and die are not exposed. The remaining 50 µm thick molding compound act as a protection layer to the underlying Si_3N_4 passivation layer to plasma etching.

In the second step, Ar/O_2 mixture plasma is used to selectively etch away the epoxy in the remaining molding compound in 2 minutes. Because no fluorine containing gas is used, Si_3N_4 and SiO_2 are not etched resulting in a remaining filler layer on top of the die. The silica filler residues, left after that the epoxy is removed from the molding compound, do not appear as a powder. Instead they form a layer of agglomerate that cannot be easily removed by gas blowing.

The final step is a safe and clean way to remove the remaining layer of silica agglomerate by ultrasonic cleaning in water for 10 seconds. The cavitations generated in water are capable to dissociate the silica agglomerate into powder efficiently, leaving a clean surface of die and bond wires. The potential mechanical damage to the bond wires due to ultrasonic cleaning process [126, 127] has to be taken into account, thus the cleaning duration is kept as short as possible.

The Si die, Si_3N_4 passivation layer, and copper bond wires are undamaged at all after this decapsulation process and remain in excellent condition for further failure analysis (see Fig. 5-11a). The surface of the copper wires after plasma etching process is smooth and the ball bonds are much less attacked compared to the acid etched counterparts (see. Fig. 5-11b, Fig. 5-10f). Electrical measurements (forward voltage at certain current) of the two bipolar diode devices in this package before and after MIP afterglow decapsulation showed no change in value. More than 20 samples are tested and all are undamaged indicating this process is safe for maintaining functionality of the device.

The $Ar/O_2/CF_4$ + Ar/O_2 plasma decapsulation process is suitable for mostly all IC packages, except gold wire bonded packages and multitier high-density wire bonded packages.

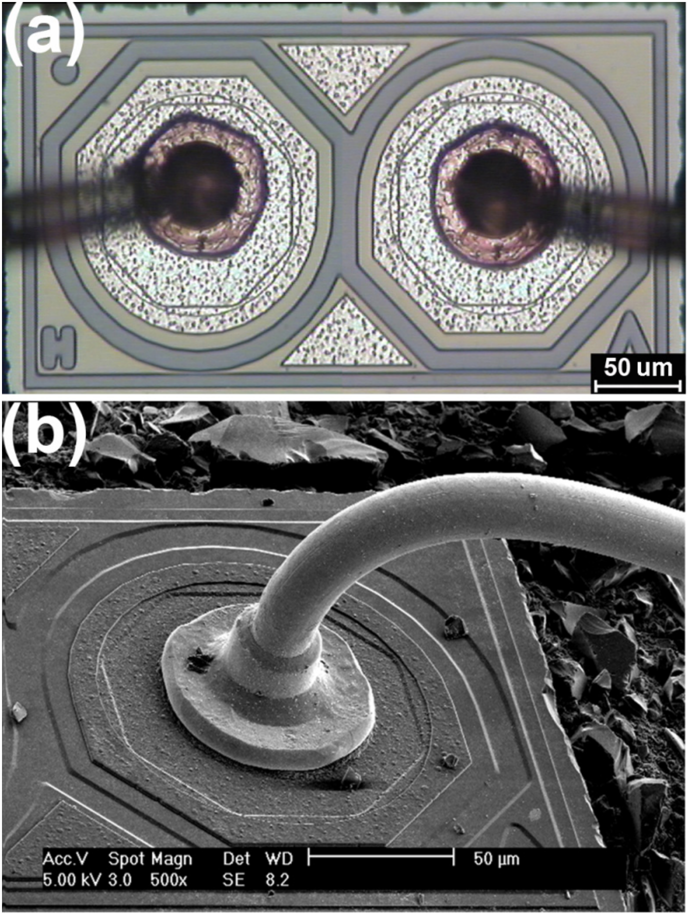

Fig.5-11 Semiconductor package decapsulated by the improved MIP etching process (a) optical image; (b) SEM image.

5.3.3 Critical Thickness to Prevent Over-etch Damage to Si_3N_4 and Si

The thickness of the blocking layer of molding compound after the first $Ar/O_2/CF_4$ etching step must be larger than 30 µm. Otherwise the fluorine radicals will penetrate through the molding compound layer and reach the underlying Si_3N_4 passivation. During $Ar/O_2/CF_4$ plasma etching, the top layer of the molding compound is porous as epoxy is partly removed by oxygen radicals while the silica fillers are slower to remove and are left on the surface. The fluorine radicals flow through these pores and cause over-etching of Si_3N_4 even though a layer of loose-structured molding compound is still left on top of the die (see Fig.5-12a). Fig.5-12b is a SEM image showing the etching process where the Si_3N_4 is completely removed in the lower area and partly removed in the upper area. Because the plasma recipe is developed to give a high molding compound etching rate, direct exposure of the die under the plasma for 10 seconds will cause complete removal of the Si_3N_4 passivation. A further exposure under CF_4 containing plasma will cause over-etching of the silicon on the die.

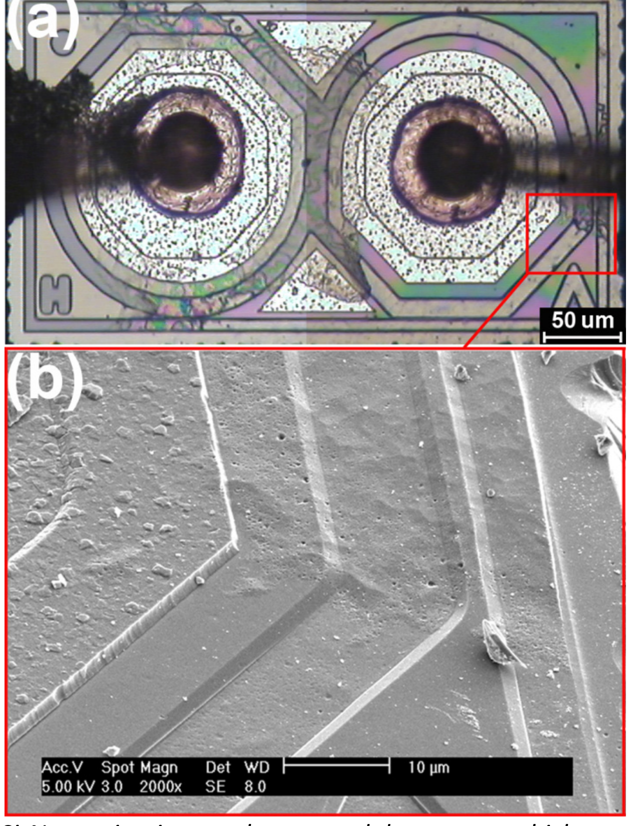

Fig.5-12 (a) Si_3N_4 passivation partly removed due to a not thick enough blocking layer of molding compound less than 30 µm thick; (b) SEM image showing the partly removed Si_3N_4 layer.

5.4 Laser-ablation + Ar/O_2 Plasma Decapsulation

Laser-ablation [30-33] is a commonly adopted process in IC industry to remove bulk layer of molding compound in plastic IC packages. Laser has the advantage of high precision and high molding compound removal rate, while the disadvantages are unavoidable damage to Si die, Si_3N_4 passivation layer, and bond wire surface. Thus laser-ablation is usually used as a pre-decapsulation process to remove bulk molding compound until the bond wire loop is exposed, then acid etching is performed to fully decapsulate the IC package [26, 34].

The reason of using laser-ablation is in some ways similar to high power Ar/O_2/CF_4 plasma etching, the two methods all remove bulk molding compound at a high rate and all cause damage to Si_3N_4 passivation layer and Si die. Since laser-ablation is a routinely used process in IC package decapsulation and it is more time saving compared to Ar/O_2/CF_4 plasma etching, replacing Ar/O_2/CF_4 plasma etching steps by laser-ablation could provide the most time-saving decapsulation solution.

This section develops a combined decapsulation process by using laser-ablation and Ar/O_2 plasma etching. The aim is to fast remove bulk molding compound by laser and then cleanly expose die and bond wires by Ar/O_2 plasma, without any process-induced damage.

5.4.1 Step 1: Laser-ablation

Decapsulation of Fine Ball Grid Array (FBGA) packages is conducted by a combination of laser-ablation and MIP afterglow etching. The sample has a 5.5 mm x 5.5 mm x 1 mm package size, 68 pins, with 20 µm diameter palladium coated copper bond wires.

Laser with 1060 nm wavelength and 0.2 mJ pulse power is used to quickly remove the bulk molding compound layer above the bond wires. After 30 seconds ablation, a cavity is left on the IC package defining the intended opening area (see Fig.5-13). The thickness of molding compound left on top of the die after laser-ablation is about 150 µm.

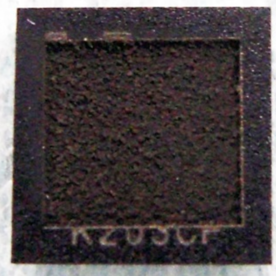

Fig.5-13 BGA package after laser-ablation, a square cavity is drilled in the center.

5.4.2 Step 2: Ar/O_2 Plasma Etching

After laser-ablation, Ar/O_2 MIP afterglow is then applied to remove epoxy in the remaining molding compound. The following process is ultrasonic cleaning in water to remove silica filler agglomerate residue. As oxygen radicals do not damage Si_3N_4 passivation layer or Si die, the only concern in processing is to prevent damage to the copper bond wires. Ar/O_2 plasma etching recipes previously developed for SOT23 package with 23 µm bare copper wires is directly applied to the FBGA package in this study. Ar/O_2 (mixing ratio = 98:2) plasma with a total gas flow rate of 1400 sccm at 40 W absorbed microwave power is used.

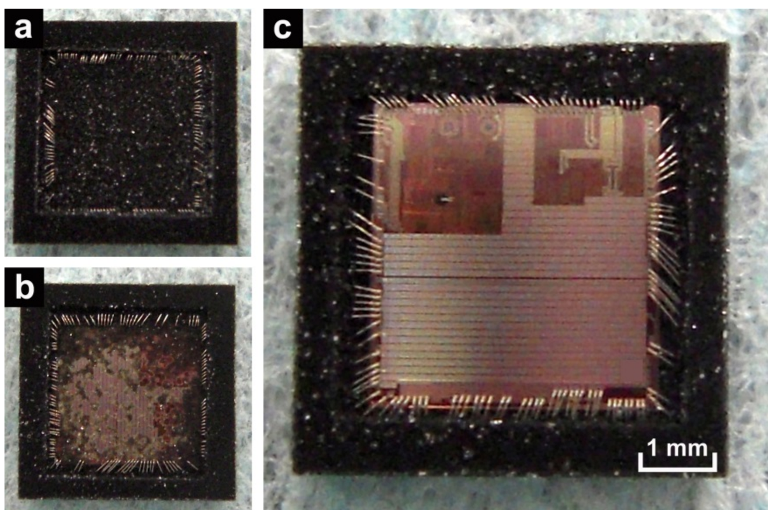

Fig.5-14 FBGA package after Ar/O_2 plasma etching and ultrasonic cleaning (a) first scan; (b) second scan; (c) third scan.

The FBGA package during plasma etching and ultrasonic cleaning process is shown in Fig.5-14a,b,c. The die is cleanly exposed after the third etching and cleaning step. The total processing time of one laser-ablated FBGA package is 30 minutes. The details on the die observed under optical microscopy and SEM analysis showed no apparent damage (see Fig.5-15a and b).

Comparing to $Ar/O_2/CF_4$ plasma etching, defining the scan path of IC packages under Ar/O_2 plasma etching is not critical. Over-exposure of the die under Ar/O_2 plasma does not cause over-etching problems. Thus, the Ar/O_2 plasma combined with ultrasonic cleaning process is best suitable for failure analysis tasks, especially for samples with little experience.

The advantage of this Laser-ablation + Ar/O_2 plasma decapsulation process is fast, no damage, and suitable for mostly all copper wire and gold wire bonded IC package decapsulation.

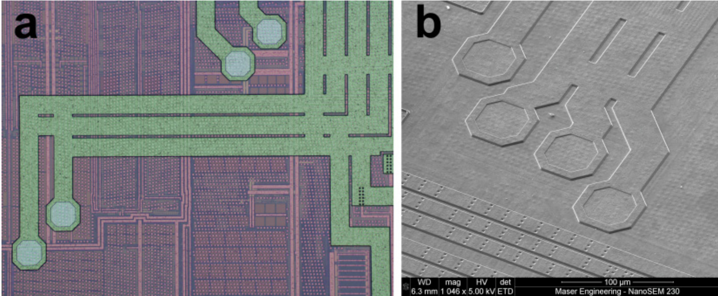

Fig.5-15 Image of the die after Ar/O_2 plasma decapsulation (a) Optical (b) SEM

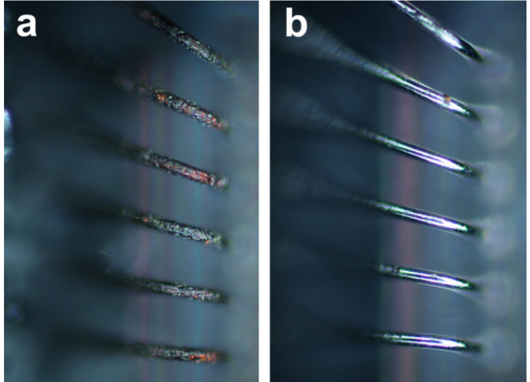

Fig.5-16 Optical microscopic image of palladium-coated copper wire after decapsulation (a) by cold acid, freshly prepared; (b) by Ar/O_2 MIP afterglow, after 6 month storage in normal air condition.

5.4.3 Comparison with Cold Acid Decapsulation

The currently adapted method in industry is to use laser-ablation followed by cold acid etching to decapsulate copper wire bonded IC packages. To compare the decapsulation performance, the same FBGA package is prepared by laser-ablation followed by HNO_3/H_2SO_4 (ratio = 5:1) acid mixture etching at 20 °C. Under optical microscope (see Fig.5-16a and b) some parts of the palladium coating on the copper wires were removed after acid etching, while after MIP afterglow etching the palladium coating remained smooth and showed no damage.

Under SEM (see Fig.5-17a and b), the acid based process reveals corrosion especially at the top region of wire loop, possibly due to the longer exposure time in acid. The acid has penetrated through the palladium protection layer and reached the copper. In comparison, after MIP afterglow etching the bond wire surface shows no damage. A few small dents appeared on the wire surface are caused by laser-ablation. It should be noted that the FBGA package decapsulated by plasma is prepared 6 month before taking the optical and SEM images. During that period, the plasma decapsulated device is stored in normal air condition and apparently no prolonged process induced damage occurred.

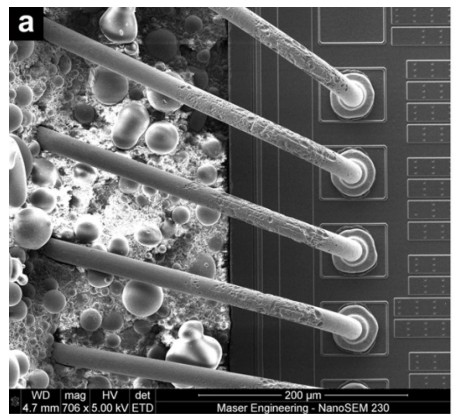

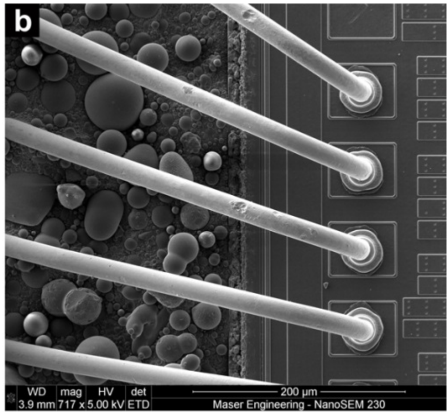

Fig.5-17 SEM image of palladium-coated copper wire package after decapsulation (a) by cold acid, freshly prepared; (b) by Ar/O_2 MIP afterglow, after 6 month storage in normal air condition.

Table 5-2 Comparison between MIP & cold acid decapsulation

	MIP afterglow decapping	Cold acid decapping
Si die quality	Good	Good
Bond wire quality	Good	Fair
Reproducibility	Good	Good
Processing time	30 minutes	15 minutes
Processing steps	plasma etching, ultrasonic cleaning	acid etching, rinsing
Process automation	automated etching, manual cleaning process	automated etching, manual cleaning process
Potential process-induced damage	oxidization on copper bond wire surface (avoidable)	corrosion on copper bond wires (unavoidable)
Recipe development	General etching recipe available. Scan route needs to be defined for different packages.	Probable range of operation available. No general etching recipe available.
Etching area	defined by scan path	defined by the gasket
When to use	Preserving fine bonding surface feature is more important.	Decapsulation speed is more important.
Most suitable application	Stressed sample after quality test Failure Analysis	Fresh sample Quality Control

Acid decapsulation normally has the major advantage of short processing time. However, decreasing the processing temperature in order to reduce corrosion on copper will lead to decrease in molding compound etching rate at the same time. Lowering the acid etching temperature will increase processing time by 10 fold, which makes cold acid etching duration becoming comparable to MIP afterglow etching. Detailed comparison between cold acid and MIP afterglow decapsulation based on this FBGA sample is listed in Table 5-2.

5.5 Laser-ablation + Low Power $Ar/O_2/CF_4$ Plasma Decapsulation

When using plasma to decapsulate IC packages with densely packed bond wires, molding compound beneath the bond wires is found to be extremely difficult to remove. Because the wire loops are located on top of the die area, plasma gas is directed to flow sideways around the wires thus causing radicals in the plasma effluent not reaching the molding compound beneath the bond wires. The result is that the ball bonds on the die are always covered by molding compound residues even after long time plasma etching. Such wire-masking effect is common to all plasma etchers [128].

The situation becomes even worse in the case of fine-pitch high-density multi-tier wire bonded packages. The wire-masking effect becomes so severe that it becomes impossible to expose the second-tier of bond wires that are located beneath the upper-tier bond wires.

In package level failure analysis, the bonding interface between copper bond wires and aluminum bond pads is often found to be the weak points in IC package. Corrosion and intermetallic formation are likely to take place at this interface. Successful exposure of the ball bond region after decapsulation is crucial to package level failure analysis. Therefore, a decapsulation process that can solve wire-masking effect and expose high-density multi-tier wire bonds in IC packages is needed. This section proposes a solution by using laser-ablation + low power $Ar/O_2/CF_4$ plasma decapsulation.

5.5.1 The Wire-masking Effect

To investigate the wire-masking effect with the eventual objective to find solutions, MIP afterglow decapsulation of IC packages with high-density multi-tier palladium-coated copper wires is conducted. The samples used in the experiment went through reliability test under High Temperature Storage (HTS) at 150°C for 1000 hours, thus the epoxy in molding compound is fully cross-linked and hardened. Laser-ablation is used to open a cavity on the package to expose the top of the bond wires (see Fig. 5-18a), and then Ar/O_2 MIP afterglow decapsulation is applied (see Fig. 5-18b). Only one set of bond wires at the upper-right corner is exposed because it is the place of interest to investigate.

The following decapsulation process used Ar/O_2 plasma etching followed by ultrasonic cleaning, which proved to work on most types of IC packages. The plasma recipe used is 1400 sccm gas mixture with 98% Ar and 2% O_2, at 40 W absorbed power. Normally, IC packages with low pin-count and low density bond wires all can be successfully decapsulated by this process.

However, the sample used in this experiment is an extreme case where the severe wire-masking effect made removal of molding compound beneath the bond wires impossible (see Fig. 5-19). The IC package is decapsulated after 9 cycles of Ar/O_2 plasma etching and ultrasonic cleaning process. The die is cleanly exposed but the molding compound beneath the bond wires is almost not removed at all. The spherical silica filler particles stick to the ball bond region. The upper-tier bond wires are exposed, while the lower-tier wires are mostly covered in molding compound.

Additional Ar/O_2 etching and ultrasonic cleaning cycles help to further remove the remaining molding compound. However, the removal rate is so low that the process becomes inefficient. Efforts have been made to vary the gas flow pattern on the bond wires, for example tilting the sample to vary the incident angle of plasma effluent, or changing the Ar flow rate in the plasma to change the turbulence flow pattern on top of the wires. Yet under the present experimental conditions, such efforts in changing gas flow pattern made little difference.

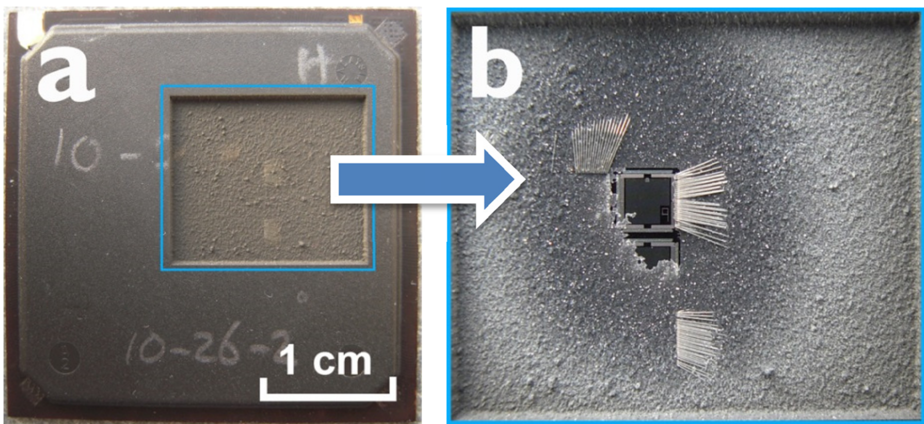

Fig.5-18 Sample (a) after laser-ablation; (b) after the subsequent MIP etching.

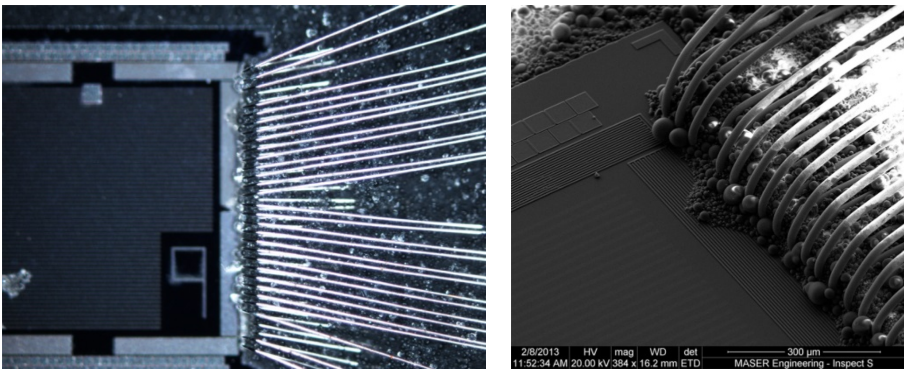

Fig.5-19 Optical (left) and SEM (right) images showing severe wire-masking problem found on HTS IC package sample after 9 cycles (3 minutes etching per cycle) of Ar/O_2 plasma etching.

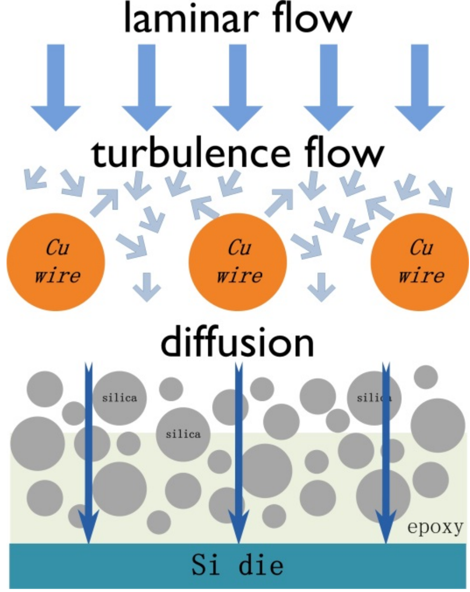

Fig.5-20 Schematic representation of the radical flow path on IC package during MIP afterglow etching. Cross-sectional view showing (from top) copper bond wires, silica filler agglomerate residue after epoxy is etched, un-etched epoxy molding compound, and silicon die.

The radical flow path during MIP afterglow etching is illustrated in Fig.5-20. Plasma effluent gas carries oxygen radicals to the surface of IC package following a laminar flow pattern. The bond wires block the path of gas flow and create turbulence at the interface. The radicals that flow through the gaps between the bond wires then diffuse into the molding compound and react with epoxy materials on the surface, creating a layer of porous-structured silica filler agglomerate.

One of the rate-limiting factors is turbulence-controlled, by which the bond wires block part of the effluent gas flow and reduce the flux of radicals that successfully reach the underlying molding compound layer. The other rate-limiting factor is diffusion-controlled, by which the densely packed silica filler residues on the molding compound surface significantly reduce the diffusion rate of radicals into the un-etched deep layer molding compound. Mitigating either of the two rate-limiting factors could help to reduce the degree of the wire-masking effect.

5.5.2 Solution to Wire-masking Effect

The efforts made to reduce the turbulence-controlled factor did not give satisfactory results. To tackle the wire-masking problem in a different approach, a new MIP etching process is developed to mitigate the diffusion-controlled factor. After laser-ablation, low power $Ar/O_2/CF_4$ MIP afterglow is scanned above the bond wire loop region. The plasma recipe used is 1400 sccm gas mixture with 97% Ar, 2% O_2, 1% CF_4, at 40 W absorbed power.

With the addition of CF_4, fluorine radicals are generated in the plasma and carried to the surface of the molding compound by the effluent flow. The agglomerate structure of silica filler agglomerate residues break due to the fluorine etching of the silica surface. The loosened silica particles are blown off by the effluent flow, exposing a fresh layer of molding compound for further etching.

The turbulence-controlled factor due to wire-masking still remains, but the radicals can reach the molding compound layer beneath the wire bond efficiently enough to achieve a reasonable etching rate. The position of the scanning path has to be determined by the etching profile of the specific plasma recipe used. In order to reduce over-etching damage on the die, the process has to be switched to low CF_4 percentage plasma etching before reaching the die. The improved process takes 7 scan cycles (each cycle takes 3 minutes) in total to fully remove the molding compound beneath the multi-tier wire bond region (see Fig. 5-21).

The improved decapsulation process successfully solves the wire-masking effect. Both layers of bond wires and the areas on the Cu/Al ball bond region are fully exposed. The aluminum bond pads and palladium-coated coppers wires are preserved excellently, even the surface layer remains undamaged. Such clean and damage-free decapsulation result for a thermally stressed multi-tier wire bonded IC package greatly facilitates following analysis on the bonding interface.

There are some areas on the die being over-etched due to a not fully optimized etching process. Fine tuning of the plasma decapsulation process by adding Ar/O_2 plasma etching as finishing step can avoid damage to the die. In this particular analysis case, the place of interest is only the ball bond region thus the silicon die area is not important and can be sacrificed.

An alternative process to bypass the wire-masking problem is to mechanically grind the sample and intentionally remove the top loop of bond wires. In this way the wire loop part that is causing the wire-masking problem is mechanically removed, leaving ball bond and some part of bond wire on the die surface. By removing the wire loop, plasma effluent can flow freely through the gaps between the vertically positioned remaining bond wires, thus the oxygen radicals can readily remove epoxy in the molding compound around the ball bond area. This process is achievable by using only an Ar/O_2 plasma and avoids using a fluorine-containing plasma, which in some applications is needed to rule out process-induced fluorine contamination.

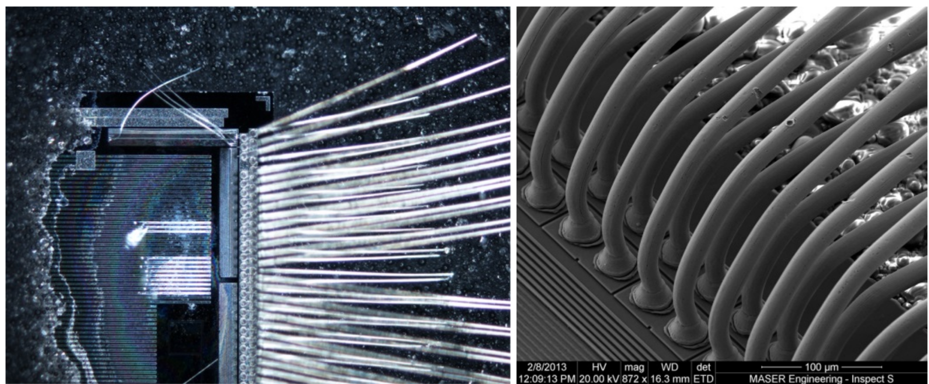

Fig.5-21 Optical (left) and SEM (right) images showing Wire-masking problem is resolved on HTS IC package sample after 7 cycles (3 minutes etching per cycle) of $Ar/O_2/CF_4$ etching.

5.6 Case Study 1: Thermally Stressed IC Packages

In quality control and failure analysis, stressed devices and failed devices are extremely useful because they represent device performance in real condition usage. Thus stressed samples contain much more reliability information than fresh samples. Yet, a prerequisite to access these reliability information on (potential) failure sites is the capability to decapsulate such IC packages without causing any process-induced damage to the copper bond wires, aluminum bond pads.

Epoxy molding compound after thermal stress usually tends to be more resistant to acid etching due to the curing of epoxy. Longer acid etching duration or higher processing temperature are often needed to expose the die. However, such etching conditions intensify corrosion on the copper wires and aluminum bond pads. Due to this reason, decapsulation of copper wire bonded IC packages that went through thermal stress often becomes impossible with conventional acid etching process.

Although decapsulation of stressed IC package is much more valuable than fresh sample decapsulation from a failure analysis perspective, this topic is rarely reported due to the lack of suitable decapsulation technologies.

5.6.1 Bare Copper Wire Bonded Package After HAST

MIP afterglow decapsulation of packages with bare copper bond wires after Highly Accelerated Stress Test (HAST) at 110°C, 85% relative humidity, for 1000 hours is studied. Compared to palladium-coated copper wires, bare copper wires are chemically more active and tend to be corroded by acid etching more quickly. The same holds true in plasma etching and it is found that bare copper wire tends to be oxidized more easily than palladium-coated copper wire when exposed in oxygen plasma at high temperature.
The process window to decapsulate bare copper wire bonded package after HAST test is small. The plasma etching process has to balance the molding compound etching rate and etching temperature, thus the package undergoes comparatively low temperature processing for a short period of time.

The MIP etching recipe we developed is capable to cleanly expose all Cu/Al bonds around the periphery of die after 30 minutes etching (see Fig. 5-22 a and b). Because the place of interest for analysis is only the ball bonds, the center die area is not exposed. The SEM image shows the surface details on the copper ball bond, edge of Cu/Al bond interface, and aluminum bond pad are well-preserved without process-induced damage (see Fig. 5-23a). Optical microscopic images showed that the copper wires (see Fig. 5-23b) and aluminum bond pads remain in excellent condition. The shiny color of the copper wires indicates even the surface layer is not oxidized, otherwise rough surface and dark-red color should be observed on oxidized copper.

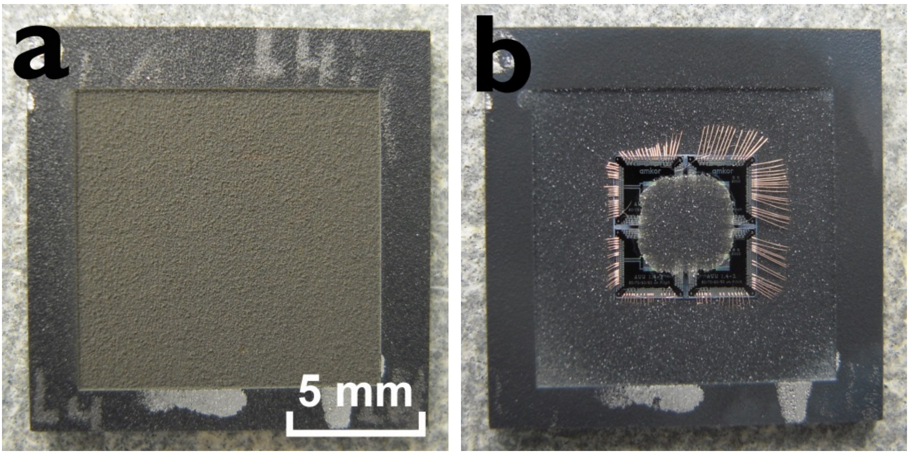

Fig.5-22 HAST bare copper wire IC package sample (a) After laser-ablation; (b) After 30 min MIP afterglow decapsulation

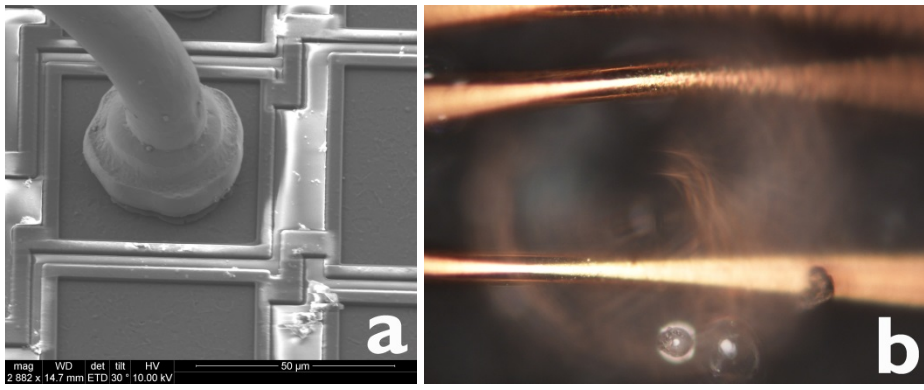

Fig.5-23 Bare copper bond wires on HAST package sample after MIP afterglow decapsulation (a) SEM image of Cu/Al bond; (b) Optical image of copper wire

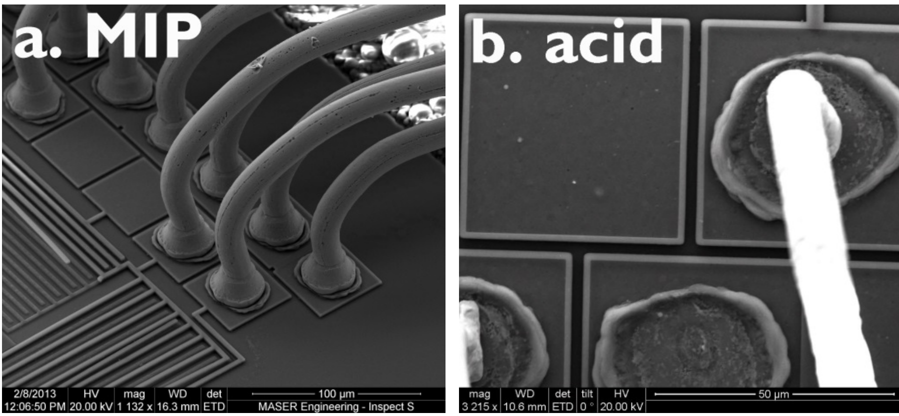

Fig.5-24 HTS IC package with palladium-coated copper wire bonds decapsulated by (a) MIP afterglow etching; (b) Cold acid etching.

5.6.2 Palladium-coated Copper Wire Bonded Package After HTS

In another example, Pd-coated Cu wire packages after High Temperature Storage (HTS) at 150°C for 1000 hours are decapsulated by MIP afterglow etching and the results are compared with cold acid decapped counterparts. MIP decapped sample shows smooth Pd-coated Cu wire surface without any observable damage (see Fig.5-24a).

For comparison, cold acid decapsulation (HNO_3/H_2SO_4 5:1 at 20 °C) of the same type HTS IC package is performed. Acid always removes the protective palladium coating layer causing corrosion of the bulk copper wire and apparent thinning of wire diameter, while in some cases lifted copper ball bonds from the aluminum bond pads are observed (see Fig.5-24b). The inevitable corrosion makes failure analysis on Cu/Al bond impossible to carry out as the valuable detail information is

removed by the acid decapsulation process. The comparison shows apparent advantage of using MIP etching for stressed package decapsulation.

Compared to unstressed IC packages, there is no apparent difference in MIP processing time under the same experiment conditions for stressed samples. It appears that MIP effluent etching is a promising solution to stressed copper wire bonded IC package decapsulation.

5.7 Case Study 2: IC Packages with Delamination Defects

To evaluate the ability to preserve minute details by MIP afterglow decapsulation, samples with delamination defects are intentionally chosen and tested (see Fig.5-25). The test vehicle used for this study is multi-tier high pin-count IC package with both gold wires and copper wires. The Fine Ball Grid Array (FBGA) package has a 7 mm x 7 mm die, 8 gold bond wires, and 300 ultrafine-pitch palladium-coated copper bond wires with a wire diameter of 18 µm.

As a pre-decapsulation process, laser-ablation is first applied to create an opening on the package surface leaving approximately 100 µm molding compound on top of the die.

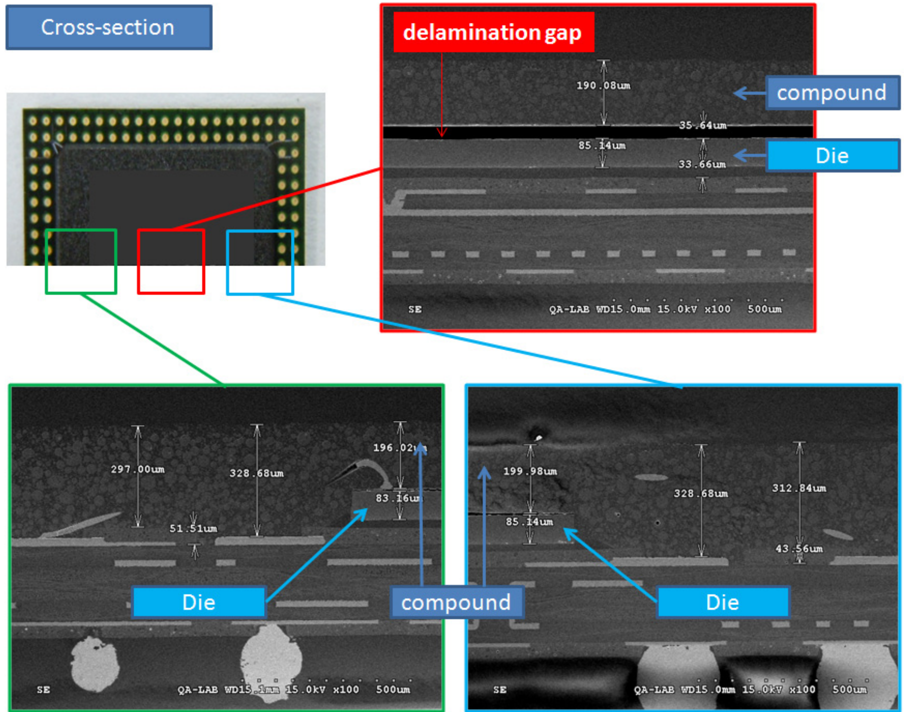

Fig.5-25 FBGA sample outline and cross-section images showing delamination defects in the package

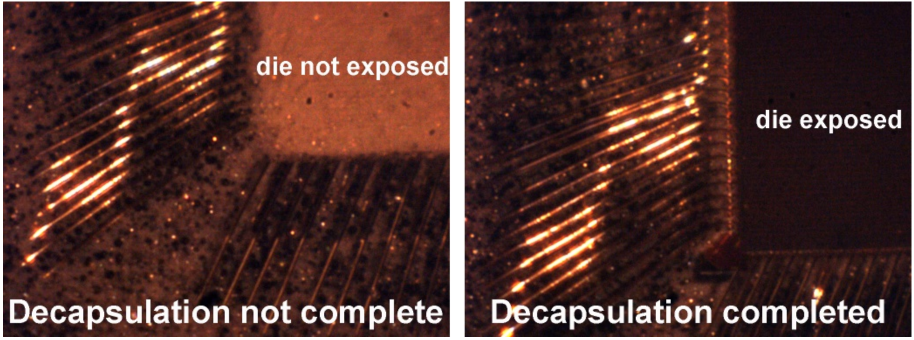

Fig.5-26 Real-time etching process monitoring by CCD camera

5.7.1 Plasma Decapsulation Results

After laser-ablation, further decapsulation process contains Ar/O_2 plasma etching followed by ultrasonic cleaning step. The whole etching process is monitored real-time under the integrated CCD camera (see Fig.5-26). Complete decapsulation of single FBGA package takes 50 minutes MIP afterglow etching with three cleaning steps (see Fig.5-27). Copper bond wires, gold bond wires, aluminum bond pads, and die structures remain undamaged after MIP decapsulation (see Fig.5-28).

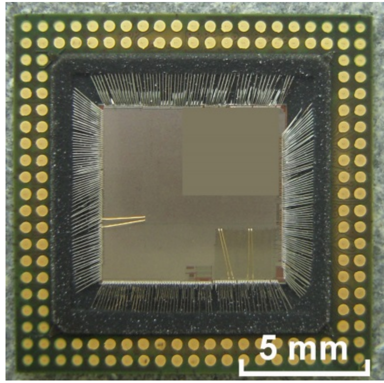

Fig.5-27 BGA package after 50 minutes MIP afterglow decapsulation

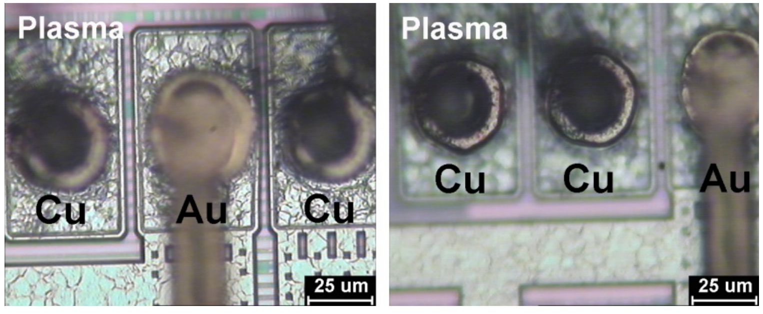

Fig.5-28 Optical microscopic images of Cu/Al and Au/Al bonds

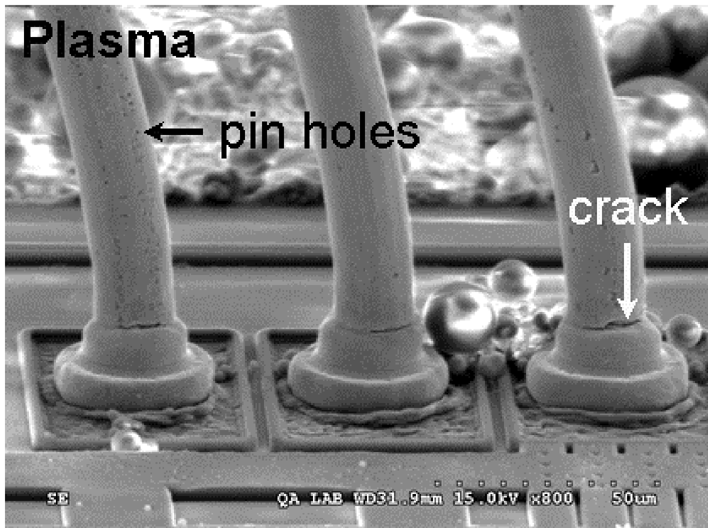

Fig.5-29 SEM image of Cu/Al bonds after MIP afterglow decapsulation

Minute crack features with sharp edges on the copper ball neck are observed after MIP afterglow decapsulation (see Fig.5-29). As the samples had delamination defects, such cracks are likely to be caused by the mechanical force in the molding compound before decapsulation. Small pin holes are found on the palladium coating layer on the copper bond wires. Because the plasma recipe used is highly selective, such pin holes are expected to be present before decapsulation.

5.7.2 Comparison with Cold Acid Decapsulation

Cold acid etching is the most widely adopted decapsulation method at the moment. Although corrosion on copper bond wires and aluminum bond pads is often found inevitable, acid decapsulation has the major advantage in shorter processing time. For comparison, same type FBGA package with delamination defects are etched by HNO_3:H_2SO_4 (3:1) acid mixture etching at 30 °C. Decapsulation of single package is achieved after 3 minutes acid etching.

Palladium coatings on the copper wire surface act as a protection layer to acid attack. Corrosion on bond wires becomes less severe compared to bare copper bond wires. However, the surface features on the Pd-coated Cu wire are still lost after acid decapsulation (see Fig.5-30). The crack feature on the ball neck observed after MIP afterglow etching is missing in the acid etched counterpart due to corrosion. Small pin holes on the Pd coating layer cannot be found, instead the wire surface becomes rough. This strongly suggests that the minute pin holes defects on the Pd coating layer that formed before decapsulation act as initial point for continuous corrosion during acid decapsulation.

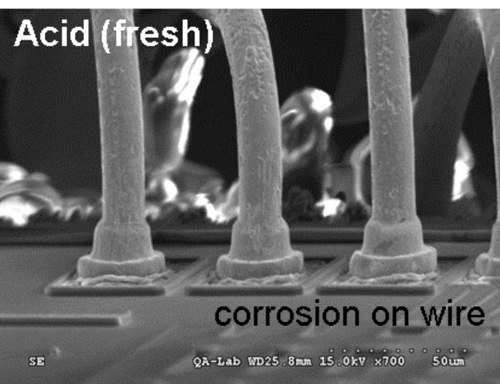

Fig.5-30 SEM image of Cu/Al bonds after cold acid decapsulation (freshly prepared)

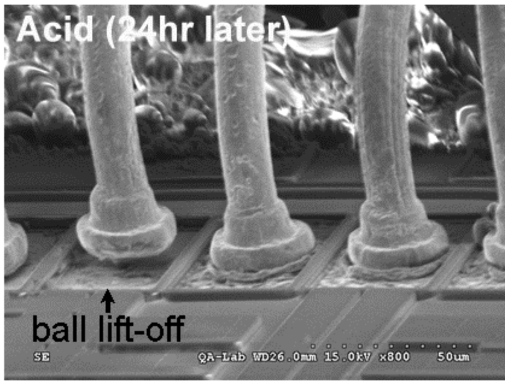

Fig.5-31 SEM image of Cu/Al bonds after cold acid decapsulation (24 hours after decapsulation)

It is recommended to analyze the samples processed by acid right after decapsulation. Although the sample is cleaned by rinsing in water, corrosion is continuing day by day. Continuing corrosion reactions will cause more surface Cu oxidation, even ball lifting can be found by aging time (Fig.5-31).

Comparing MIP afterglow with acid decapsulation, MIP excels in preservation of bond wire and bond pad surface features while acid excels in processing time. The current MIP configuration has an effective etching area of 12 mm^2, thus for decapsulation of IC packages with small die area MIP and acid processing duration is similar. However, IC packages with large die area require scanning procedure under MIP etching and the processing duration increases linearly with respect to the die area. On the performance side, MIP can protect the Cu wire from corrosion, hence the wire surface is smooth when comparing to the parts after acid decapsulation. For observation and analysis on the bond wire, bond pads, and Cu/Al intermetallic compound, MIP afterglow etching is the better choice.

5.8 Case Study 3: Solving Failure Analysis Dilemma by MIP Decapsulation

One of the requests we received from an industrial partner is to decapsulate a group of thin copper wire bonded Shrink Small-Outline Package (SSOP) components that went through HAST quality tests.

Initially, some of the SSOP components after going through HAST quality tests were decapsulated by cold acid etching. Wire-pull and ball-shear mechanical tests on the Cu/Al bonds were performed after acid decapsulation to evaluate whether there is degradation on the wire bond strength after HAST test. The evaluation result will determine whether this type of bond wire used in the SSOP component passes quality tests and can be massively used in production.

Two observations emerged in failure analysis and created a dilemma. The first observation is the mechanical tests showed the bond strength is below specified value thus does not meet quality requirements. The second observation is the thin copper bond wires suffered shrinkage in size after acid decapsulation due to corrosion damage. The two problems together create a dilemma in failure analysis, is the degradation of Cu/Al bond strength due to HAST test or to decapsulation damage.

The evaluation comes to an impasse and the company turned to MIP system for help. The same type copper wire SSOP components after HAST quality tests are decapsulated by laser-ablation + Ar/O_2 or $Ar/O_2/CF_4$ MIP etching process. After MIP decapsulation, the copper wire bonds and silicon die are exposed cleanly without process-induced damage. Further mechanical tests on the Cu/Al ball bonds were performed on multiple MIP decapsulated samples. The bond strength measured is found to be within specified range, thus proving the copper wire bonds pass HAST quality test and the reason of bond degradation on acid decapsulated samples was due to corrosion damage by acid.

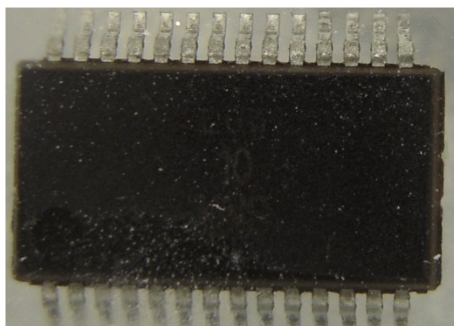

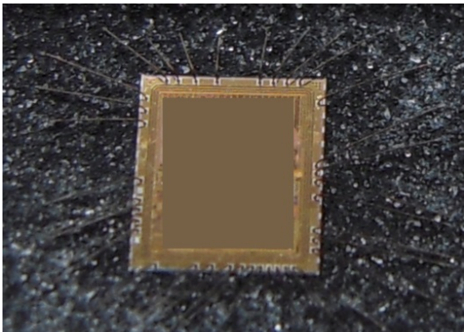

Fig.5-32 Copper wire bonded SSOP package after HAST test. Left: Before decapsulation. Right: After MIP decapsulation.

5.9 Conclusions

Obstacles encountered in using MIP afterglow etching for copper wire bonded IC package decapsulation applications are investigated. Practical problems on non-uniform etching, over-etching damage, and wire-masking effects are solved by developing processes and selecting suitable plasma etching recipes.

$Ar/O_2/CF_4$ plasma decapsulation process removes molding compound at a high rate. Copper wire bonded IC packages can be decapsulated without damage to the bond wires and bond pads. However, over-etching of Si_3N_4 passivation layer and Si die is inevitable due to the fluorine atoms in the plasma effluent. Thus the application of this decapsulation process is limited to wire bond analysis only.

$Ar/O_2/CF_4$ + Ar/O_2 plasma decapsulation process solves the over-etching problem on Si_3N_4 passivation layer and Si die. By adding Ar/O_2 plasma etching followed by ultrasonic cleaning steps before the die is exposed, over-etching of Si_3N_4 and Si is successfully avoided. The critical thickness of molding compound blocking layer is found to be 30 µm and below this value $Ar/O_2/CF_4$ plasma over-etching of Si_3N_4 passivation on top of the die takes place. This process is suitable for mostly all IC package decapsulation, except gold wire bonded packages and multitier high-density wire bonded packages.

Laser-ablation + Ar/O_2 plasma decapsulation process is similar to $Ar/O_2/CF_4$ + Ar/O_2 plasma decapsulation process. By replacing $Ar/O_2/CF_4$ plasma etching step with commonly used laser-ablation step in IC industry, overall decapsulation duration can be shortened. However, laser-ablation instrument is costly thus decreasing the affordability of such process to end users. The advantage of this decapsulation process is fast, no damage, and suitable for mostly all copper wire and gold wire bonded IC package decapsulation. The only limitation is the process cannot solve multitier high-density wire bonded package decapsulation.

Laser-ablation + low power $Ar/O_2/CF_4$ plasma decapsulation process solves a specific case that no other processes can tackle. When high-density multi-tier ultrafine-pitch bond wires are present in an IC package, the wires create a wire-masking effect to the plasma effluent flow thus making exposure of multi-tier wire bonds impossible. This shadowing effect that jeopardizes the removal of molding compound especially around the ball bond region can be resolved by introducing low power $Ar/O_2/CF_4$ plasma etching at suitable locations on top of the bond wires.

The four different decapsulation processes covers all types of plastic IC package decapsulation tasks. Typical decapsulation duration by MIP etching is in the range from 6~60 minutes per sample depending on the complexity and the size of the

particular IC package. The speed of decapsulation is at least 20 times faster than conventional plasma etching, while comparable to cold acid etching process.

The plasma etching recipes takes into account the molding compound etching rate, processing temperature, potential oxidization damage, and process reproducibility. As a result, Si_3N_4 passivation layer, Si die, Cu bond wires, Pd-coated Cu bond wires, Au bond wires, and Al bond pads inside the IC package can be cleanly exposed without any process-induced damage after MIP afterglow decapsulation.

Electrical functionality of the die inside the IC package after MIP decapsulation showed no degradation in I-V characteristics due to plasma etching. Wire-pull and ball-shear mechanical tests on the Cu/Al bonds showed no bond strength degradation due to plasma etching.

Comparisons between MIP and cold acid decapsulation performance are made on different types of samples. The cold acid decapsulated components always show unavoidable corrosion damage on the Pd-coated Cu wires or bare Cu wires, removing valuable surface features thus hindering further failure analysis. The minute surface features on the Pd coating layer and the Cu wires remain undamaged only after MIP decapsulation.

Decapsulation of components that went through thermal stressing after quality tests has always been impossible for acid etching because of the hardening of epoxy in the plastic molding compound. However, it is found that hardened epoxy in molding compound after thermal stressing does not bring additional difficulties to MIP etching. Plasma recipes developed on unstressed samples can be directly applied to the stressed or failed components, making MIP etching to be the ideal solution to such challenging tasks. The capability of MIP in solving challenging failure analysis tasks that acid decapsulation is not able to tackle was demonstrated in a case with thin copper wire bonded samples after HAST quality tests.

The high epoxy molding compound etching rate and selectivity, low stray field, good localization control, and real time imaging ability makes the MIP system an ideal solution to decapsulation of copper or gold wire bonded semiconductor packages. Various types of IC packages with or without original defects are successfully decapsulated, demonstrating the high efficiency and flexibility of this technology. The superior performance of MIP afterglow decapsulation in a reasonable processing time demonstrates the benefits of using this technology in copper wire bonded IC packages failure analysis and quality control applications.

Chapter 6

Microwave Induced Plasma Decapsulation of LED Packages

6.1 Introduction

Light-emitting diodes (LED) are packaged to protect the die from environment and improve the light extraction efficiency. Although high-power LED products have been delivered into the market in recent years and efforts have been made to improve the performance and reliability of LEDs [129-131], techniques that enable fast and safe decapsulation of high-power LED packages for failure analysis applications are still missing.

Silicone is commonly used as the encapsulation material for high-power LED packages due to its excellent thermal stability, optical transparency, and chemical stability. However, these material properties pose difficulties to the currently adapted plastic semiconductor package decapsulation methods like mechanical polishing, laser-ablation, fuming nitric and sulfuric acid mixture wet etching [24, 25]. Due to the elastic property of silicone, mechanical polishing cannot be used because of inevitable damage on the bond wires and die. Due to the light transparency property of silicone, laser-ablation cannot be used because of inevitable thermal damage on the die. The major elemental composition in silicone is silicon, carbon, oxygen, hydrogen, which is similar to that of molding compound that is widely used in plastic semiconductor packages. However, the chemical bonds and arrangement of molecules between silicone and molding compound are so different that conventional nitric and sulfuric acid are not capable for efficient silicone removal.

The best available solution in industry to decapsulate LED packages is long soaking or reflux boiling in one of the following solvents: Ardrox silicon rubber remover #2312, Panasolve, Tetramethylguanidine, etc. [132]. However, the duration of a clean removal of silicone lens on high-power LED package is often on the scale of hours depending on the type and thickness of the silicone encapsulant used.

Conventional dry plasma etching by O_2/CF_4 plasma used for polydimethylsiloxane (PDMS) patterning [95-97] in principle can be used to remove silicone encapsulant. However, it is not a practical solution to LED package decapsulation as the silicone etching rate with conventional reduced-pressure plasma etcher is often found too low, resulting in processing time from hours to days.

It is obvious that a fast and damage-free new technology for decapsulation of high-power LED packages is needed. In this chapter, commercially available LED

packages from leading manufacturers are tested to investigate the feasibility of using the MIP technology for high-power GaN based LED package decapsulation.

6.2 Flip-chipped Sapphire Substrate GaN-based High-power LED

There are two types of packaging structure used in commercial high-power LED, either flip-chipped or wire bonded. Fig.6-1.a shows a flip-chipped GaN-based sapphire substrate high-power LED package. A thin layer of silicone encapsulant and a 1500 µm thick hemispherical silicone lens encapsulates the LED die, transient-voltage-suppression (TVS) diode, ceramic substrate, and metal leads inside (see Fig.6-1.b).

Studies on MIP afterglow etching of silicone materials have been discussed in Section 4.7 in this thesis. MIP with 1400 sccm Ar, 5 sccm O_2, 16 sccm CF_4, 60 W input microwave power is a suitable etching recipe for removal of silicone lens. The complete etching process is monitored by the integrated CCD camera (see Fig.6-2). After 7 minutes plasma etching, the silicone lens (1.5 mm thick) on a flip-chipped sapphire substrate GaN based high power LED package can be completely removed.

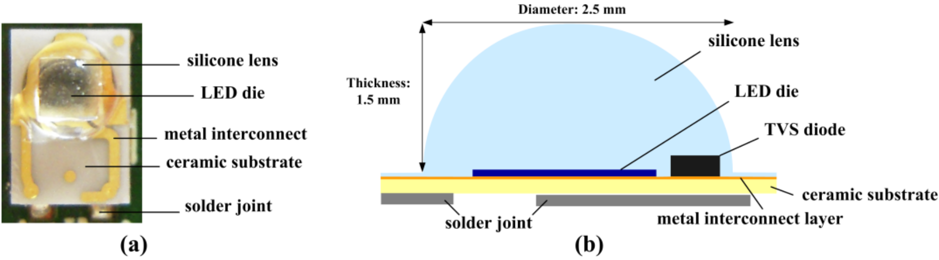

Fig.6-1 (a) A sapphire substrate flip-chipped high-power GaN-based LED package. (b) Schematic representation of the cross-sectional structure of the flip-chipped LED package.

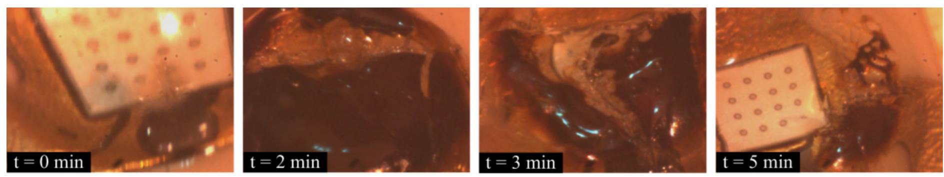

Fig.6-2 Silicone lens under MIP afterglow etching at different time spans. Images are taken by the integrated CCD camera in the MIP system.

One of the major concerns in plasma decapsulation of semiconductor packages is the over-etching damage to the die. Usually additional process steps are needed. However, for this type of LED package such concerns are not necessary. The substrate material of the LED die used in this study is sapphire, which is Al_2O_3 in

composition. The die is packaged in flip-chip structure thus the sapphire substrate is located on the top side in direct contact with the silicone encapsulant. $Ar/O_2/CF_4$ plasma does not etch Al_2O_3 thus the plasma do not cause over-etching damage to the LED die. However, exposure of the LED package under plasma at high microwave power level can result in melting of the solder joint and induce damage site formation or removal. As long time high temperature stress is a major source of failure generation and evolution, low plasma etching temperature with short etching duration is preferred to minimize potential process induced damage by plasma decapsulation. Etching recipe optimized for decapsulation have a plasma effluent gas temperature of 600 °C resulting in a LED package bulk temperature of about 200 °C.

Endpoint detection of the silicone lens etching process can be achieved by installing an interferometer in the MIP system. However, such solution will add complexity and cost. Experimentally we found an alternative solution by utilizing the already integrated CCD camera. By visual inspection through the CCD camera, it is difficult to distinguish whether the colorless and transparent silicone has been completely removed from the LED die. Therefore we directed a beam of light to the LED package during MIP afterglow decapsulation. The smooth silicone surface reflects the incident light while the LED die surface does not, the difference can be distinguished through the images from the CCD camera thus end point detection can be achieved.

As light-emitting-diodes are electroluminescence devices, the emission spectrum is the best indication to evaluate its functionality after plasma decapsulation. Flip-chipped sapphire substrate GaN based high power LED package without phosphor layer is used in the experiment (see Fig.6-3).

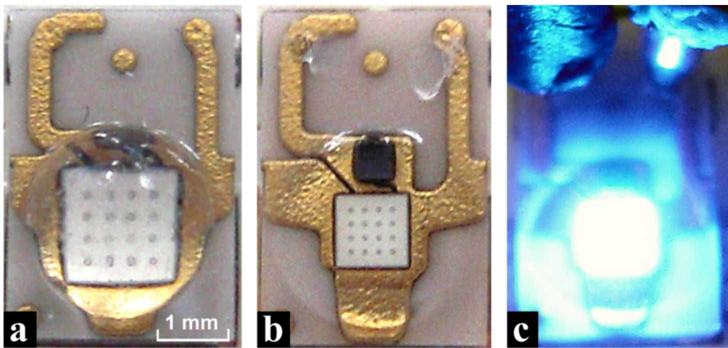

Fig.6-3 (a) Flip-chipped sapphire substrate GaN-based high-power LED package used for functionality test. (b) After 7 minutes MIP decapsulation, LED die is cleanly exposed. (c) LED after decapsulation remains functional.

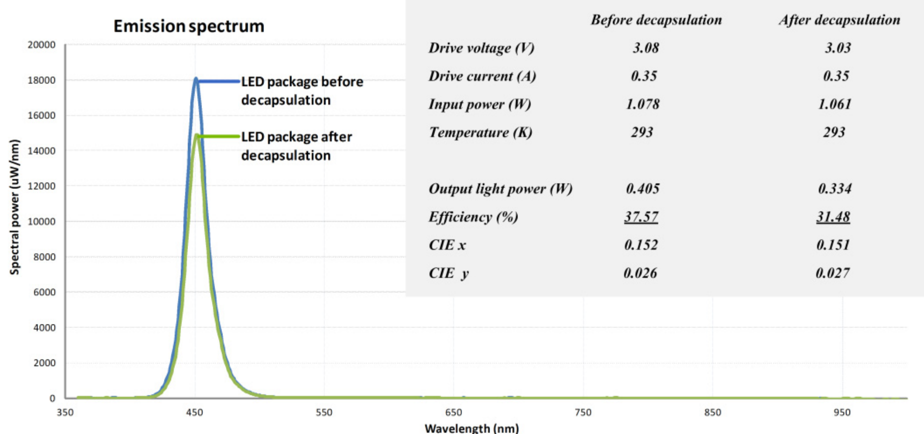

	Before decapsulation	After decapsulation
Drive voltage (V)	3.08	3.03
Drive current (A)	0.35	0.35
Input power (W)	1.078	1.061
Temperature (K)	293	293
Output light power (W)	0.405	0.334
Efficiency (%)	37.57	31.48
CIE x	0.152	0.151
CIE y	0.026	0.027

Fig.6-4 Optical emission spectrum of LED before and after MIP effluent decapsulation

The emissivity of the same LED die before and after plasma decapsulation is measured by an integral sphere. The measurement condition and results are shown in Fig.6-4. The shift in emission spectrum and CIE values of the same LED die before and after MIP decapsulation is small. The major difference is in the efficiency value, which is the ratio of the light output versus the overall electrical power input. The efficiency of LED package before decapsulation is 38%, while after decapsulation efficiency dropped to 31%.

The drop in LED light emission and efficiency after decapsulation should be due to the light extraction ability of the hemispherical silicone lens. For a bare flip-chipped LED die where the sapphire substrate is in direct contact with air, the large difference in refractive index between sapphire (n=1.76) and air (n=1) causes large amount of light emitted from the LED die to suffer from partly or totally internal reflection at the sapphire-air interface. Due to this phenomenon, the efficiency of a bare LED die is comparatively low.

Encapsulating the LED die in a hemispherical-shaped silicone lens can help to extract more light to the environment. Two interfaces have to be investigated in order to understand the function of the silicone lens. At the sapphire-silicone interface, the difference in refractive index between sapphire (n=1.76) and silicone (n=1.5~1.6) is much smaller compared to the sapphire-air case. Thus more light can be extracted from the LED die into the silicone medium. The second interface is silicone-air, where light has to be extracted into the air medium in order to achieve high photon out-coupling efficiency. The hemispherical shape of the silicone lens cause more light emitted from the LED die to reach the silicone-air interface near 0 °C incident angle, thus greatly reducing the amount of light been totally reflected at the second interface. It should be noted that silicone lens at the same time absorbs UV and visible light and the amount of light absorption

is proportional to its thickness. Optimized hemispherical silicone lens can increase light extraction efficiency of a bare LED die by 20~30% [133, 134], which is in similar range to our electroluminescence measurement data.

LED packages with the same packaging structure but different light-emitting composite materials can be decapsulated by the same MIP etching process with high reproducibility. The packaging structure and the landing material determine if $Ar/O_2/CF_4$ MIP etching will cause possible over-etching damage or not. Fig.6-5 shows optical microscopic images of a green-light sapphire substrate flip-chipped LED after MIP decapsulation. The die remains functional after silicone lens removal. Clear images on detailed die structures beneath the sapphire substrate can be obtained through optical microscopy, indicating the removal of silicone encapsulant is complete.

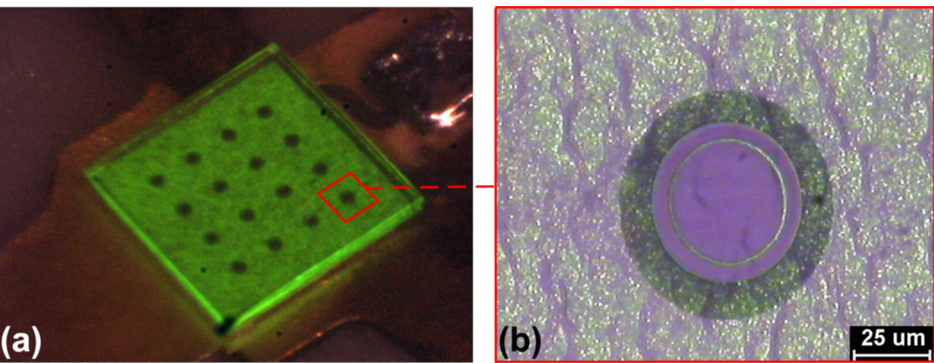

Fig.6-5 (a) Cleanly exposed sapphire substrate flip-chip high-power green-light LED die remains functional after MIP decapsulation; (b) Optical microscopy image of the die after decapsulation (LED in on-state).

6.3 Wire-bonded GaN-based High-power LED

For wire-bonded high-power LED packages, the commonly used bond wire type is gold (see Fig.6-6a). From experiment, it is found that the effluent of an Ar/CF_4 or an $Ar/O_2/CF_4$ microwave induced plasma etches gold at high rate under elevated temperature (see Section 4.8.4 for gold etching details). As fluorine radicals are needed in the plasma effluent to effectively etch silicone, MIP etching poses difficulties in decapsulating gold wire bonded high-power LED packages.

The solution to gold bond wire over-etching problem is to decrease the processing temperature such that the etching product of gold and fluorine does not evaporate. The gold wires exposed to $Ar/O_2/CF_4$ plasma etching forms a layer of gold fluoride on the wire surface. If the processing plasma effluent temperature is below 300 °C, gold fluoride does not evaporate thus the bulk gold wire will not be continuously removed by plasma.

Decapsulation process of gold wire-bonded high-power LED packages is carried out in two steps. First step is high power $Ar/O_2/CF_4$ plasma etching with 1400 sccm Ar, 5 sccm O_2, 16 sccm CF_4, 60 W input microwave power. After 7 minutes etching the bulk silicone lens is removed and a thin layer of silicone is left covering the gold bond wire and LED die (see Fig.6-6b). The second step is to use low-temperature $Ar/O_2/CF_4$ plasma etching to remove the remaining silicone layer. To decrease plasma effluent temperature, lower power and higher argon gas flow is used. Plasma etching recipe is 2800 sccm Ar, 25 sccm O_2, 2 sccm CF_4, 40 W input microwave power. After 5 minutes etching, the remaining silicone layer and dispersed phosphors in the silicone are removed (see Fig.6-6c). Gold bond wires and LED die are cleanly exposed. LED is still functional after decapsulation and gives off blue light because the removal of phosphors.

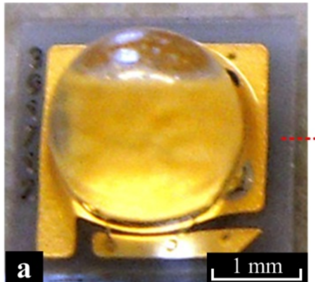

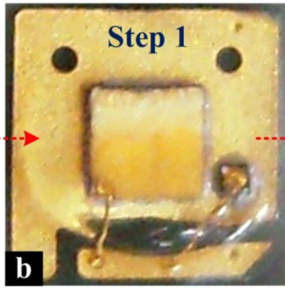

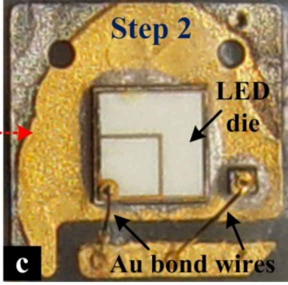

Fig.6-6 (a) Single large die LED package with proximate conformal phosphors distribution. (b) In first step, after 7 minutes high-power $Ar/O_2/CF_4$ MIP decapsulation, the bulk silicone lens is removed. (c) In second step, another 5 minutes low-temperature $Ar/O_2/CF_4$ MIP decapsulation removes the remaining silicone layer, exposing the die and gold bond wires.

6.4 Conclusions

Decapsulation of high-power LED packages by atmospheric pressure microwave induced $Ar/O_2/CF_4$ plasma afterglow is investigated. Plasma etching recipe that has 65 – 85% of CF_4 in the O_2/CF_4 etchant gas results in high silicone etching rate at approximately 200 µm/min under 60 W input power levels. Such recipes that balance etching rate, processing temperature, and controllability are recommended for LED decapsulation applications.

The process window for flip-chipped GaN-based sapphire substrate LED decapsulation is large as there are no concerns on over-etching damages. For gold wire-bonded high-power LED packages, MIP decapsulation has to be carried out in two steps using different etching recipes to prevent over-etching damage to gold wire bonds.

The high silicone etching rate and selectivity ensures single high-power LED packages to be decapsulated in 7 minutes for flip-chipped packages, and 12 minutes for wire-bonded packages. The LED die and gold wire bonds can be cleanly exposed for further analysis. Decapsulation processing time by using MIP is at least 10 times shorter than conventional wet etching alternatives.

Electroluminescence measurements on LED show efficiency dropped from 38% to 31% after decapsulation. The decrease in efficiency is most likely due to the light extraction ability of the hemispherical silicone lens, rather than damage on the device due to the MIP etching process.

It appears that MIP afterglow technology has a high potential for fast and safe decapsulation of high-power LED packages for failure analysis applications.

Chapter 7

Business Development

Re-innovation of a former innovation in the past rejuvenates the technology and brings new ideas that benefit our society by introducing innovative solutions. This Chapter describes how the Microwave Induced Plasma (MIP) decapsulation system came into existence, how the MIP technology advanced during the years with respect to industrial needs, and how the commercialization of MIP decapsulation system progressed.

From 1976 to 2009 (see Fig.7-1)

Microwave resonant cavities are known for many decades, their use were mostly in microwave applications. In 1976, Kees Beenakker introduced the use of a TM_{010} mode microwave resonant cavity to improve the element selective detection capability in gas chromatography [39]. The cavity is one of the very few designs that can sustain atmospheric pressure helium plasma and was widely adopted in gas chromatography and later referred to by chemists as the Beenakker cavity.

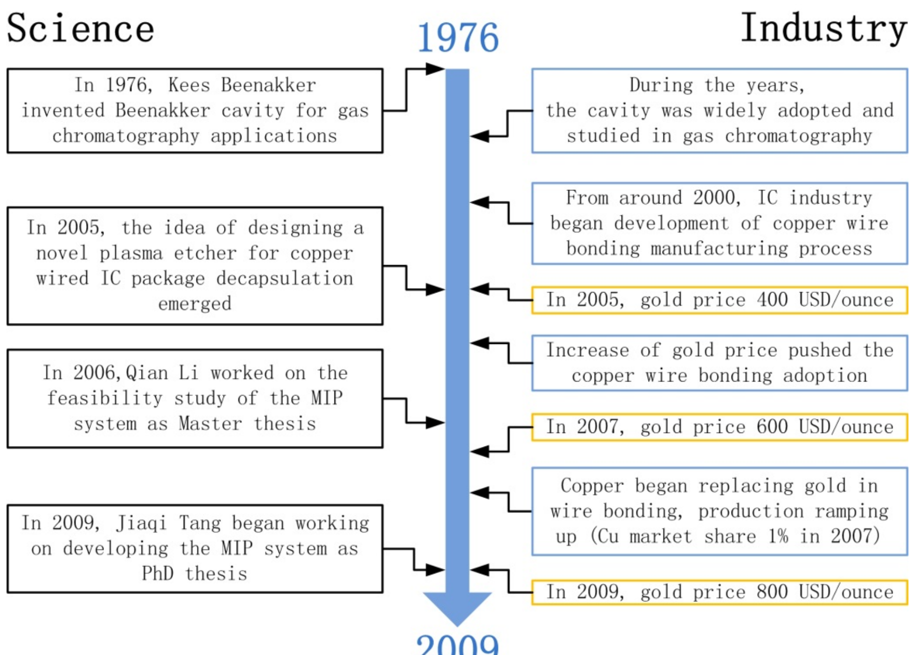

Fig.7-1 Timeline from 1976 to 2009, left column are the advancements in scientific research on Beenakker cavity, right column are applications in industry and the emergence of copper wire bonding in production due to the increasing gold price.

Development of fine-pitch copper wire bonding started as early as in 1990, however the adoption of this new technology was on halt due to not enough industrial motivation. In 2005, development on copper wire bonding manufacturing process was still ongoing. In the same year, the idea of developing a novel plasma etcher for copper-wired IC package decapsulation emerged, resulted from a discussion between Kees Beenakker and Charles Vath III (by that time head of development, ASM Pacific in Singapore) on the foreseeable difficulties in copper-wired package failure analysis.

In 2006, Qian Li worked on the feasibility study of using a MIP for decapsulation application and the results were promising [135, 136]. In 2009, Jiaqi Tang started PhD research on the MIP decapsulation system development. During 2005 to 2009, gold price rapidly increased from 400 USD/ounce to 800 USD/ounce and drove IC assembly industry to begin replacing gold wire bonding by copper wire bonding.

From 2010 to 2013 (see Fig.7-2)

Since the beginning of PhD project the objectives has been set clear, develop a prototype MIP system that can be commercialized. Scientific research and business development progressed side by side.

A good technology does not speak for itself unless it can reach the right audience. In the beginning, we had zero industrial partners. We started presenting our technology and approaching companies that might be interested within our reach. Most of the companies were not really interested in what we do basically because they were the wrong audience. But we successfully found one partner and established long term collaboration.

Presenting our work on international conferences initially attracted attention from the audience, however the follow-ups were not solid, and the most likely reason is the audience felt that MIP is still a research project in the lab that is far from industrial application. Situation changed when we opened the doors to invite companies to send samples to us, and we did decapsulation evaluation on their copper-wired samples free of charge.

Especially with the help of our contacts in industry, we were introduced to the correct person in the correct position who was involved in copper wire bonding technology. As a result, more companies began collaboration with us. In order to meet the demanding sample preparation requirements posed by them, we put efforts in developing certain aspects in the MIP system that eventually yielded technical breakthroughs that are useful in real applications.

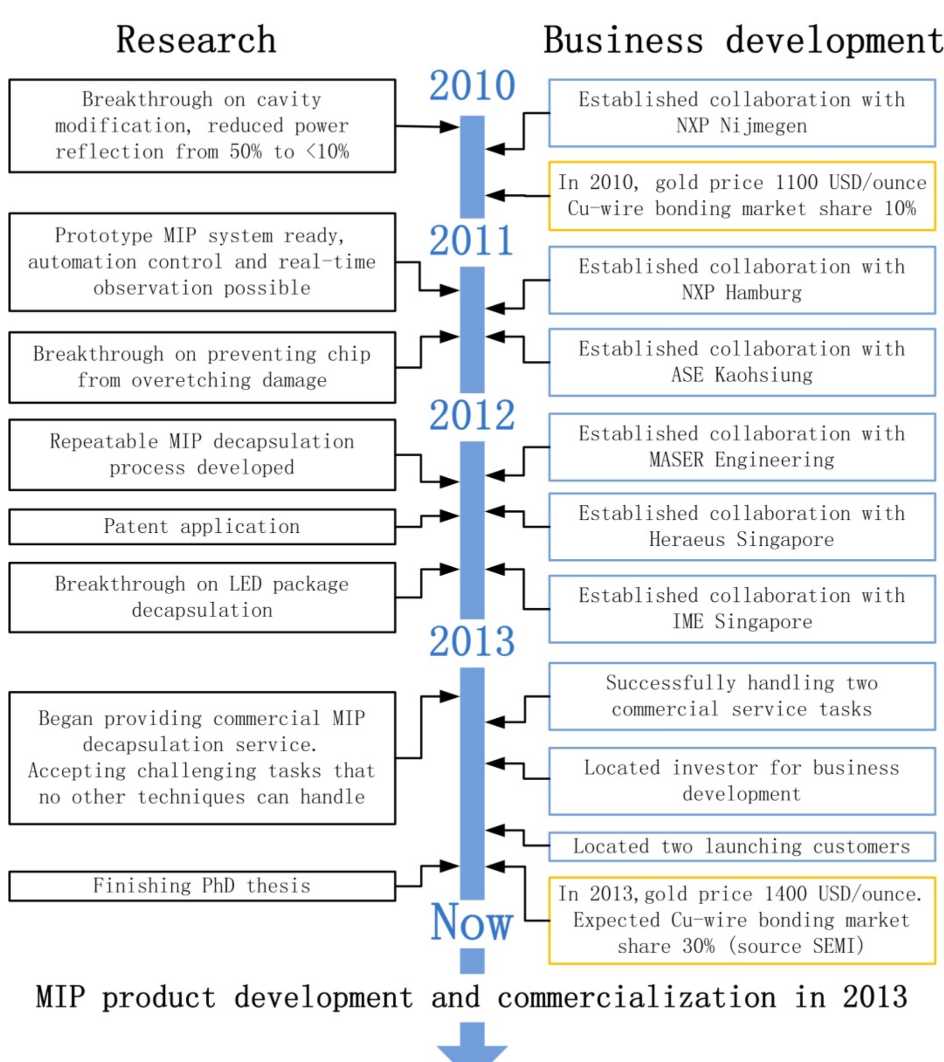

Fig.7-2 Timeline from 2010 to 2013, left column are the milestones in scientific research on MIP system development, right column are the milestones in business development on commercialization of the MIP system

Transition from a research project to business development was the most difficult task especially for technical researchers, but luckily we had a team and consultancy. The MIP system needs to generate revenue in order to support a company. In the various options we had, we decided to provide commercial

decapsulation service first and then start a company together with another already-established company that is experienced in instrument manufacturing.

Two commercial decapsulation service tasks were handled in 2013 and the MIP system proved to solve copper-wired package failure analysis difficulties that no other alternative techniques can tackle. More importantly, a paid decapsulation service is a feedback from the market that such MIP decapsulation capability is really in need.

Looking back, besides a good technology the crucial elements that made us achieved so far are: 1. Contacts that connected us to the end users; 2. Good relation with the end users; 3. A good team for business development; 4. Spirit of entrepreneurship and fall in love with what you do.

With gold price high as 1400 USD/ounce, copper wire bonding is estimated to continue steadily replacing gold wire bonding and reaching a market share of 30% in 2013 [137]. Product development and commercialization of MIP system is under way to address this high-tech niche market. Collaborations with leading industrial partners have been and will continue to be the focus of Jiaco Instruments to meet the challenges in making microelectronics better.

Chapter 8

Conclusions and Recommendations

8.1 Conclusions

In this thesis, the development of a Microwave Induced Plasma (MIP) system and its applications in decapsulation of copper wire bonded and other types of semiconductor packages are presented.

Microwave Induced Plasma System Setup

The major components in the MIP system include microwave generator, Beenakker-type resonant cavity, discharge tube, mass flow controller, programmable XYZ-stage, and CCD camera. The system works under atmospheric pressure thus vacuum components are not needed.

Modifications to the Original Beenakker Cavity

The core component in the MIP system is a Beenakker-type TM_{010} mode microwave resonant cavity, which is the plasma source that determines the plasma etching performance. The impedance mismatch problem when sustaining atmospheric pressure argon plasma by the original Beenakker cavity can be solved by adding a variable antenna to the original coupling loop inside the cavity. Microwave power reflection of the system is reduced from 50% to 0% when sustaining argon plasma.

The addition of O_2 or CF_4 etchant gas into the argon plasma detunes the impedance of original Beenakker cavity, thus inducing instability to plasma. The plasma process window can be broadened by adding modification elements that reduces the cavity's quality factor.

Counted from the output port of the microwave generator, the power efficiency of the MIP system is estimated to be 80%. The volume power density of MIP sustained by the modified Beenakker cavity is 1600 W/cm^3 under 40 W input power.

Development of Microwave Induced Plasma Afterglow Etching Recipes

The suitable MIP etching conditions have a plasma effluent temperature of around 400°C, resulting in an etching reaction interface temperature of 250°C and a bulk IC package temperature of 100°C.

MIP afterglow etching recipes are developed for Si, SiO_2, Si_3N_4, epoxy, epoxy molding compound, and silicone, which includes all kinds of non-metal materials

that may appear in an IC package. $Ar/O_2/CF_4$ plasma etching recipes that give high material removal rates are O_2/CF_4 (1:1) for epoxy molding compound, O_2/CF_4 (3:7) for Si and SiO_2, O_2/CF_4 (2:8) for silicone. Depending on material composition, normal range of vertical etching rate is 20~100 µm/min, and volumetric etching rate is 0.1~0.5 mm^3/min.

During MIP afterglow decapsulation of IC packages, preservation of metal bond wire and bond pad structure is as crucial as achieving high encapsulation material removal rate. The oxygen and fluorine atoms generated in an $Ar/O_2/CF_4$ MIP afterglow reacts with metals, forming metal oxides and fluorides, respectively. $Ar/O_2/CF_4$ plasma with high effluent temperature rapidly etches gold because gold fluoride is volatile at 300°C. The key element in fluorine-containing plasma etching of aluminum and palladium is found to be moisture.

Copper Wire Bonded IC Package Decapsulation by MIP Afterglow Etching

$Ar/O_2/CF_4$ plasma decapsulation process removes molding compound at a high rate. However, over-etching of Si_3N_4 passivation layer and Si die is inevitable due to the fluorine atoms in the plasma effluent.

$Ar/O_2/CF_4$ + Ar/O_2 plasma decapsulation process solves the over-etching problem on Si_3N_4 passivation layer and Si die. By adding Ar/O_2 plasma etching followed by ultrasonic cleaning steps before the die is exposed, over-etching of Si_3N_4 and Si is successfully avoided. This process is suitable for mostly all IC package decapsulation.

Laser-ablation + Ar/O_2 plasma decapsulation process is similar to $Ar/O_2/CF_4$ + Ar/O_2 plasma decapsulation process and the overall decapsulation duration is shortened.

Laser-ablation + low power $Ar/O_2/CF_4$ plasma decapsulation process is found to be the only solution to multitier high-density wire bonded package decapsulation. The severe wire-masking effect that jeopardizes the removal of molding compound especially around the ball bond region can be resolved by this process.

The four different decapsulation processes covers all types of plastic IC package decapsulation tasks, including thermally stressed package decapsulation that cannot be handled by other techniques. After MIP afterglow decapsulation, Si_3N_4 passivation layer, Si die, Cu bond wires, Pd-coated Cu bond wires, Au bond wires, and Al bond pads inside the IC package can be cleanly exposed without any process-induced damage.

Comparisons showed that the minute surface features on the Cu bond wires remain undamaged only after MIP decapsulation, while after cold acid

decapsulation the corrosion damage on the Cu bond wires is inevitable thus causing removal of valuable surface features and hindering further failure analysis.

Typical decapsulation duration by MIP etching is in the range from 6~60 minutes per sample depending on the complexity and the size of the particular IC package. The speed of decapsulation is at least 20 times faster than conventional plasma etching, while comparable to cold acid etching process. The superior performance of MIP afterglow decapsulation in a reasonable processing time demonstrates the benefits of using this technology in copper wire bonded IC packages failure analysis and quality control applications.

LED Package Decapsulation by MIP Afterglow Etching

High-power LED packages can be cleanly decapsulated by MIP afterglow etching without influencing the functionality of the LED die. The process window for flip-chipped GaN-based sapphire substrate LED decapsulation is large as there are no concerns on over-etching damages. For gold wire-bonded high-power LED packages, MIP decapsulation has to be carried out in two steps using different etching recipes to prevent over-etching damage to gold wire bonds. Typical decapsulation duration for single package is 7 minutes for flip-chipped packages and 12 minutes for wire-bonded packages, which is at least 10 times shorter than conventional wet etching alternatives.

8.2 Future work

In this thesis, a prototype Microwave Induced Plasma (MIP) instrument is built. The lab-built instrument is an alpha machine that has the basic functionalities for IC package decapsulation application. However, there are some topics that still need to be further investigated in order to develop the MIP instrument to a beta machine and improve its performance.

Beta Machine Development

The beta machine is a 90% ready commercial machine that meets the operation standards and requirements in industrial use. Components used in the alpha machine have to be re-selected to meet the manufacturing standards. Integration of the complete system and a well-written user interface software need to be developed to make the beta machine robust and easy to use in operation. Safety requirements on electricity, gas, microwave, and other points have to be considered during the design phase of the beta machine. Qualification certificates and block-design for the easiness of repairing also need to be addressed.

Decapsulation Process Development

The removal of silica filler in epoxy molding compound has always been a bottle-neck in plasma decapsulation. Blowing by high gas flow introduces unwanted damage to the bond wires and provides very little help in filler removal. Addition of fluorine in plasma helps removal of filler residue but at the same time introduces unwanted over-etching damage on silicon die. The improved process proposed in this thesis is to use oxygen plasma etching before reaching the die and then use ultrasonic cleaning to remove the filler residues. Although the process proved to be efficient, the handling of the ultrasonic cleaning step takes time and creates engineering difficulties in designing a 100% automated MIP decapsulation instrument. A new method to efficiently remove silica fillers during plasma etching need to be developed to further improve the automation level of MIP decapsulation.

Plasma Source Development

IC packages have various sizes due to the different chips they encapsulate. The effective etching area in the current MIP instrument is not large enough to cover the entire surface of IC packages with large surface areas. New plasma source that generates a larger area stable atmospheric pressure plasma can further reduce the processing time when decapsulating large-sized IC packages. However, the filamentation phenomenon in atmospheric pressure plasma creates a technical barrier and this topic needs to be further investigated.

List of abbreviations

Al: aluminum
Ar: Argon
Au: Gold
CCD: Charge-coupled Device
CF_4: Carbon-tetra-fluoride
Cu: Copper
EDX: Energy-Dispersive X-ray Spectroscopy
FBGA: Fine Ball Grid Array
FIB: Focused Ion Beam
HAST: Highly Accelerated Stress Test
HF: Hydrogen Fluoride
HTS: High Temperature Storage
IC: Integrated Circuits
ICP: Inductively-coupled Plasma
LED: Light-emitting Diode
MIP: Microwave Induced Plasma
O_2: Oxygen
PCB: Printed Circuit Board
Pd: Palladium
PDMS: Polydimethylsiloxane
RF: Radio Frequency
RIE: Reactive Ion Etching
SAM: Scanning Acoustic Microscopy
SEM: Scanning Electron Microscopy
Si: Silicon
Si_3N_4: Silicon Nitride
SiF4: Silicon Fluoride
SiO_2: Silicon Oxide
SOT: Small-outline Transistor
SSOP: Shrink Small Outline Package
TC: Temperature Cycling
TEM: Transmission Electron Microscopy

About the Author

Jiaqi Tang was born in Beijing, China, in 1984. He received B.S. degree in materials science from Fudan University in 2007. In 2009, he received M.Sc. degree in materials science from University of Pennsylvania. His research topic focused on organic memory devices.

From September 2009 he has been working towards his Ph.D. degree at Delft Institute of Microsystems and Nanoelectronics (DIMES), Delft University of Technology. His main research activities focus on developing a Microwave Induced Plasma (MIP) instrument for copper wire bonded semiconductor package decapsulation application. During this period, he also worked on business development of the MIP instrument.

Since September 2013, he is CEO of Jiaco Instruments, a TU Delft start-up company he co-founded to commercialize the MIP instrument.

List of Publications

Patent Application

- **J. Tang**, C. I. M. Beenakker, J. B. J. Schelen, “Plasma jet etching device and method for removing an encapsulation portion of a sample via plasma jet etching”, Application no. 2008943, 2012

Journal Papers

- **J. Tang**, D. Gruber, J. B. J. Schelen, H. –J. Funke, and C. I. M. Beenakker, “Fast Etching of Molding Compound by an $Ar/O_2/CF_4$ Plasma and Process Improvements for Semiconductor Package Decapsulation”, ECS Journal of Solid State Science and Technology,1 (4), P175-P178, 2012.
- **J. Tang**, J. B. J. Schelen, and C. I. M. Beenakker, “A novel approach to fast decapsulation of high-power light-emitting diode packages for failure analysis applications”, IEEE Transactions on Device and Materials Reliability, to be submitted.

Conference Proceedings

- **J. Tang**, C.H. Chen, S.K. Liang, E.G.J. Reinders, C.Th.A. Revenberg, J.B.J. Schelen, and C.I.M. Beenakker, “Microwave Induced Plasma Decapsulation of Stressed and Delaminated High Pin-count Copper Wire Bonded IC Packages”, IEEE Electronic Components and Technology Conference (ECTC), 1717-1723, 2013
- **J. Tang**, A.R.G.W. Knobben, E.G.J. Reinders, C.Th.A. Revenberg, J.B.J. Schelen, and C.I.M. Beenakker, “Microwave Induced Plasma Decapsulation of Thermally Stressed Multi-tier Copper Wire Bonded IC Packages” IEEE International Conference on Electronic Packaging Technology & High Density Packaging (ICEPT), 2013
- **J. Tang**, E.G.J. Reinders, C. Th. A. Revenberg, J. B. J. Schelen, and C. I. M. Beenakker, “Decapsulation of High Pin Count IC Packages with Palladium Coated Copper Wire Bonds Using an Atmospheric Pressure Plasma”, IEEE Electronics Packaging Technology Conference (EPTC), 165-169, 2012.
- **J. Tang**, J.B.J. Schelen, and C.I.M. Beenakker, “Process Control in Plasma Decapsulation: Preventing Damage to the Copper Wire Bonds & Controlled Removal of Si3N4 Passivation Layer”, IEEE International Conference on Electronic Packaging Technology & High Density Packaging (ICEPT), 1194-1199, 2012.
- **J. Tang**, J.B.J. Schelen, and C.I.M. Beenakker, “Flexible system for real-time plasma decapsulation of copper wire bonded IC packages”, IEEE Electronic Components and Technology Conference (ECTC), 1764-1769, 2012.

- **J. Tang**, H. Ye, J.B.J. Schelen, and C.I.M. Beenakker, "Plasma Decapsulation of Plastic IC Packages with Copper Wire Bonds for Failure Analysis", IEEE International Conference on Electronic Packaging Technology & High Density Packaging (ICEPT), 1-5, 2011. **(Outstanding conference paper)**
- **J. Tang**, J.B.J. Schelen, and C.I.M. Beenakker, "Plasma etching for failure analysis of integrated circuit packages", ECS Trans. 34, 913-918, 2011.
- **J. Tang**, J.B.J. Schelen, and C.I.M. Beenakker, "Optimization of the Microwave Induced Plasma System for Failure Analysis in Integrated Circuit Packaging", IEEE International Conference on Electronic Packaging Technology & High Density Packaging (ICEPT), 1034-1038, 2010. **(Best student paper)**

Summary

The majority of Integrated Circuit (IC) devices are encapsulated in wire-bonded plastic IC packages. Epoxy molding compound is used as the encapsulation material and gold was used as the bonding wire material. However, the increase of gold material price from 400 USD/ounce in year 2005 to 1400 USD/ounce in year 2013 results in a major cost issue in IC assembly and prompt industry to search for alternative bond wire materials. Due to its cost and performance advantages, copper wire bonding is steadily replacing traditional gold wire bonding in IC assembly. The share of copper wire bonding has increased from 1% in year 2007 to 10% in year 2010 and is expected to reach 30% in year 2013.

In package level failure analysis, decapsulation is an important step to open the IC package to inspect the condition of internal components and locate possible failure sites for root cause analysis. Thus the requirement of a good decapsulation process is to selectively remove the epoxy molding compound encapsulation layer, while not damaging the semiconductor chip and metal bonding wires that locate inside the IC package.

The mostly used conventional decapsulation technique is to use hot nitric or nitric and sulfuric mixture acid to etch away the molding compound, such process has been routinely used for gold wire bonded plastic IC package decapsulation. However, because copper wires are more susceptible to be corroded and damaged by the acid, the switching to copper wire bonding in IC industry has raised a problem for acid decapsulation. Copper bond wires suffer inevitable corrosion after acid decapsulation, thus further failure analysis on copper/aluminum bonding becomes difficult especially in the case of IC packages that went through thermal stressing conditions after quality tests. Conventional plasma decapsulation and laser-ablation also have inherent disadvantages, thus their application in copper-wired IC package decapsulation are limited.

In this thesis, we introduce a solution to the copper-wired IC package decapsulation by using a Microwave Induced Plasma (MIP) system. The MIP system combines the high etching selectivity of a plasma with the speed and absence of RF fields of acid decapsulation. Characteristics of the MIP system are high power density, atmospheric pressure operation and absence of exposure of the samples to ions. As a result, fast, selective and safe decapsulation of copper wire bonded IC packages is achieved. The performance of this MIP system outperforms acid decapsulation in preservation of fine surface details on the

copper wire bonds. Compared to conventional plasma etchers, the MIP system is at least 20 times faster and does not damage the functionality of the chip.

The prototype setup of the MIP decapsulation system is described in Chapter 2. The core component in the MIP system is a Beenakker-type TM_{010} mode microwave resonant cavity, which is the plasma source that determines the plasma etching performance. Chapter 3 investigates problems when using the original Beenakker cavity as the source of the plasma. Modifications are proposed that enable generation of an atmospheric pressure high-power density stable $Ar/O_2/CF_4$ plasma. High power reflection in the MIP system is reduced by adding a variable antenna to the original coupling loop inside the cavity. Broad and stable plasma process window is achieved by adding another modification element that reduces the cavity's quality factor. The power efficiency of the MIP system is estimated to be 80%, while the volume power density of MIP sustained by the modified Beenakker cavity is 1600 W/cm^3 under 40 W input power.

Based on the plasma chemistry, MIP afterglow etching recipes for a variety of materials are developed in Chapter 4. $Ar/O_2/CF_4$ plasma etching of epoxy molding compound, Si, SiO_2, Si_3N_4, silicone, copper, aluminum, palladium, and gold are conducted. Those materials are of special interest because they are commonly used in semiconductor packages. The optimal recipes for high etching rates as well as the rate-limiting factors of etching each material are given. The results provide reference to plasma etching selectivity and preservation of certain materials during MIP decapsulation of IC packages.

Chapter 5 focuses on the application of MIP afterglow etching in IC package decapsulation. Four different MIP decapsulation processes are proposed and their pros & cons are analyzed. These four processes covers all types of plastic IC package decapsulation tasks, including thermally stressed package decapsulation that cannot be handled by other techniques. After MIP afterglow decapsulation, Si_3N_4 passivation layer, Si die, Cu bond wires, Pd-coated Cu bond wires, Au bond wires, and Al bond pads inside the IC package can be cleanly exposed without any process-induced damage. Comparison of MIP decapsulation with the currently used alternative solution of cold acid decapsulation is made. The superior ability of preserving minute surface features by MIP decapsulation in a reasonable time that facilitates further failure-site analysis is demonstrated through case studies.

The application of MIP afterglow etching in LED package decapsulation is explored in Chapter 6. High-power LED packages are cleanly decapsulated by MIP afterglow etching without influencing the functionality of the LED die. Different decapsulation processes for flip-chipped and gold wire-bonded LED packages are developed. Typical decapsulation duration for single LED package is 7 minutes for flip-chipped packages and 12 minutes for wire-bonded packages, which is at least 10 times shorter than conventional wet etching alternatives.

The business development of the MIP system is described in Chapter 7. A review of the milestones in both scientific research and business development are given to show how both matter progressed together. Experiences and thoughts are shared which hopefully could be a reference for entrepreneurs in scientific world.

Samenvatting

De meerderheid van de geïntegreerde circuits (IC) zijn ingekapseld in met bonddraad verbonden plastic IC verpakkingen. Epoxy moulding compound wordt gebruikt als inkapselingsmateriaal en goud wordt gebruikt als bonddraad materiaal. De toename van de goud materiaal prijs van 400 USD/ounce in het jaar 2005 tot 1400 USD/ounce in 2013 resulteerde in een significante toename van kosten in de IC assemblage, en dreef de industrie tot het zoeken naar alternatieve bonddraad materialen. Mede dankzij de kostprijs en de performance voordelen, is koper bonddraad langzamerhand de traditionele gouden bonddraad aan het vervangen in de IC assemblage. Het aandeel van koper bonddraad is toegenomen van 1% in het jaar 2007 naar 10% in het jaar 2010 en de verwachtingen zijn dat 30% wordt bereikt in het jaar 2013.

Voor faal analyse op verpakkingsniveau, is de decapsulatie een belangrijke stap om de IC verpakking te openen voor de inspectie van de staat van de interne componenten, en voor het lokaliseren van mogelijke faal locaties voor een oorzaak analyse. De eis voor een goed decapsulatie proces is daarom de mogelijkheid tot het selectief verwijderen van epoxy moulding compound terwijl geen schade wordt toegebracht aan de halfgeleider chip en de metalen bonddraden welke kunnen worden gelokaliseerd in de IC verpakking.

De meest gebruikte conventionele decapsulatie techniek is het gebruik van heet salpeterzuur of een mix van salpeter en zwavelzuur voor het weg etsen van de moulding compound, dit proces wordt als routine gebruikt voor plastic IC verpakkingen met gouden bonddraden. Omdat koperen bonddraden meer vatbaar zijn voor schade en het corroderen in zuur, heeft de schakeling naar koperen bonddraden geleid tot een probleem in de industrie voor zuur decapsulatie. Koperen bonddraden lijden onder onvermijdelijke corrosie na zuur decapsulatie, daarom wordt verdere faal analyse op koper/aluminium verbindingen moeilijk, met name in het geval van IC verpakkingen welke door een thermische spanningsconditie zijn geweest na kwaliteitstesten. Conventionele plasma decapsulatie en laser-ablatie technieken hebben ook inherente nadelen, de toepassing daarvan is daarom gelimiteerd voor decapsulatie van koper bonddraad IC verpakkingen.

In dit proefschrift introduceren we een oplossing voor decapsulatie van IC verpakkingen met koperen-draad verbindingen met behulp van een Microgolf Geïnduceerde Plasma (MIP) systeem. Het MIP systeem combineert de hoge ets

selectiviteit van een plasma met de snelheid en afwezigheid van RF velden van zuur decapsulatie. Karakteristieken van het MIP systeem zijn een hoge vermogensdichtheid, operatie onder atmosferische druk en de afwezigheid van blootstelling van de samples aan ionen. Het behaalde resultaat is een snelle, selectieve en veilige decapsulatie van koperen bonddraad IC verpakkingen. De performance van het MIP systeem ten opzichte van zuur decapsulatie in het behoud van fijne oppervlakte details is beter. In vergelijking tot conventionele plasma etsers is het MIP systeem ten minste 20 keer sneller en het brengt geen schade toe aan de functionaliteit van de chip.

Het prototype setup van het MIP system wordt beschreven in Hoofdstuk 2. Het kern onderdeel in het MIP systeem is een Beenakker-type TM_{010} mode microgolf resonerende holte, welke de plasma bron is die de plasma ets performance bepaalt. Hoofdstuk 3 onderzoekt problemen die ontstaan met het gebruik van de originele Beenakker holte als de bron van het plasma. Aanpassingen worden voorgesteld die het genereren van een atmosferische druk, hoge vermogensdichtheid en stabiele $Ar/O_2/CF_4$ plasma mogelijk maakt. De hoge vermogen reflectie in het MIP systeem wordt gereduceerd door toevoeging van een variabele antenne aan de originele koppeling lus in de holte. Brede en stabiele plasma procesvensters werden behaald met toevoeging van andere modificatie elementen welke de kwaliteit factor van de holte verandert. De vermogensefficiëntie van het MIP systeem wordt geschat op 80%, terwijl de volgehouden volume vermogensdichtheid van MIP bij de Beenakker holte 1600 W/cm^3 onder 40 W input vermogen is.

Op plasma chemie gebaseerde MIP nagloei ets recepten voor een variëteit aan materialen zijn ontwikkeld in Hoofdstuk 4. $Ar/O_2/CF_4$ plasma etsen van epoxy moulding compound, Si, SiO_2, Si_3N_4, siliconen, koper, aluminium, palladium en goud werden uitgevoerd. Deze materialen zijn van speciaal belang omdat ze veel worden toegepast in halfgeleider verpakkingen. De optimale recepten voor hoge ets snelheden en de beperkende factoren van het etsen van elk materiaal worden gegeven. De resultaten geven referenties naar plasma ets selectiviteit en behoud van bepaalde materialen tijdens MIP decapsulatie van IC verpakkingen.

Hoofdstuk 5 focusseert op de applicatie van het MIP nagloei etsen in IC verpakking decapsulatie. Vier verschillende MIP decapsulatie processen worden voorgesteld en hun voor & nadelen worden geanalyseerd. Deze vier processen overdekken alle types van plastic IC verpakking decapsulatie taken, inclusief thermisch gestreste verpakking decapsulatie welke niet behandeld kan worden door andere technieken. Na MIP nagloei decapsulatie, Si_3N_4 passivatie laag, Si chip, Cu bonddraden, Pd-gecoate Cu bonddraden, Au bonddraden, en Al bondvlakken in IC verpakkingen kunnen schoon worden blootgesteld zonder dat enige schade wordt veroorzaakt door het proces. Vergelijkingen van MIP decapsulatie met de huidige gebruikte alternatieve oplossingen van koude zuur

decapsulatie word gemaakt. De superieure mogelijkheid voor het behoud van minutieuze oppervlakte structuren door MIP decapsulatie in een redelijke tijd faciliteert verdere faal-plek analyses en wordt gedemonstreerd door middel van case studies.

De toepassing van MIP afterglow etsen in LED verpakking decapsulatie is onderzocht in Hoofdstuk 6. Hoog vermogen LED verpakkingen worden schoon gedecapsuleerd met MIP nagloei etsen zonder de functionaliteit van de LED chip te beïnvloeden. Verschillende decapsulatie processen voor flip-chipped en gouden bonddraad verbonden LED verpakkingen zijn ontwikkeld. Typische decapsulatie tijd voor enkele LED verpakkingen is 7 minuten voor flip-chipped verpakkingen en 12 minuten voor bonddraad verpakkingen, welke ten minste 10 minuten korter zijn dan conventionele nat ets alternatieven.

De bedrijfsontwikkeling van het MIP systeem is beschreven in Hoofdstuk 7. Een recensie van mijlpalen in wetenschappelijk onderzoek en bedrijfsontwikkeling wordt gegeven om te laten zien hoe beide zaken samen ontwikkelen. Ervaring en gedachten worden gedeeld welke hopelijk kunnen dienen als referentie voor ondernemers in de wetenschappelijke wereld.

Acknowledgments

Four years of Ph.D. life has been an enjoyable journey to me. Now that the time comes to a conclusion, I would like to express my gratitude to all who helped me and encouraged me along the way.

First and foremost I would like to express my sincere thanks and gratitude to my supervisor, Prof. Kees Beenakker, for his guidance, inspiration, and full support to my research work even in times that we held different opinions. When we first spoke during the phone interview in 2009, I couldn't have imagined how valuable this Ph.D career would mean to my life, and neither could I foresee the final answer to your question 'Do you want to start a business after Ph.D.?'. You introduced me not only to the scientific research, but also to the semiconductor back-end industry. I am especially grateful for the times we test the breakthroughs on the cavity together in MEMs lab, and thanks for traveling with me to establish contact with industrial partners, even to places like everywhere-Non-Smoking Taiwan.

I am grateful to Charles Vath III from COMSOL Consulting Singapore for sharing views in packaging technology, giving recommendations on MIP system development, and introducing me to so many industrial contacts.

I would like to thank Ben Schelen from DEMO for supporting me to build the alpha machine from scratch. It seems you provide engineering solutions to everything, mechanical, electrical, temperature, microwave… you name it.

I would also like to offer my gratitude to my Ph.D. committee members for your efforts on reviewing my thesis and your suggestions. Special thanks to Prof. Daan Schram from TU Eindhoven, I appreciate his advice on plasma physics and his passion in scientific research. Also, I would like to thank Prof. Rob Wolters from Twente University for the inspirational discussion on plasma etching chemistry.

In the 4th year of my Ph.D., the process of establishing a start-up company got really serious. The most important reason is that I had a fantastic business advisor, Rene van Eijkelenburg, thank you for guiding me through the obstacles and coaching me to think in a different way other than the technical approach.

I have had the pleasure of collaborating with several companies, and I would like to extend my thanks to them for their important contribution to this thesis, their

warm hospitality when inviting me over for a visit, their generous advice on my work, and their difficult samples that brought me challenges and stimulated me to dive deeper into research. Special thanks to Kees Revenberg and Ewald Reinders from MASER Engineering; Richart Stegink, Marcel van der Straaten, Frank Zachariasse, and Henk Pomp from NXP Nijmegen; Daniel Gruber and Hans-Juergen Funke from NXP Hamburg; John Wang and Theo Martens from NXP Kaohsiung; Bernd Appelt, Curtis Chen, and Sky Liang from ASE Group Kaohsiung; Johnny Yeung from Heraeus Singapore; Sharon Furcone from Freescale USA; Alastair Trigg from Institute of Microelectronics Singapore; James Zhong from Goodark Suzhou; John Beleran from UTAC Group Singapore; Aram Sarkissian from Evans Analytical Group USA; Vahe Sarkissian from ABACA USA; Johannes Bruckmeier and Claudia Keller from Infineon Neubiberg.

I would like to thank Rob Fastenau, Dean of EWI faculty, for his support to the start-up company and initiating the 'EEMCS goes Silicon Valley' trip, the experience of the visit and the trainings will benefit EWI entrepreneurs lifelong. I also like to thank Ronald Gelderblom and Ad Kleingeld from Valorization Center; Erik van Westing from M2i for their support on the patent applications.

None of the work in this thesis would be possible without Dimes: To Prof. Kouchi Zhang, for pushing me to make and realize ambitious goals every year, and arranging SSL group BBQ party in summer time; to Prof. Lina Sarro, for making ECTM a family– including chasing after the Ph. D.'s to get their homework done; to Cadmus Yuan and Willem van Driel, for your suggestions on LED and providing me all kinds of samples; to Henk van Zeijl, for your strange ideas on my research and introducing me to Infineon, in addition, you are a fantastic off-road driver; to Atef Akhnoukh, for our fruitful discussions on microwaves; to Silvana Milosavljevic, my first teacher in the cleanroom; to Cassan Visser, for making me nice photos for the Annual Review Report; to Alex van den Bogaard, for helping me with MFCs and temperature measurements; to Ron van Viersen, for arranging me the gas connections and bottles; to Gregory Pandraud, for always calling me 'boss' in the MEMs lab; to Marian Roozenburg, Marysia Lagendijk-Korzeniewski, and Bianca Knot, for always giving me patient help on administration and tons of sample shipment.

I want to express my gratitude to my colleagues, Huaiyu Ye, Sau Koh, Jing Zhang, Sima Tarashioon, for the unforgettable trips we had to conferences and meetings; Rene Poelma for translating my summary into Dutch even you are short on time; Jianfei Dong for the drinks; Jia Wei, Chengang Shen, Yujian Huang, Pan Liu, An Tran, Cell Wong, Jin Zhang, Fabio Santagata, Lin Qi, An Xiao, Xianping Chen, Lingen Wang, Xueming Li, Pengfei Sun, for the nice discussions and chats we had, it has been a great pleasure to work with you. My dear office mates, thank you for making my office time so enjoyable, clearly each of you has a role, Thomas brings

cake, Daniel brings laughter, Sten brings humor and life - plants & fish, Aslihan brings sunshine.

Also, I would like to extend special thanks to my friends and roommates, you enriched my staying in Delft in many aspects. Roland, Lily, Cecilia, to me you are more like family rather than friends, thank you for always been there to support me.

Moreover, I want to express my deepest appreciation to my family, for your endless love, understanding, and encouraging me to pursue my dream.

And most of all, with all my love, to my wife Jing Wang, thank you for your enduring love, for sharing the joys and tears, and for making my life beautiful. The past three years with you has been the best years of my life. We have the whole future awaiting for us to explore.

Bibliography

[1] R. R. Tummala, *Fundamentals of Microsystems Packaging*: McGraw-Hill, 2001.

[2] G. Q. Zhang, W. D. van Driel, and X. J. Fan, *Mechanics of Microelectronics*: Springer, 2006.

[3] *Intel Packaging Databook*, 1999.

[4] T. Panczak, "Copper Wirebonding OSAT Viewpoint," Amkor report, 2011.

[5] S. R. C. Magno, J. Ramos, E. Pecolera, and C. Stai, "Copper as a viable solution for IC packaging," *Circuits Assembly,* vol. 19, p. 22, 2008.

[6] B. K. Appelt, A. Tseng, C. H. Chen, and Y. S. Lai, "Fine pitch copper wire bonding in high volume production," *Microelectronics Reliability,* vol. 51, pp. 13-20, 2011.

[7] S. K. Prasad, *Advanced Wirebond Interconnection Technology*: Kluwer Academic Publishers, 2004.

[8] S. Kaimori, T. Nonaka, and A. Mizoguchi, "The development of Cu bonding wire with oxidation-resistant metal coating," *IEEE Transactions on Advanced Packaging,* vol. 29, pp. 227-231, 2006.

[9] I. Singh, I. Qin, H. Xu, C. Huynh, S. Low, H. Clauberg, B. Chylak, and V. L. Acoff, "Pd-coated Cu wire bonding technology: Chip design, process optimization, production qualification and reliability test for high reliability semiconductor devices," in *62nd Electronic Components and Technology Conference (ECTC)* 2012, pp. 1089-1096.

[10] T. Uno, S. Terashima, and T. Yamada, "Surface-enhanced copper bonding wire for LSI and Its Bond Reliability under Humid Environment," in *59th Electronic Components and Technology Conference (ECTC)* 2009, pp. 1486-1495.

[11] S. L. Khoury, D. J. Burkhard, D. P. Galloway, and T. A. Scharr, "A comparison of copper and gold wire bonding on integrated circuit devices," *IEEE transactions on components, hybrids, and manufacturing technology,* vol. 13, pp. 673-681, 1990.

[12] S. Murali, N. Srikanth, Y. M. Wong, and C. J. Vath Iii, "Fundamentals of thermo-sonic copper wire bonding in microelectronics packaging," *Journal of Materials Science,* vol. 42, pp. 615-623, 2007.

[13] N. Srikanth, S. Murali, Y. M. Wong, and C. J. Vath Iii, "Critical study of thermosonic copper ball bonding," *Thin Solid Films,* vol. 462-463, pp. 339-345, 2004.

[14] L. England and T. Jiang, "Reliability of Cu wire bonding to Al metallization," in *57th Electronic Components and Technology Conference (ECTC)* 2007, pp. 1604-1613.

[15] H. Abe, K. Dong Chul, T. Yamamoto, T. Yagihashi, Y. Endo, H. Saito, T. Horie, H. Tamate, Y. Ejiri, N. Watanabe, and T. Iwasaki, "Cu wire and Pd-

Cu wire package reliability and molding compounds," in *62nd Electronic Components and Technology Conference (ECTC)* 2012, pp. 1117-1123.
[16] C. J. Vath III, M. Gunasekaran, and R. Malliah, "Factors affecting the long-term stability of Cu/Al ball bonds subjected to standard and extended high temperature storage," *Microelectronics Reliability,* vol. 51, pp. 137-147, 2011.
[17] S. Peng, H. Seki, P. Chen, S. Zenbutsu, S. Itoh, L. Huang, N. Liao, B. Liu, C. Chen, W. Tai, and A. Tseng, "An evaluation of effects of molding compound properties on reliability of Cu wire components," in *61st Electronic Components and Technology Conference (ECTC)*, 2011, pp. 363-369.
[18] "International Technology Roadmap for Semiconductors (ITRS) Assembly and Packaging Report " 2011.
[19] A. D. Trigg, C. T. Chong, S. Y. P. Fen, J. L. T. Kwee, C. C. H. Ming, S. C. S. Mung, C. Ping, V. P. Ganesh, B. Low, T. L. Chu, and E. P. Leng, "Copper wire bond reliability evaluation using a modular test chip," in *14th Electronics Packaging Technology Conference (EPTC)*, 2012, pp. 170-173.
[20] T. M. Moore and R. G. McKenna, *Characterization of Integrated Circuit Packaging Materials*: Butterworth-Heinemann, 1993.
[21] H. Ardebili and M. Pecht, *Encapsulation Technologies For Electronic Applications*: Elsevier, 2009.
[22] F. Beck, *Integrated Circuit Failure Analysis: A Guide to Preparation Techniques*: John Wiley & Sons Ltd., 1998.
[23] N. Soo Whye, Z. Hong Bo, L. Kaeng Nan, W. Lee, and L. Ren De, "Copper wirebond package decapsulation technique using mixed acid chemistry," in *19th IEEE International Symposium on the Physical and Failure Analysis of Integrated Circuits (IPFA)*, 2012, pp. 1-5.
[24] S. Murali and N. Srikanth, "Acid decapsulation of epoxy molded IC packages with copper wire bonds," *IEEE Transactions on Electronics Packaging Manufacturing,* vol. 29, pp. 179-183, 2006.
[25] C. P. Liu, Y. F. Liu, C. H. Li, H. C. Cheng, Y. C. Kung, and J. Y. Lin, "A novel decapsulation technique for failure analysis of epoxy molded IC packages with Cu wire bonds," *Microelectronics Reliability,* vol. 52, pp. 725-734, 2012.
[26] M. J. Lefevre, F. Beauquis, J. Yang, M. Obein, P. Gounet, and S. Barberan, "New method for decapsulation of copper wire devices using LASER and sub-ambient temperature chemical etch," in *13th Electronics Packaging Technology Conference (EPTC)*, 2011, pp. 769-773.
[27] S. Dzioba, G. Este, and H. M. Naguib, "Decapsulation and photoresist stripping in oxygen microwave plasmas," *J Electrochem Soc,* vol. V 129, pp. 2537-2541, 1982.
[28] M. Pfarr and A. Hart, "The use of Plasma Chemistry in Failure Analysis," in *18th Annual Reliability Physics Symposium*, 1980, pp. 110-114.

[29] J. Thomas, J. Baer, P. Westby, K. Mattson, F. Haring, G. Strommen, J. Jacobson, S. S. Ahmad, and A. Reinholz, "A unique application of decapsulation combining laser and plasma," in *59th Electronic Components and Technology Conference (ECTC)*, 2009, pp. 2011-2015.

[30] P. Schwindenhammer, H. Murray, P. Descamps, and P. Poirier, "Determination of temperature change inside IC packages during laser ablation of molding compound," *Microelectronics Reliability,* vol. 48, pp. 1263-1267, 2008.

[31] A. Aubert, L. Dantas de Morais, and J. P. Rebrassé, "Laser decapsulation of plastic packages for failure analysis: Process control and artefact investigations," *Microelectronics Reliability,* vol. 48, pp. 1144-1148, 2008.

[32] M. Krüger, J. Krinke, K. Ritter, B. Zierle, and M. Weber, "Laser-assisted decapsulation of plastic-encapsulated devices," *Microelectronics Reliability,* vol. 43, pp. 1827-1831, 2003.

[33] H. Qiu, H. Y. Zheng, X. C. Wang, and G. C. Lim, "Laser decapsulation of molding compound from wafer level chip size package for solder reflowing," *Materials Science in Semiconductor Processing,* vol. 8, pp. 502-510, 2005.

[34] P. Schwindenhammer, P. Poirier, and P. Descamps, "Microelectronics failure analysis using laser ablation of composite materials in system in package," in *8th Electronics Packaging Technology Conference (EPTC)*, 2006, pp. 752-759.

[35] C. Tendero, C. Tixier, P. Tristant, J. Desmaison, and P. Leprince, "Atmospheric pressure plasmas: A review," *Spectrochimica Acta - Part B Atomic Spectroscopy,* vol. 61, pp. 2-30, 2006.

[36] A. E. Croslyn, B. W. Smith, and J. D. Winefordner, "A review of microwave plasma sources in atomic emission spectrometry: Literature from 1985 to the present," *Critical Reviews in Analytical Chemistry,* vol. 27, pp. 199-255, 1997.

[37] K. A. Forbes, E. E. Reszke, P. C. Uden, and R. M. Barnes, "Comparison of microwave-induced plasma sources," *Journal of Analytical Atomic Spectrometry,* vol. 6, pp. 57-71, 1991.

[38] C. I. M. Beenakker, B. Bosman, and P. W. J. M. Bousman, "An assessment of a microwave-induced plasma generated in argon with a cylindrical TM010 cavity as an excitation source for emission spectrometric analysis of solutions," *Spectrochimica Acta Part B: Atomic Spectroscopy,* vol. 33, pp. 373-381, 1978.

[39] C. I. M. Beenakker, "A cavity for microwave-induced plasmas operated in helium and argon at atmospheric pressure," *Spectrochimica Acta Part B: Atomic Spectroscopy,* vol. 31, pp. 483-486, 1976.

[40] C. I. M. Beenakker and P. W. J. M. Boumans, "Additional experience with the cylindrical TM010 cavity for generating an MIP in helium and argon at atmospheric pressure," *Spectrochimica Acta Part B: Atomic Spectroscopy,* vol. 33, pp. 53-54, 1978.

[41] B. Agdur and B. Enander, "Resonances of a microwave cavity partially filled with a plasma," *Journal of Applied Physics,* vol. 33, pp. 575-581, 1962.
[42] S. J. Buchsbaum, L. Mower, and S. C. Brown, "Interaction between cold plasmas and guided electromagnetic waves," *Physics of Fluids,* vol. 3, pp. 806-819, 1960.
[43] D. J. Rose and S. C. Brown, "Methods of measuring the properties of ionized gases at high frequencies. III. Measurement of discharge admittance and electron density," *Journal of Applied Physics,* vol. 23, pp. 1028-1032, 1952.
[44] S. Offermanns, "Electrodeless high-pressure microwave discharges," *Journal of Applied Physics,* vol. 67, pp. 115-123, 1990.
[45] S. Offermanns, "Resonance characteristics of a cavity-operated electrodeless high-pressure microwave discharge system," *IEEE Transactions on Microwave Theory and Techniques,* vol. 38, pp. 904-911, 1990.
[46] J. L. Shohet and C. Moskowitz, "Eigenvalues of a microwave-cavity-lossy-plasma system," *Journal of Applied Physics,* vol. 36, pp. 1756-1759, 1965.
[47] A. Dattner, "Resonance densities in a cylindrical plasma column," *Physical Review Letters,* vol. 10, pp. 205-206, 1963.
[48] S. L. Halverson and A. J. Hatch, "FREQUENCY-SHIFTING METHOD OF EXCITING A PLASMA IN A RESONANT CAVITY," *Applied Physics Letters,* vol. 14, pp. 79-81, 1969.
[49] I. L. Kosow, *Microwave Theory and Measurements*. New Jersey: Prentice-Hall, INC., 1962.
[50] R. D. Deutsch and G. M. Hieftje, "Development of a microwave-induced nitrogen discharge at atmospheric pressure (MINDAP)," *Applied Spectroscopy,* vol. 39, pp. 214-222, 1985.
[51] A. T. Zander and G. M. Hieftje, "Determination of trace metals by microwave plasma spectrometry with an atmospheric pressure helium discharge," *Analytical Chemistry,* vol. 50, pp. 1257-1260, 1978.
[52] A. Bollo-Kamara and E. G. Codding, "Considerations in the design of a microwave induced plasma utilizing the TM010 cavity for optical emission spectroscopy," *Spectrochimica Acta Part B: Atomic Spectroscopy,* vol. 36, pp. 973-982, 1981.
[53] N. Rait, D. W. Golightly, and C. J. Massoni, "An improved Beenakker-type cavity for microwave induced plasma spectrometry," *Spectrochimica Acta Part B: Atomic Spectroscopy,* vol. 39, pp. 931-937, 1984.
[54] D. L. Haas, J. W. Carnahan, and J. A. Caruso, "An Internally Tuned TM010 Microwave Resonant Cavity for Moderate Power Microwave-induced Plasmas," *Appl. Spectrosc.,* vol. 37, pp. 82-85, 1983.
[55] K. G. Michlewicz, J. J. Urh, and J. W. Carnahan, "A microwave induced plasma system for the maintenance of moderate power plasmas of

helium, argon, nitrogen and air," *Spectrochimica Acta Part B: Atomic Spectroscopy,* vol. 40, pp. 493-499, 1985.
[56] J. P. J. van Dalen, P. A. de Lezenne Coulander, and L. de Galan, "Improvements of the cylindrical TM010 cavity for an atmospheric pressure microwave-induced plasma," *Spectrochimica Acta Part B: Atomic Spectroscopy,* vol. 33, pp. 545-549, 1978.
[57] L. G. Matus, C. B. Boss, and A. N. Riddle, "Tuning and matching the TM_{010} cavity," *Review of Scientific Instruments,* vol. 54, pp. 1667-1673, 1983.
[58] J. Hubert, M. Moisan, and A. Ricard, "A new microwave plasma at atmospheric pressure," *Spectrochimica Acta Part B: Atomic Spectroscopy,* vol. 34, pp. 1-10, 1979.
[59] M. Moisan, Z. Zakrzewski, and R. Pantel, "The theory and characteristics of an efficient surface wave launcher (surfatron) producing long plasma columns," *Journal of Physics D: Applied Physics,* vol. 12, p. 219, 1979.
[60] M. Moisan, R. Grenier, and Z. Zakrzewski, "The electromagnetic performance of a surfatron-based coaxial microwave plasma torch," *Spectrochimica Acta Part B: Atomic Spectroscopy,* vol. 50, pp. 781-789, 1995.
[61] M. Moisan and J. Pelletier, *Microwave Excited Plasmas*. New York: Elsevier, 1992.
[62] R. P. Cardoso, T. Belmonte, C. Noel, F. Kosior, and G. Henrion, "Filamentation in argon microwave plasma at atmospheric pressure," *Journal of Applied Physics,* vol. 105, pp. 093306-8, 2009.
[63] Y. Kabouzi, M. D. Calzada, M. Moisan, K. C. Tran, and C. Trassy, "Radial contraction of microwave-sustained plasma columns at atmospheric pressure," *Journal of Applied Physics,* vol. 91, pp. 1008-1019, 2002.
[64] *ANSYS Fluent software*. Available: http://www.ansys.com/Products/Simulation+Technology/Fluid+Dynamics/Fluid+Dynamics+Products/ANSYS+Fluent
[65] C. Prokisch, A. M. Bilgic, E. Voges, J. A. C. Broekaert, J. Jonkers, M. Van Sande, and J. A. M. Van Der Mullen, "Photographic plasma images and electron number density as well as electron temperature mappings of a plasma sustained with a modified argon microwave plasma torch (MPT) measured by spatially resolved Thomson scattering," *Spectrochimica acta, Part B: Atomic spectroscopy,* vol. 54, pp. 1253-1266, 1999.
[66] A. Besner, M. Moisan, and J. Hubert, "Fundamental properties of radiofrequency and microwave surface-wave induced plasmas," *Journal of Analytical Atomic Spectrometry,* vol. 3, pp. 863-866, 1988.
[67] C. K. Chen and J. Phillips, "Impact of aerosol particles on the structure of an atmospheric pressure microwave plasma afterglow," *Journal of Physics D: Applied Physics,* vol. 35, pp. 998-1009, 2002.
[68] J. Y. Jeong, J. Park, I. Henins, S. E. Babayan, V. J. Tu, G. S. Selwyn, G. Ding, and R. F. Hicks, "Reaction chemistry in the afterglow of an oxygen-helium,

atmospheric-pressure plasma," *Journal of Physical Chemistry A,* vol. 104, pp. 8027-8032, 2000.
[69] K. Fricke, S. Reuter, D. Schroder, V. Schulz-Von Der Gathen, K. D. Weltmann, and T. Von Woedtke, "Investigation of surface etching of poly(ether ether ketone) by atmospheric-pressure plasmas," *IEEE Transactions on Plasma Science,* vol. 40, pp. 2900-2911, 2012.
[70] G. Park, H. Lee, G. Kim, and J. K. Lee, "Global model of He/O2 and Ar/O2 atmospheric pressure glow discharges," *Plasma Processes and Polymers,* vol. 5, pp. 569-576, 2008.
[71] N. Knake, S. Reuter, K. Niemi, V. Schulz-Von Der Gathen, and J. Winter, "Absolute atomic oxygen density distributions in the effluent of a microscale atmospheric pressure plasma jet," *Journal of Physics D: Applied Physics,* vol. 41, 2008.
[72] S. Reuter, J. Winter, A. Schmidt-Bleker, D. Schroeder, H. Lange, N. Knake, V. Schulz-Von Der Gathen, and K. D. Weltmann, "Atomic oxygen in a cold argon plasma jet: TALIF spectroscopy in ambient air with modelling and measurements of ambient species diffusion," *Plasma Sources Science and Technology,* vol. 21, 2012.
[73] S. Reuter, K. Niemi, V. Schulz-Von Der Gathen, and H. F. Döbele, "Generation of atomic oxygen in the effluent of an atmospheric pressure plasma jet," *Plasma Sources Science and Technology,* vol. 18, 2009.
[74] X. Yang, S. E. Babayan, and R. F. Hicks, "Measurement of the fluorine atom concentration in a carbon tetrafluoride and helium atmospheric-pressure plasma," *Plasma Sources Science and Technology,* vol. 12, pp. 484-488, 2003.
[75] A. Barry, "Tailoring Surfaces with Silanes," *Gelest Corporation Technical Paper*.
[76] Y. Xie, C. A. S. Hill, Z. Xiao, H. Militz, and C. Mai, "Silane coupling agents used for natural fiber/polymer composites: A review," *Composites Part A: Applied Science and Manufacturing,* vol. 41, pp. 806-819, 2010.
[77] C. J. Mogab, A. C. Adams, and D. L. Flamm, "Plasma etching of Si and SiO2 - The effect of oxygen additions to CF4 plasmas," *Journal of Applied Physics,* vol. 49, pp. 3796-3803, 1978.
[78] C. I. M. Beenakker, J. H. J. Van Dommelen, and R. P. J. Van De Poll, "Decomposition and product formation in CF4-O2 plasma etching silicon in the afterglow," *Journal of Applied Physics,* vol. 52, pp. 480-485, 1981.
[79] B. Lamontagne, A. M. Wrobel, G. Jalbert, and M. R. Wertheimer, "Large-area microwave plasma etching of polyimide," *Journal of Physics D: Applied Physics,* vol. 20, pp. 844-850, 1987.
[80] F. Emmi, F. D. Egitto, and L. J. Matienzo, "Etching behavior of an epoxy film in O_2/CF_4 plasmas," *Journal of Vacuum Science & Technology A: Vacuum, Surfaces, and Films,* vol. 9, pp. 786-789, 1991.
[81] F. D. Egitto, F. Emmi, R. S. Horwath, and V. Vukanovic, "Plasma etching of organic materials. I. Polyimide in O_2--CF_4," *Journal of Vacuum Science &*

Technology B: Microelectronics and Nanometer Structures, vol. 3, pp. 893-904, 1985.
[82] G. N. Taylor and T. M. Wolf, "OXYGEN PLASMA REMOVAL OF THIN POLYMER FILMS," *Polymer Engineering and Science,* vol. 20, pp. 1087-1092, 1980.
[83] A. M. Wrobel, B. Lamontagne, and M. R. Wertheimer, "Large-area microwave and radiofrequency plasma etching of polymers," *Plasma Chemistry and Plasma Processing,* vol. 8, pp. 315-329, 1988.
[84] S. R. Cain, F. D. Egitto, and F. Emmi, "Relation of polymer structure to plasma etching behavior: Role of atomic fluorine," *Journal of Vacuum Science & Technology A: Vacuum, Surfaces, and Films,* vol. 5, pp. 1578-1584, 1987.
[85] V. Vukanovic, G. A. Takacs, E. A. Matuszak, F. D. Egitto, F. Emmi, and R. S. Horwath, "Plasma etching of organic materials. II. Polyimide etching and passivation downstream of an O2--CF4--Ar microwave plasma," *Journal of Vacuum Science & Technology B: Microelectronics and Nanometer Structures,* vol. 6, pp. 66-71, 1988.
[86] G. S. Oehrlein, Y. Zhang, D. Vender, and O. Joubert, "Fluorocarbon high-density plasmas. II. Silicon dioxide and silicon etching using CF_4 and CHF_3," *Journal of Vacuum Science & Technology A: Vacuum, Surfaces, and Films,* vol. 12, pp. 333-344, 1994.
[87] F. Gaboriau, G. Cartry, M. C. Peignon, and C. Cardinaud, "Etching mechanisms of Si and SiO2 in fluorocarbon ICP plasmas: Analysis of the plasma by mass spectrometry, Langmuir probe and optical emission spectroscopy," *Journal of Physics D: Applied Physics,* vol. 39, pp. 1830-1845, 2006.
[88] J. Ding, J. Jenq, x, S, G. Kim, H, H. L. Maynard, J. S. Hamers, N. Hershkowitz, and J. W. Taylor, "Etching rate characterization of SiO_2 and Si using ion energy flux and atomic fluorine density in a CF_4/O_2/Ar electron cyclotron resonance plasma," *Journal of Vacuum Science & Technology A: Vacuum, Surfaces, and Films,* vol. 11, pp. 1283-1288, 1993.
[89] R. d'Agostino and D. L. Flamm, "Plasma etching of Si and SiO_2 in SF_6-O_2 mixtures," *Journal of Applied Physics,* vol. 52, pp. 162-167, 1981.
[90] W. E. Vanderlinde, C. J. Von Benken, and A. R. Crockett, "Rapid integrated circuit delayering without grass," 1996, pp. 260-271.
[91] M. Schaepkens, T. E. F. M. Standaert, N. R. Rueger, P. G. M. Sebel, G. S. Oehrlein, and J. M. Cook, "Study of the SiO2-to-Si3N4 etch selectivity mechanism in inductively coupled fluorocarbon plasmas and a comparison with the SiO2-to-Si mechanism," *Journal of Vacuum Science and Technology A: Vacuum, Surfaces and Films,* vol. 17, pp. 26-37, 1999.
[92] Y. Zhang, G. S. Oehrlein, and F. H. Bell, "Fluorocarbon high density plasmas. VII. Investigation of selective SiO2-to-Si3N4 high density plasma etch processes," *Journal of Vacuum Science and Technology A: Vacuum, Surfaces and Films,* vol. 14, pp. 2127-2137, 1996.

[93] G. H. Kim, S. B. Kim, and C. I. Kim, "Selective etching of SiO2 over Si3N4 in a C5F8/O2/Ar plasma," *Microelectronic Engineering,* vol. 83, pp. 2504-2509, 2006.
[94] J. Tang, D. Gruber, J. B. J. Schelen, H.-J. Funke, and C. I. M. Beenakker, "Fast Etching of Molding Compound by an Ar/O2/CF4 Plasma and Process Improvements for Semiconductor Package Decapsulation," *ECS Journal of Solid State Science and Technology,* vol. 1, pp. P175-P178, 2012.
[95] B. Balakrisnan, S. Patil, and E. Smela, "Patterning PDMS using a combination of wet and dry etching," *Journal of Micromechanics and Microengineering,* vol. 19, 2009.
[96] S. J. Hwang, D. J. Oh, P. G. Jung, S. M. Lee, J. S. Go, J. H. Kim, K. Y. Hwang, and J. S. Ko, "Dry etching of polydimethylsiloxane using microwave plasma," *Journal of Micromechanics and Microengineering,* vol. 19, 2009.
[97] J. Garra, T. Long, J. Currie, T. Schneider, R. White, and M. Paranjape, "Dry etching of polydimethylsiloxane for microfluidic systems," *Journal of Vacuum Science and Technology, Part A: Vacuum, Surfaces and Films,* vol. 20, pp. 975-982, 2002.
[98] J. W. Lee, Y. D. Park, J. R. Childress, S. J. Pearton, F. Sharifi, and F. Ren, "Copper dry etching with Cl2/Ar plasma chemistry," *Journal of the Electrochemical Society,* vol. 145, pp. 2585-2589, 1998.
[99] K. S. Choi and C. H. Han, "Low temperature copper etching using an inductively coupled plasma with ultraviolet light irradiation," *Journal of the Electrochemical Society,* vol. 145, pp. L37-L39, 1998.
[100] S. Lee and Y. Kuo, "Chlorine Plasma/Copper Reaction in a New Copper Dry Etching Process," *Journal of the Electrochemical Society,* vol. 148, pp. G524-G529, September 1, 2001 2001.
[101] F. Wu, G. Levitin, and D. W. Hess, "Low-temperature etching of Cu by hydrogen-based plasmas," *ACS Applied Materials and Interfaces,* vol. 2, pp. 2175-2179, 2010.
[102] F. Wu, G. Levitin, and D. W. Hess, "Temperature effects and optical emission spectroscopy studies of hydrogen-based plasma etching of copper," *Journal of the Electrochemical Society,* vol. 159, pp. H121-H124, 2012.
[103] N. Wiberg, *Holleman-Wiberg's Inorganic Chemistry*: Walter de Gruyter, 1995.
[104] G. Liu and Y. Kuo, "Additive-Gas Effects on Cl2 Plasma-Based Copper-Etch Process and Sidewall Attack," *Journal of the Electrochemical Society,* vol. 155, pp. H97-H102, 2008.
[105] J. W. Kim, Y. C. Kim, and W. J. Lee, "Reactive ion etching mechanism of plasma enhanced chemically vapor deposited aluminum oxide film in CF4/O2 plasma," *Journal of Applied Physics,* vol. 78, pp. 2045-2049, 1995.
[106] P. E. Riley, "Plasma etching of aluminum metallizations for ultralarge scale integrated circuits," *Journal of the Electrochemical Society,* vol. 140, pp. 1518-1522, 1993.

[107] N. Hara, S. Mukuhara, K. Ohtomo, Y. Shimizu, and K. Sugimoto, "Corrosion Behavior of Stainless Steel and Aluminum in a Downstream Environment of CF 4 / O 2 Microwave Plasma," *Journal of the Electrochemical Society,* vol. 149, pp. B297-B305, July 1, 2002 2002.

[108] K. H. Ernst, D. Grman, R. Hauert, and E. Hollaender, "Fluorine-induced corrosion of aluminum microchip bond pads: An XPS and AES analysis," *Surface and Interface Analysis,* vol. 21, pp. 691-696, 1994.

[109] K. R. Williams and R. S. Muller, "Etch rates for micromachining processing," *Journal of Microelectromechanical Systems,* vol. 5, pp. 256-269, 1996.

[110] K. R. Williams, K. Gupta, and M. Wasilik, "Etch rates for micromachining processing - Part II," *Journal of Microelectromechanical Systems,* vol. 12, pp. 761-778, 2003.

[111] S. Alberici, D. Coulon, P. Joubin, Y. Mignot, L. Oggioni, P. Petruzza, D. Piumi, and L. Zanotti, "Surface treatment of wire bonding metal pads," *Microelectronic Engineering,* vol. 70, pp. 558-565, 2003.

[112] F. Fracassi, R. d'Agostino, and A. Cacucci, "Dry etching of palladium thin films in fluorine containing plasmas: X-ray photoelectron spectroscopy investigation," *Journal of Vacuum Science and Technology A: Vacuum, Surfaces and Films,* vol. 13, pp. 63-66, 1995.

[113] D. R. Lide, *CRC Handbook of Chemistry and Physics*: Taylor and Francis Group, 2013.

[114] R. M. Randade, S. S. Ang, and W. D. Brown, "Reactive ion etching of thin fold films," *Journal of the Electrochemical Society,* vol. 140, pp. 3676-3678, 1993.

[115] F. T. Aldridge, "High speed anisotropic reactive ion etching of gold films," *Journal of the Electrochemical Society,* vol. 142, pp. 1563-1565, 1995.

[116] T. Y. Kang, G. Kim, I. H. Cho, D. Seo, and S. J. Hong, "Process optimization of CF4/Ar plasma etching of Au using I-optimal design," *Thin Solid Films,* vol. 517, pp. 3919-3922, 2009.

[117] K. L. Saenger and C. P. Sun, "Yellow emission bands produced during gold etching in O_2-CF_4 rf glow-discharge plasmas: Evidence for gas-phase AuF," *Physical Review A,* vol. 46, pp. 670-673, 1992.

[118] S. Andreev and J. J. Belbruno, "Detection of AuF by emission spectroscopy in a hollow cathode discharge," *Chemical Physics Letters,* vol. 329, pp. 490-494, 2000.

[119] N. N. Greenwood and A. Earnshaw, *Chemistry of the Elements*: Elsevier 1994.

[120] M. J. Vasile, T. J. Richardson, F. A. Stevie, and W. E. Falconer, "Preparation and characterization of gold pentafluoride," *Journal of the Chemical Society, Dalton Transactions,* pp. 351-353, 1976.

[121] B. K. Appelt, A. Tseng, Y.-S. Lai, and C.-H. Chen, "Copper Wire Bonding in High Volume Manufacturing," *ECS Transactions,* vol. 34, pp. 857-864, March 21, 2011 2011.

[122] M. Pfarr and A. Hart, "USE OF PLASMA CHEMISTRY IN FAILURE ANALYSIS," *Annual Proceedings - Reliability Physics (Symposium),* pp. 110-114, 1980.
[123] K. S. Suslick, "Sonochemistry," *Science,* vol. 247, pp. 1439-1445, 1990.
[124] J. H. Bang and K. S. Suslick, "Applications of ultrasound to the synthesis of nanostructured materials," *Advanced Materials,* vol. 22, pp. 1039-1059, 2010.
[125] K. A. Kusters, S. E. Pratsinis, S. G. Thoma, and D. M. Smith, "Ultrasonic fragmentation of agglomerate powders," *Chemical Engineering Science,* vol. 48, pp. 4119-4127, 1993.
[126] Y. Jiang, D. Tang, X. Song, and T. F. Lam, "The effect of ultrasonic cleaning on the bond wires," in *Proc. 12th International Symposium on the Physical and Failure Analysis of Integrated Circuits*, 2005, pp. 237-241.
[127] B. P. Richards, P. Burton, and P. K. Footner, "Effects of ultrasonic cleaning on device degradation," *Circuit World,* vol. 16, pp. 20-25, 1990.
[128] K. D. Staller, "Low temperature plasma decapsulation of copper-wire-bonded and exposed copper metallization devices," in *Proc. International Symposium for Testing and Failure Analysis*, 2010, pp. 127-132.
[129] E. F. Schubert, J. K. Kim, H. Luo, and J. Q. Xi, "Solid-state lighting - A benevolent technology," *Reports on Progress in Physics,* vol. 69, 2006.
[130] M. Meneghini, A. Tazzoli, G. Mura, G. Meneghesso, and E. Zanoni, "A review on the physical mechanisms that limit the reliability of GaN-based LEDs," *IEEE Transactions on Electron Devices,* vol. 57, pp. 108-118, 2010.
[131] M. Dal Lago, M. Meneghini, N. Trivellin, G. Meneghesso, and E. Zanoni, "Degradation mechanisms of high-power white LEDs activated by current and temperature," *Microelectronics Reliability,* vol. 51, pp. 1742-1746, 2011.
[132] F. Beck, *Integrated Circuit Failure Analysis*: John Wiley & Sons, 1998.
[133] H. C. Hsu, C. J. Wang, H. R. Lin, and P. Han, "Optimized semi-sphere lens design for high power LED package," *Microelectronics Reliability,* vol. 52, pp. 894-899, 2012.
[134] H. Luo, J. K. Kim, E. F. Schubert, J. Cho, C. Sone, and Y. Park, "Analysis of high-power packages for phosphor-based white-light-emitting diodes," *Applied Physics Letters,* vol. 86, pp. 1-3, 2005.
[135] Q. Li, C. I. M. Beenakker, and C. J. Vath III, "A novel decapsulation technique for failure analysis of integrated circuits," in *7th International Conference on Electronics Packaging Technology*, Shanghai, 2007.
[136] Q. Li, "A New Technology for Failure Analysis of CopperWire Bonded Plastic ICs," Master Thesis, Delft University of Technology, Delft, 2006.
[137] L. Chamness. (2012, Semiconductor Materials Market to Surpass $50 Billion in 2013. Available: http://www.semi.org/en/node/43361